

Exploring the Effects of Electric Fields and Surface Charging on Magnetic Properties of Nanostructures : an *ab initio* Study

Dissertation

zur Erlangung des akademischen Grades
doktor rerum naturalium (Dr. rer. nat.)

vorgelegt der

Mathematisch-Naturwissenschaftlich-Technischen Fakultät
(mathematisch-naturwissenschaftlicher Bereich)
der Martin-Luther-Universität Halle - Wittenberg

von Herrn Tamene Regassa Dasa
geb. am März 18 1984 in Addis Ababa, Ethiopia

angefertigt am
Max-Planck-Institut für Mikrostrukturphysik
Halle (Saale) verteidigt am 12.06.2014

Gutachter:

1. Prof. Dr. Wolfram Hergert
2. PD Dr. Arthur Ernst
3. Prof. Dr. Gustavo M. Pastor

Halle (Saale), 12.06.2014

Abstract

Neue Möglichkeiten die magnetischen Eigenschaften der nanometer-großen metallenen Oberflächenstrukturen (von Nanodrähten und Dünen Folien) zu untersuchen und zu beeinflussen werden vorgeschlagen und diskutiert auf der Basis von voll-relativistischen *ab initio* Berechnungen.

Der Einfluss der geometrischen Relaxationen und der chemischen Zusammensetzung metallener Nanodrähte auf deren magnetische Stabilität und Anisotropie wird untersucht. Starke Zunahme der magnetischen Anisotropie Energie (MAE) wird festgestellt in Co Nanodrähten auf einer Pt Oberfläche, folgend der Legierung mit Platin (Pt). In Fe Nanodrähten kann so eine Legierung sogar einen Umschwung der Magnetisierung hervorrufen. Außerdem wird gezeigt, dass elektrische Felder dazu eingesetzt werden können, die magnetische Anisotropie der Nanodrähte zu beeinflussen; ein Effekt, der mit der Abschirmung des elektrischen Feldes durch Oberflächen- und Nanodraht-Elektronen zustande kommt.

Für Fe und Co Multilagen auf einer Pt(001) Oberfläche wird festgestellt, dass deren Spin Polarisation und Anisotropie mit zunehmender Fe oder Co Schichtdicke oszilliert. Dieses Effekt lässt sich ausgezeichnet mit der Existenz der *d*-elektronen Quantentopf-Zustände in der Multilage erklären. Die Quantentopf-Zustände, und damit auch die Spin Polarisation und Anisotropie der Multilagen, lassen sich mit einem externen elektrischen Feld beeinflussen.

Die magnetischen Eigenschaften atomarer Strukturen können mit einer Vielzahl an magneto-elektrischen Phänomenen beeinflusst werden. In dieser Arbeit zeigen wir, dass auch durch Beeinflussung der internen Ladungsträger (durch Elektronen- oder Elektronen-Loch-Zufuhr) können magnetische Eigenschaften von metallenen Multilagen kontrolliert werden können. So kann, zum Beispiel, die Ausrichtung der Magnetischen Momente geändert oder die Austauschkopplung zweier Monolagen umgekehrt werden.

Abstract in English

In the present thesis, several novel possibilities to tune the magnetic properties of nanoscale metallic structures (atomic chains and multilayers) are presented and discussed, on the basis of *ab initio* density functional theory (DFT) including a self-consistent treatment of spin-orbit coupling.

Taking structural relaxation into account, the dependence of the magnetic anisotropy of linear atomic chains on the chemical composition is discussed. A strong enhancement of the magnetic anisotropy energy in mixed Co-Pt chains, compared to pure Co chains, is found. Moreover, alloying linear Fe chains on Pt(997) surface with Co leads to magnetization reversal. The study on the influence of electric field on magnetic properties gives clear evidence that an externally applied electric field could allow one to tailor magnetic anisotropy in Co and Co-Pt atomic chains. These effects are related to the spin-dependent screening of an external electric field at the chains.

Thickness dependence of the MAE and the spin polarization (SP) in Fe and Co multilayers on a Pt(001) substrate are investigated. As the thickness of thin films is increased, an oscillatory behavior of the MAE and SP of the systems is observed. Capping of Fe and Co multilayers with platinum results, in majority of cases, in a strong enhancement of the MAE. We give an explanation to the oscillatory behavior of the MAE – it is associated with the spin-polarized quantum well states (QWS). It is also shown that both the MAE and the spin polarization of the QWS are sensitive to external electric field and can be tailored therewith.

The magnetic states of atomic particles and thin films can be tuned by electric means via a variety of magneto-electric phenomena. We investigate the possibility to do so by controlling the density of the intrinsic charge carriers of these nanostructures. The interplay of injected surface charge with the magnetic anisotropy and the interlayer exchange coupling is investigated. Clear evidence is found that surface charging can reverse the easy axis of magnetization from in-plane to out-of plane. Additionally, it is revealed, for the first time, that switching of the interlayer exchange coupling of magnetic layers separated by a Cu spacer could be accomplished only by charge injection or removal.

Contents

Introduction	1
1 Understanding and tuning magnetism at the nanoscale	3
1.1 Magnetic properties of atomic structures	3
1.1.1 Magnetic adatoms on metal surface	3
1.1.2 One-dimensional atomic chains on metal surface	6
1.2 Quantum size effect in thin films	9
1.2.1 1-D quantum confinement	9
1.3 Tailoring magnetism by means of magneto-electric couplings	12
1.3.1 External electric field	13
1.3.2 Charging of metallic surfaces	15
Objectives of the study	17
2 Theoretical framework of the study	21
2.1 Density functional theory (DFT)	21
2.1.1 The exchange correlation functionals	22
2.1.2 Spin polarized systems	23
2.1.3 SOC and non-collinear magnetism	24
2.2 The plane wave pseudopotential method	26
2.3 The projector augmented wave (PAW) technique	28
2.4 Alteration of charge carriers in supercell approach	29
2.4.1 External electric field	29
2.4.2 Surface charging	31
2.5 Current approaches to calculate magnetic anisotropy energy (MAE)	32
2.5.1 Force theorem	32
2.5.2 Self consistent method	34
3 Magnetic properties of linear atomic chains on metal surfaces	37
3.1 Overview	37
3.2 Co and Co-Pt chains on Pt(111)	38
3.2.1 Monoatomic Co chains on Pt(111)	38
3.2.2 Atomic Co-Pt chain on Pt(111)	40
3.3 Co(Fe) chains on Pt(997) surface	43
3.4 The impact of electric fields on linear atomic chains	46

4	Tailoring magnetic properties of thin films with QWS	51
4.1	Quantum size effect and magnetic properties of thin films	51
4.2	Fe multilayers on Pt(001) surface	53
4.3	Capping $[\text{Fe}]_{\text{N}}/\text{Pt}(001)$ with a Pt-monolayer	57
4.4	Co multilayers on Pt(001) surface	60
4.5	Capping $[\text{Co}]_{\text{N}}/\text{Pt}(001)$ with Pt monolayer	61
4.6	Influence of non-magnetic capping layers	65
4.6.1	Pt overlayers on Co ultra-thin films	65
4.6.2	Pt(Cu) multilayers on Fe monolayer	69
4.7	Effect of electric field on magnetic thin films	70
4.7.1	Effect of electric field on Fe and Co monolayers Pt(001)	71
4.7.2	Effect of electric field on spin-dependent QWS	71
5	Surface charge tuning of MAE and interlayer exchange coupling	77
5.1	Surface charging of alloy multilayers	77
5.2	Surface charging and magnetic anisotropy	79
5.2.1	Fe(Co) monolayers capped with Pt	80
5.2.2	Fe bilayers capped with Pt	81
5.3	Switching of IEC by interface charging	86
5.3.1	Fe/ Cu_{N} /Fe	86
5.4	Summary	92
	References	95
	Publications (Veröffentlichungen)	106
	Curriculum	107

Introduction

Modern technology utilizes nano-magnets for a tremendous number of applications, and these systems have been the subject of intensive experimental and theoretical studies. One of the topics which attracts much attention in the field of nanoscience is the behavior of single domain nano-magnets, f.e. the influence of scaling down of the current micro-sized single magnetic domains to nano-sized ones [1]. This issue has been the standard motivation for most studies dealing with magnetic phenomena, either for scientific interest or engineering applications. For the realization of single-domain nano-magnets, it was suggested that magnetic nano-particles on metal surface are promising candidates [1, 2]. It seems that employing atomic-scale magnets is unavoidable in order to have significant reduction in the size of the magnetic data storage memory units. Besides, one should also find a way to minimize the mutual interaction between these units. Bottom line is: the future of data storage and processing is still considered to be in the utilization of the spin degree of freedom, a concept known as spintronics [1, 3] or spin-electronics [4]. Although, quite recently a new trend has emerged – magnonics [5], a new branch of solid state research, competing with spintronics for the right to achieve a breakthrough in energy efficient and fast data storage and processing.

Above all, the advancement of the research in the field of spintronics continues to provide new intriguing and fundamental realizations. The actual technological application have also been closely following the benchmark discoveries of scientific research. For example, in relation to device application an important breakthrough was made by P. Grünberg and A. Fert [6, 7] with the discovery of the giant magnetoresistance (GMR) which has quickly made its way into the read heads of modern hard disk drives [8]. The noteworthy fact is, however, that the write heads of magnetic storage devices, contrary to their read counterparts, are still using magnetic coils and fields to store information in the magnetization state of ferromagnetic bit domains and have been doing so since the earliest storage devices, such as magnetic tapes [8]. Albeit, the accessible size of one bit has shrunk by several orders of magnitude over time and novel methods, e.g. the heat-assisted magnetic recording (HAMR), [9] are continuously been developed and implemented. Nevertheless, this goes to show that sensing magnetism on the nanoscale is much easier than controlling it, and that the latter still leaves a lot of space for research.

The goal of this thesis is to understand and find novel possibilities to influence the magnetism of metallic nanostructures of different dimensionality on metallic surfaces. The main accent is made on the effects of electric field and surface charging, as two of the most promising tools for tailoring magnetism at the nanoscale. Three main properties define the magnetism of a nanoscale system: its spin moment, orbital moment and its magnetic anisotropy. The first two are intrinsic characteristics of the material/chemical elements used and are responsible for the extent of the magnetic effects in the system. Magnetic anisotropy energy is also a very important parameter in nano-magnetism since it is responsible for the stability and dynamics of the magnetic system [4].

The first chapter of the present thesis is devoted to summarizing the state of the art understanding of what parameters of the system define its magnetic properties. The influence of dimensionality and quantum size effects on magnetism shall be discussed in the first part of Chapter 1. The second part of that chapter shall be devoted to the mechanisms through which electric field and charging can affect chemical and physical properties of a nanoscale system.

Chapter 2 includes the theoretical frameworks that have been employed in the study. It begins with a general introduction of density functional theory (DFT) and the exchange correlation functionals. The representation of magnetic systems in the framework of non-collinear DFT is discussed in the next part of this chapter. Later on modern techniques of solving the Kohn-Sham equations will be discussed. The last part of this chapter deals with various ways of incorporating the effect of electric field or surface charging in supercell approaches. The overview on the two essential methods of calculating magnetic anisotropy will be covered at the end.

Dimensionality is one aspect of nanoscale magnets which strongly affects their magnetic properties, and in Chapter 3 this issue will be addressed by a thorough investigation of the magnetic properties of atomic chains on metal surfaces. First we will present the results about the inter-chain exchange coupling for different chemical composition of the atomic chain, then it will be followed by a discussion on the magnetic and orbital anisotropies of Co and Co-Pt chains on Pt(111). The next section is devoted to magnetic properties of atomic chains on Pt(997) surface. Lastly, the influence of electric field on magnetic anisotropy will be presented.

In Chapter 4 the relation between 1-D quantum well states in thin films with magnetic properties will be covered. The correlation between spin-dependent quantum well states and magnetic properties of Fe and Co thin films is presented, consequently. It is shown that the magnetic anisotropy has an oscillatory behavior as a function of Fe and Co layer thickness. The second part this chapter is dedicated to the strong impact of non-magnetic overlayers on magnetic properties of Fe(Co)-Pt(Cu) multilayers. A reorientation of magnetization from in-plane to out-of plane is observed as the thickness of a non-magnetic overlayer increases. Furthermore, the effect of external electric field on the quantum well states and thus on the magnetic anisotropy is discussed.

The last chapter deals with the recent achievements on the effect of surface charging on magnetic anisotropy and interlayer exchange coupling. We demonstrate that a modest amount of charge injection or removal in alloy multilayers can bring significant change to the magnetic anisotropy energy and inter-layer exchange coupling. Explicitly, for FePt ultra-thin films injection of negatively charged particles results in the reversal of easy axis of magnetization. Last but not least, it was revealed that the process of switching of the interlayer exchange coupling between Fe layers mediated by Cu layers could possibly be accomplished with interface charge doping.

Chapter 1

Understanding and tuning magnetism at the nanoscale

In this chapter an overview of magnetic properties of sub-nano-scale structures on metallic surfaces will be presented. Effects of dimensionality, chemical composition and quantum size effect shall be outlined. The fundamental developments and achievements regarding magnetic adatoms, chains and thin films on metal surfaces will be presented. Strong emphasis will be given to magnetic anisotropy energy and spin (orbital) magnetic orders. Finally, the latest developments and trends in tuning mechanisms of magnetization together with suitable examples will be provided. From various ways of exploiting magnetoelectric phenomena to induce changes in the magnetic properties of nanostructures, particular attention will be given to external electric field and charge injection or removal.

1.1 Magnetic properties of atomic structures

When dealing with magnetic nanostructures it is paramount to understand how their ferromagnetism differs from their bulk counterparts. De Heer *et al.* have illustrated the evolution of magnetic properties as the size and dimensionality of the system changes from bulk to nano-scale, as small as ~ 30 atoms [10]. The most important finding for our case was that the spin magnetic moment tends to increase for magnetic clusters (Fe, Co and Ni) as their size is reduced from bulk to the nano-scale. Interestingly, the values of the magnetic moments for the nano-clusters are close to the value of the magnetic moments from atomic based localized moment model. For instance the spin magnetic moment of nano-cluster of Fe (~ 50 atoms) is $3 \mu_B$, and the bulk spin magnetic moment is $2.2 \mu_B$ [10, 11]. The high value of the spin-magnetic moment for the nano-clusters is attributed to the localization of the $3d$ electrons as a result of reduced coordination number, since there are more surface atoms in reduced dimensions. In the coming sections we present an overview of magnetic adsorbates, adatoms and chains, on surfaces.

1.1.1 Magnetic adatoms on metal surface

Magnetic adatoms are the smallest magnetic entities that can be adsorbed on a metal surface, and these entities can possibly be the smallest permanent magnets if there is a way to manipulate their magnetization. Moreover, either for the fundamental research or engineering applications detailed understanding of the magnetic stability and excitations of

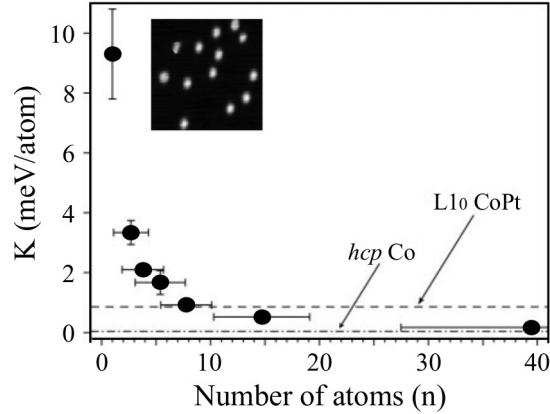


Figure 1.1: The magnetic anisotropy as a function of cluster size (in number of atoms) on Pt(111) surface. For the reason of comparison, the dashed and dashed-dotted lines show the MAE per Co atom of the $L1_0$ CoPt alloy and *hcp*-Co, respectively. STM image of isolated Co adatom on Pt(111) surface depicted on the inset. It has Co coverage of 0.01 ML and each side of the image is 85\AA [13].

finite size magnetic clusters is essential. The determining factor for the magnetic stability of nano structures or bulk is the magnetic anisotropy energy (MAE) and it is this property in nano-magnets that makes them so useful. Specifically, it describes the tendency of the spatial alignment of magnetic moments of the systems along specific directions instead of their random fluctuation. In order to realize the objective of decreasing the size of magnetic data storage units one has to increase the magnetic anisotropy per atom of the adsorbates. Numerous studies both experimental and theoretical have been conducted in order to achieve that goal [2, 12, 13, 14].

MAE arises from the spin-orbit coupling which connects the spin magnetization with the crystal field of the magnetic system [13], and high MAE is mandatory for the stability of magnetic systems against thermal fluctuations. It is common to use $3d$ elements with heavy metals (*e.g.* Pd, Pt, Rh) as substrate, in order to enhance the MAE of magnetic particles [13, 15, 12]. The electronic d -orbitals of these elements are partially filled and thus lie close to the Fermi energy. Using heavy elements as substrates alters the magnetic properties of the adsorbates via the mixing of orbitals. Furthermore, metals like Pt have high spin-orbit coupling and can induce stronger impact on the value of the MAE. However, one can also modify the MAE by varying the particle size and shape. Employing this combination of $3d$ elements with high spin-orbit coupling species, Gambardella *et al.* have studied structures as small as adatoms (Co) on a Pt(111) surface. They used X-ray Magnetic Circular Dichroism (XMCD), which is one of the various ways of probing atomic structures on a metal surfaces, to study the evolution of magnetization with cluster size. A microscope image of the sample is depicted in the inset of Fig. 1.1. The orbital anisotropy, orbital moment difference between easy and hard axes, and the MAE per atom is inversely proportional to the size of the Co clusters. As an illustration, the MAE versus the size of the Co clusters on Pt(111) surface is shown in Fig. 1.1. The most striking finding was the giant magnetic anisotropy of ~ 9 meV for Co adatoms on Pt(111). The easy axis hereby is oriented perpendicular to the surface [13, 12]. The spin and orbital magnetic moments of the Co adatom were found to be $2.1 \mu_B$ and $1.1 \mu_B$, respectively.

Apart from XMCD the magnetization of individual magnetic atoms on a metal surface

can be probed by using spin polarized scanning tunneling spectroscopy (SP-STS). Basically, in spin polarized scanning tunneling spectroscopy (SP-STS), differential conductance dI/dV of the sample-tip system is measured with a magnetic tip as a function of the bias voltage V applied between the sample and the tip. Under certain assumptions [16], this quantity provides information about the local density of states of the sample. If the mutual magnetization orientations of the tip and sample can be varied, (*e.g.* with an external magnetic field), the local energy-resolved polarization of the sample can be assessed by taking the dI/dV asymmetry as a measure [15, 17]. In this manner also magnetization curves of single adatoms as a function of the externally applied magnetic field can be plotted. Evaluating the remanence and switching field of these hysteresis curves, Wiesendanger *et al.* have been able to study magnetic nano-structures which have been investigated previously by XMCD, Co adatoms on Pt(111) surface [17, 15]. In Fig. 1.2(A) the STM topographic images of nano-clusters ranging from single adatom to monolayer of Co are depicted. The magnetization curves of single Co adatoms on *fcc* and *hcp* sites of a Pt(111) substrate are presented in Fig. 1.2(B). In this figure the spin-resolved differential tunneling conductance signal above single Co adatoms as a function of the externally applied magnetic field is shown, from which the magnetic moment of the Co adatoms can be extracted. The variations of the extracted magnetic moments are not caused by the differences in the adsorption site but in the spatially inhomogeneous polarization of the Pt substrate induced from the random distributed Co adatoms [17, 18].

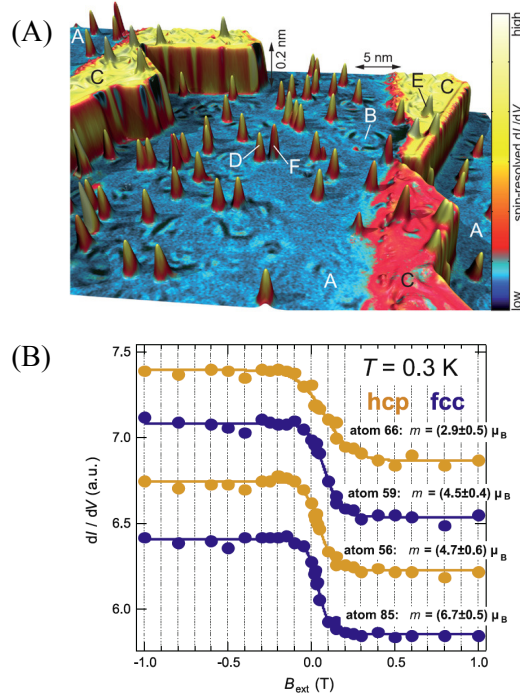


Figure 1.2: [A] The three dimensional overview of the STM topography of Co adsorbed on Pt surface with spin resolved dI/dV map. The sample is composed of Pt(111) terrace (A), Co monolayer stripes (C) attached to the step edge, Co adatoms (D and E) and Co dimers (F) [15]. [B] Experimentally measured magnetization curves for single Co adatoms on *fcc* and *hcp* sites of a Pt(111) substrate at a temperature of 0.3 K. From the spin-resolved differential tunneling conductance signal above single Co adatoms as a function of the externally applied magnetic field, the magnetic moment of the Co adatoms can be extracted [18, 17].

STM combined with inelastic electron tunneling spectroscopy is yet another experimental technique which can probe magnetic properties of adsorbates, *e.g.* the spin excitation spectra of individual adatoms on surfaces. Unlike in the case of elastic tunneling, inelastic tunneling process is based on the energy transferred between the tunneling electron and the sample. The latter can only take place if the energy of the electron is transferred to an excitation of the sample. If the bias is applied between the tip and the sample, electrons can tunnel transferring their energy to all the excitations with energies (E_i) equal or less than the electron energy defined by the bias voltage V . This energy exchange between the tunneling electron and an excitation/deexcitation in the sample contributes to the tunneling current and is often called an "inelastic conduction channel" [19]. In practice the bias voltage is gradually increased, and as it exceeded the energy of the next excitation, a jump in the conductance is observed [19, 20]. Knowing the excitation spectra of the samples one can fit them to a certain model to extract the physical properties of interest, *e.g.* the magnetic moments and anisotropies. Heinrich *et al.* have used this technique in order to investigate the spin excitation spectra of individual Mn atoms adsorbed on a Al_2O_3 surface [19]. Explicitly, they have exploited the dependence of magnetic excitation on the external magnetic field, showing that the external magnetic field and the threshold voltage are proportional. In this study it was revealed that the spin excitation of Mn atoms is sensitive to the adsorption sites of the substrate [19]. In addition to the magnetic adatoms, dimers and trimers of Fe and Co have been studied with inelastic tunneling spectroscopy, and the magnetic anisotropy of Fe adatoms on Pt(111) surface was found to be 6.5 meV. The very high perpendicular MAE of Co adatom was also affirmed in this study. The reduced MAE of Fe adatoms as compared to Co is associated with smaller hybridization of Fe with Pt substrate. The magnetic anisotropy of dimers and trimers of Co and Fe have comparable MAE of 5 meV per atom [21].

As we see, individual magnetic adatoms on surfaces exhibit exceptional magnetic properties, such as increased magnetic moment and, most importantly, high anisotropies. Let us now see, how these properties depend on the dimensionality of the system, going from single adatoms (0-D) to one-dimensional (1-D) atomic chains on metal substrate, and from there to monolayers (1-D,2-D) and to the bulk (3-D).

1.1.2 One-dimensional atomic chains on metal surface

Experimentally, there are two ways of creating one-dimensional atomic chains or nanoclusters on metal surfaces, either by means of STM manipulation [22, 23, 24] or using atomic self assembly [2, 25, 14, 26]. The former employs the exceptional ability of the STM to manipulate single atoms on surface one by one. For instance linear atomic chains of Au (1-20 atoms) on NiAl(110) surface were constructed and the electronic properties were derived from scanning tunneling spectroscopy by Niluis *et al.* [22]. Similarly, one can organize Co-Cu chains of various length and composition on Cu(111) surface, by using low temperature STM. On the other hand, Kern *et al.* have shown the other way of constructing 1D nanostructures on metal surfaces, the diffusion controlled aggregation [25]. This method makes uses of the dependence of the mobility of the atoms on the surface and the temperature. Almost a decade later Gambardella *et al.* constructed long uniform monatomic chains of Co on vicinal surfaces of Pt(997) substrate by atomic self assembly. An STM images of these Co chains on Pt(997) surface is shown in Fig 1.3(a). The magnetism of these Co wires was also studied by using XMCD in which the spin magnetic moment per Co atom is enhanced from $1.57 \mu_B$ (bulk value) to $2.08 \mu_B$ (in chains). Such enhancement is attributed to the narrow minority

d -bands of Co atoms in the chain as result of localized electronic structure which leads to high density of states near the Fermi energy. A rather large MAE of 2 meV has also been observed, which is an important prerequisite for the long range magnetic order [27]. Indeed, in absence of additional stabilizing factors, such as MAE, “one or two dimensional isotropic spin- S Heisenberg model with finite-range exchange interaction can be neither ferromagnetic nor antiferromagnetic” as was proven by Mermin and Wagner [28]. With the additional stability of spins provided by the magnetic anisotropy long range ferromagnetic order has been achieved for one dimensional single domain particles. The stable long range magnetic order is, however, not an absolute property and is dependent on the experimental measuring time and the temperature. This means that below a certain temperature known as blocking temperature, these atomic sized particles could be able to maintain ferromagnetic order for a longer time than the experimental time of observation. Thus, below certain blocking temperature long range ferromagnetism could be maintained and probed [27, 29].

Fig 1.3 shows the magnetization of monoatomic Co wires as function of the magnetic field at (a) 45 K and (b) 10 K. The zero remnant magnetization (M) at $B = 0$ reveals the absence of long-range ferromagnetic order. But, at temperature lower than the blocking temperature of the Co wires ($T=10$ K) the shape of the magnetization curve indicates the presence of long range magnetic order, and therefore of significant inter-atomic exchange coupling in the chains [13, 27].

Another important feature of 1-D nanostructures is the quantum size effect present therein [27, 30, 24], *i.e.* the magnetic properties of these structures strongly depend on their size. For instance, mono-atomic Cu chains on Cu(111) surface exhibit one dimensional quantum confinement in which the confined states are mainly unoccupied. The underlying phenomena is general for atomic chains supported by a substrate characterized by pseudo band gap in the projected band structure [30].

The transition from 1-D systems to 2-D like systems of both Co and Fe atomic chains was also studied experimentally [27, 14]. Finite Fe chains on Pt(997) have been studied in the form of sub-monolayers adsorbates [14, 11]. From the magnetization measurements it was found that the easy axis of finite Fe chains (0.1 ML) points along in-plane direction [14]. Interesting results were found by increasing the iron coverage from 0.1 to 0.2 ML where the average magnetization decreases by more than a factor of 4. This phenomena was associated with the coordination-dependent competition of ferromagnetic FM and antiferromagnetic AFM exchange coupling of Fe atoms.

Moreover, by increasing the lateral width of Co chain an interesting variation of the magnetic properties was shown [27]. For example, the easy axis of magnetization, MAE, and coercive field have shown an oscillatory behavior with respect to the width of the wire. In Fig. 1.4 the coercive field of as function of the width of the wire is presented, as an illustration.

The transition from monolayer structures to multilayers is accompanied by much the same effects as the chain to monolayer transition. Here as well, the quantum size effects are known to play a dominant role in determining the magnetic properties of nanostructures [31, 32].

As we see, quantum size effects are responsible for some of the most interesting features of atomic scale magnets with respect to their dependence on the dimension and size. In the next section we will further elaborate the concept of quantum size effect and its impact on magnetic properties of nanostructures, particularly thin films.

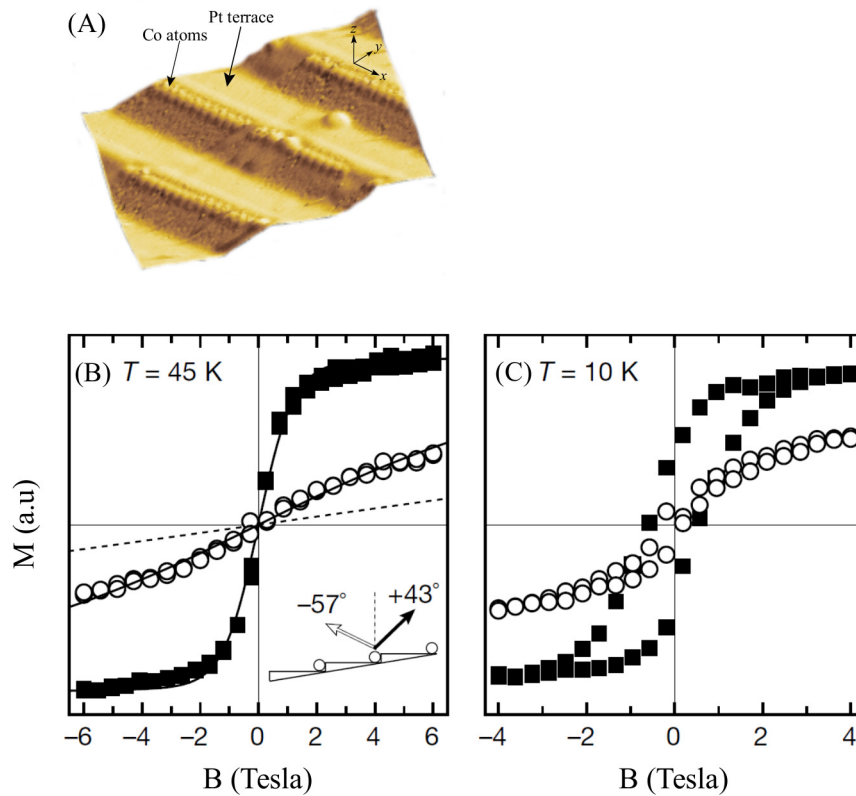


Figure 1.3: (A) The scanning tunneling microscopy (STM) images of linear Co monatomic wires on Pt(997). The vertical dimension is enhanced for better contrast, and the chains are linearly aligned and have a spacing equal to the terrace width. (B) Magnetization as a function of the applied field at $T = 45$ K and (C) $T = 10$ K measured along the easy direction (squares) and at 80 degree away from the easy direction (circles) in-plane perpendicular to the wire axis [13].

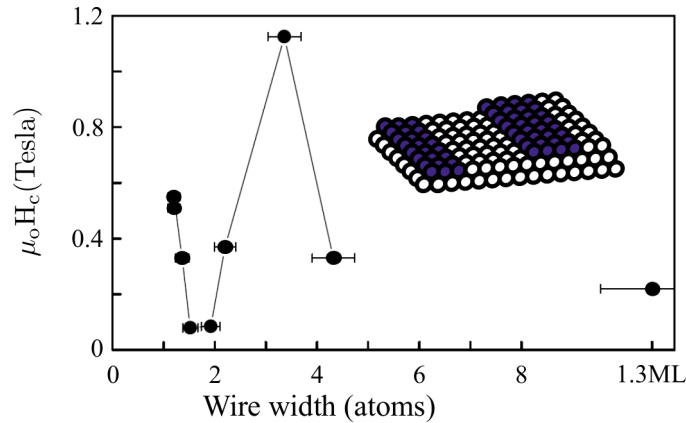


Figure 1.4: The behavior of the coercive field (H_c) as function of the width of the wire (number of atoms), which shows strong oscillatory behavior. The values of H_c were measured at 10 K, and for the case of 1.3 ML H_c was measured at $T = 45$. [2].

1.2 Quantum size effect in thin films

Quantum confinement in thin films is an active field of research since there is room for utilization of thin films for practical applications in electronic devices along with basic scientific interest. When such systems are reduced to the nanoscale range or when the thickness of the film is comparable with the de Broglie wavelength of electron quantum size effect (QSE) will be important. In addition, quantum confinement of electrons at the nanoscale leads to the formation of discrete energy levels, quantum well states (QWS) [33, 34]. Hence, small variation in the size of such systems will modify their electronic structure.

1.2.1 1-D quantum confinement

The simplest case used to describe quantum confinement is the model for free electron in a 1D box, bound by an infinite potential barrier. The quantum well state of wave vector k should satisfy the condition of integer number of half-waves fitting into the width of the quantum well ($k = n\pi/d$), where n is an integer quantum number and d is the width of the well. The respective energy levels are given by [35],

$$E = \frac{\hbar^2}{2m} \left(\frac{n\pi}{d} \right)^2. \quad (1.2.1)$$

In realistic nanostructures the existence of QWS requires two main conditions to be fulfilled: the system should contain delocalized electrons available for confinement and it should have a confining (bounding) potential. As an example, in semiconductor systems the intrinsic fundamental band gap of one semiconductor can act as a confinement for the electrons occupying the dispersive bands of the other semiconductor. Similarly, in metals delocalized shared electrons can be confined by metal-vacuum, metal-insulator or metal-metal interfaces (the latter requires the metals to be chemically different). In any case, the potential landscape of real systems in which the electrons are confined is much more complex than a simple infinite potential well. In Fig. 1.5 a sketch of a 1-D confinement in a metallic overlayer is presented. The “floor” of the potential well is “paved” by coulomb potentials of single atoms. The walls of the well are the vacuum repulsive potential and the chemical

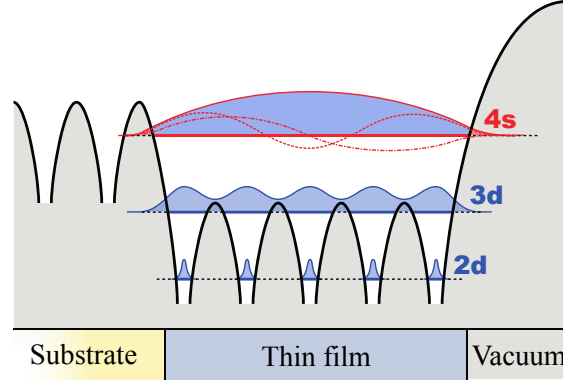


Figure 1.5: A schematic representation of the potential landscape of thin films (*e.g.* Fe) on a solid substrate, and the orbital spectrum from low lying states ($2d$) to high lying states ($4s$). Normally, the s -states which are highly delocalized are expected to be confined but the d -orbital can also form QWS.

potential mismatch at the substrate-overlayer interface [35, 36, 34]. Depending on the energy of the electrons the confinement shall have a different character, as shall be discussed shortly.

The band dispersion $E(k)$ for real solid thin films is different from the one for free electrons (Eq. 1.2.1), since the confining potentials in thin films are finite and have different shape. Additionally, the low level components of the confined electrons ($3d$) are affected by the corrugation of the potential, periodically modulated potential of the thin film (see Fig. 1.5). Confinement of higher-energy electrons in thin films can be illustrated from the band energy perspective by Bohr-Sommerfeld quantization conditions [37],

$$\phi_s(E) + \phi_v(E) + 2kd = 2\pi n, \quad (1.2.2)$$

where ϕ_s and ϕ_v are the scattering phase shifts at the substrate-film and film-vacuum interfaces, respectively, and k is the wave number of the envelope function of a Bloch state perpendicular to the surface plane of the film with thickness d . The phase shift of the confined states at the interface with the substrate (ϕ_s) is a function of the thin film band mismatch with the substrate,[38] and ϕ_v depends on the vacuum energy level, which is deduced from the Fermi energy and work function of the thin film. In fact, many properties of nano-sized thin films, *e.g.* magnetic anisotropy, surface reactivity, superconductivity, are directly affected by QWS [31, 39, 40].

Commonly 1-D quantum confinement in thin films is associated with sp -like states, since these states are highly delocalized or have smaller effective masses (Fig. 1.5) [41, 42]. Experimental observation of 1-D confinement in Ag thin films on Fe surface was associated with nearly free like sp electrons [42]. However, sometimes the d -band energies are high enough for the d -electrons to be (at least partially) delocalized (see Fig. 1.5). Chaing *et al.* were able to observe such d -confinement in Ag thin films [43]. This addressed the issue that metallic thin films can also host d -electrons which are slightly less localized and have dispersive bands, similar to sp -bands [43, 42, 31, 44]. Still, the influence of d -QWS is only limited to ~ 25 ML while it is four times larger for the case of sp -QWS.

Recently, Yoshimatsu *et al.* have shown quantum well state of d -character in a strongly correlated oxide using angle resolved photoemission spectroscopy (ARPES) [45]. Artificial thin film of SrVO_3 were deposited on Nb doped SrTiO_3 (STO) substrate, with thickness varying layer by layer. The $3d$ states of V which are located close to the Fermi energy were

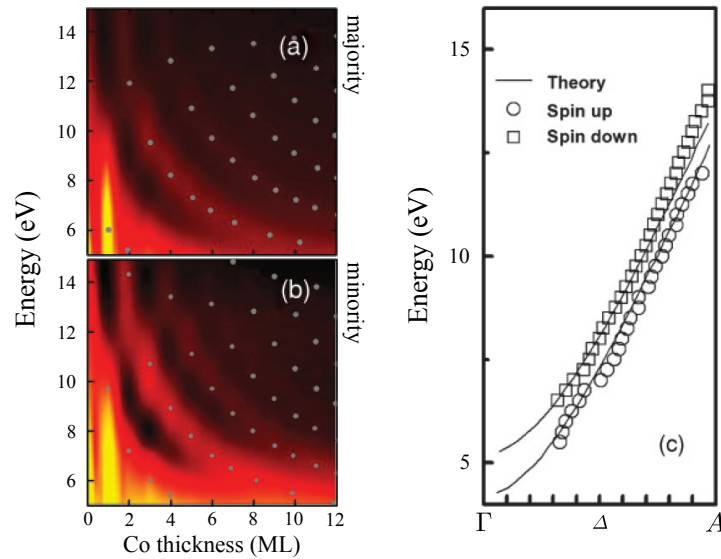


Figure 1.6: Electron reflectivity for (a) spin-down electrons and (b) spin-up electrons shows layer resolved quantum well states. (c) Spin-split energy bands retrieved from the spin-polarized quantum well states [32].

found to undergo confinement by the two interfaces with the substrate and the vacuum.

Above we have stated the condition that have to be fulfilled for thin films to exhibit quantum confinement. These conditions assume the existence of having delocalized electrons and bounding potentials. If either the intrinsic band structure or the confining potential are spin-polarized, the QWS will also acquire a spin-dependent character, which is important to remember for evaluating spin-sensitive parameters of the system [31].

Przybylski *et al.* have revealed an oscillatory uniaxial magnetic anisotropy of magnetic thin films as function of the thickness [31]. The period of oscillation was in the order of few monolayers and such variation of the magnetic anisotropy was associated with the quantum confinement of *d*-electrons. Basically, the discrete electronic states or QWS of the delocalized electrons can depend on the spin symmetry, and it is caused by either by spin-polarized electronic structure or bounding potential. A good examples for the former case are the oscillatory MAE [31] and the inverse photoemission study of Fe layers on Au(001) substrate where signatures of the spin-dependent QWS were observed [46, 47].

Furthermore, using spin polarized low energy electron microscope a spin dependent electron reflectivity was investigated on epitaxially grown Co films by Park *et al.* [32] Here it should be stressed that the spin polarization alternates its sign upon variation of the thickness of the film and the electron energy, which is attributed to the spin-dependent quantum well states of the film. In Fig. 1.6(a) and (b) the QWSs of the spin up and spin down electrons are shown, and one can see the occurrence of QWS every integer multiple of Co layers. The well resolved spin-split band dispersion of majority and minority bands in comparison with *ab-initio* calculations (referred therein) is presented [32].

An example of spin-dependent QWS being caused by spin-polarized boundary condition can be found in metallic films like Cu or Ag attached to magnetic substrates [46, 48]. Spin polarized photoemission study of Garison *et al.* indicated that the QWS in Cu thin films supported by Co(001) substrate are strongly spin-polarized and has mostly minority spin character [41, 48]. The QWSs have character of *sp* orbitals and *d* orbitals which are

hybridized with each other, influencing the coupling between layers.

The spatial variation of the local density of states which is the result of quantum confinement, can have a profound effect on the local magnetic properties of the system. Oka *et al.* have shown the spin-dependent quantum confinement can be the determining force for the local spin-polarization of electrons confined to a triangular Co nano-island grown on a Cu(111) surface [49].

In the following section the idea of controlling magnetization of nano-scale magnets with electric field and surface charging is presented.

1.3 Tailoring magnetism by means of magneto-electric couplings

Up to now various aspects of nano-adsorbates on metal surface were discussed. From these studies one can infer that atomic scale magnets seem to be the most promising candidates for future applications. However, local controlling mechanism of these entities is one big problem, which still waits for more efficient solutions. Even though magnetic field is doubtlessly the most common tool for controlling magnetism, it has some drawbacks. For instance, it has inherently non-local character and consumes much energy. In this aspect active research of recent years has yielded quite a few alternative possibilities to control magnetic entities. One possible option is the use of electron spin both as a carrier of information and as a switching tool. This concept is the basis for modern spin-transfer torque [50, 51] based devices [52, 53]. But, the critical current density required for the switching mechanism by usual spin-transfer torque method remains significantly high [54].

The alternative mechanism that has already been suggested for controlling magnetic order is to utilize the coupling between electric and magnetic properties of a material, *i.e.* magnetoelectric effect [55, 56]. There are two mainstream approaches to exploit this phenomena, the first one is based on multiferroics, multifunctional materials, where the coupling between the magnetic properties and the external electric field (EF) is provided by the change of the structure due to the field induced-polarization [57, 58, 59, 60].

Multiferroics that are of interest to us, are the ones exhibiting magnetoelectric-coupling. It was shown that magneto electric coupling can be used to control magnetic ordering and domains [61, 62, 63, 64], as well as anisotropy, coercivity and magnetic hysteretic behavior [64, 65]. Other studies have shown that electric field can induce a change in the direction of anisotropy in a ferromagnet, coupled to a multiferroic [66].

Another way to couple the electric field and magnetic properties is implemented in magnetic semiconductors with carrier-mediated magnetic interaction. A strong magneto-electric effect can be observed in materials, where magnetic properties are predominantly governed by charge (electron or hole) carrier concentration [53, 67, 68, 69, 70, 54, 60]. Here the motive is to manipulate one of the degrees of freedom of an electron which is its charge. The applied field alters the concentration of carriers, thus varying the magnetic interaction and, consequently, the magnetic order. As an example, Ohno *et al.* succeeded in controlling ferromagnetism in a thin-film semiconductor alloy, where ferromagnetic exchange couplings between localized magnetic moments are mediated by valence-band holes [68]. The EF modifies the concentration of charge carriers, thus allowing one to tune the transition temperature of the hole-mediated ferromagnetic state. Here the carrier concentration is controlled by the field effect in a semiconductor-insulator-metal system. The gate voltage controls the concentration

of holes mediating the interaction between Mn dopants.

Unfortunately, both the latter and the ferroelectrics approaches have a major drawback: the critical temperature, at which thermal fluctuations destroy magnetic order, is too low for most semiconductors and multiferroics [67]. Only very recently a magnetic semiconductor, which allows to switch its magnetic state from the paramagnetic to the ferromagnetic one at room temperature by means of the gate voltage, has been introduced [71].

1.3.1 External electric field

In this thesis we will focus on more transparent magneto-electric coupling mechanism, relying on varying the magnetic properties of nano-sized systems by altering their intrinsic charge carriers. Let us first discuss the emergent physics that we expect to find when a metallic surface is exposed to electric field or additional charge, and each mechanism will be followed by an illustrative example.

When a surface of a metal is exposed to external EF the conduction electrons at the surface find themselves in a non-flat electrostatic potential, dashed line in Fig 1.7, and strive to screen the field and occurrence of charge density redistribution (filled curves, Fig 1.7). In the case of a magnetic surface, electrons of different spin character experience a different degree of redistribution, a phenomenon termed spin-dependent screening [72, 73, 74] (the two differently filled curves in the lower panel of Fig 1.7 (b) are shown to illustrate that). Both spin-dependent and paramagnetic screening obviously change the concentration of charge carriers at the surface, and thus affecting both structure and magnetism on the surface of the adsorbates and the processes thereon.

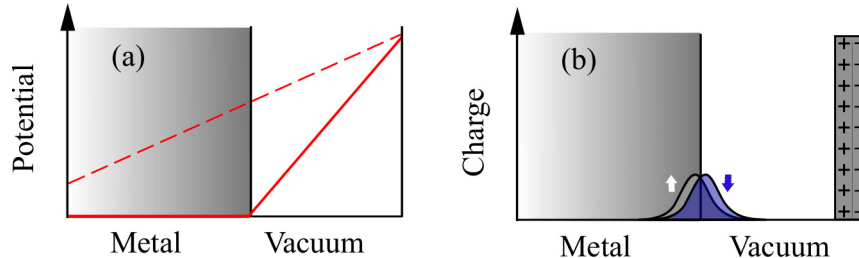


Figure 1.7: A model of the effect of the external electric field as result of the (a) potential landscape and consequently the (b) charge redistribution. The two charge density plots illustrate spin-dependent screening, *i.e.* electrons of different spin character show a different response to the external field.

As an illustration, metallic Pd thin films were shown to exhibit electric field-induced ferromagnetism [75]. The mechanism is related to the material-dependent Stoner instability [76]. The charge redistribution induced by the EEF changes the occupation of the Fermi level thus toppling the delicate balance and inducing ferromagnetism, a change which is equally profound and hard to control precisely.

Application of a constant external electric field (EEF) to ferromagnetic systems varies the charge concentration which leads to a more stable change in magnetic moment and anisotropy of the sample. Theoretical studies have shown that this scenario is realistic for metallic slabs. Duan and coworkers [77] have predicted, that ferromagnetic Fe, Ni and Co exhibit magneto-electric effects in presence of EF. The reason is indeed the spin-dependent screening of Fig. 1.8 (a) shows calculated redistribution of majority (solid line) and minority

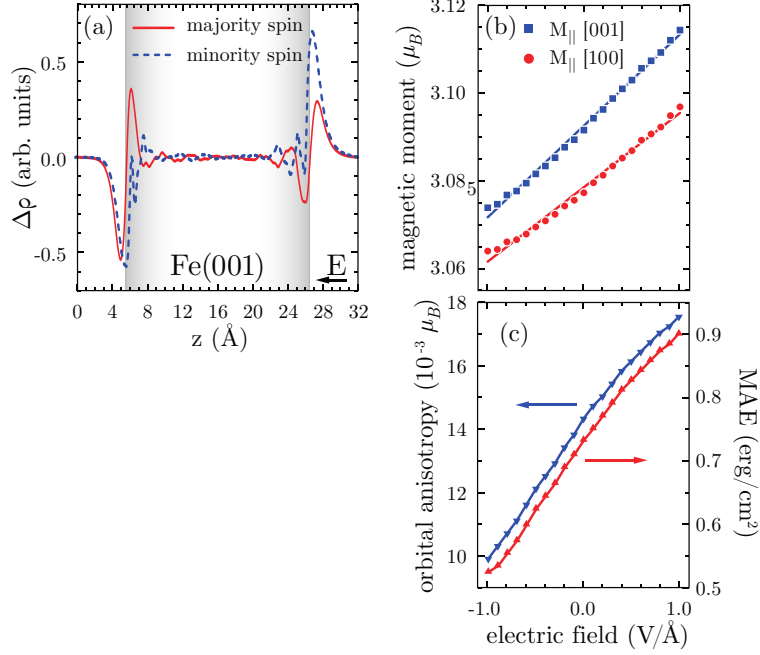


Figure 1.8: (a) Charge density redistribution induced by EEF in a 21 Å thick Fe film for majority- (solid line) and minority- (dashed line) spin electrons. The applied external electric field is $1.0 \text{ V}/\text{\AA}$, pointing from right to left. (b) Total magnetic moments on the (001) Fe surface as a function of applied electric field for the magnetic moment lying in the plane of the film (along the [100] direction) and perpendicular to the plane (along the [001] direction). The solid lines are a linear fit to the calculated data. (c) Electric-field-induced changes in calculated orbital moment anisotropy in units of 10^{-3} of the surface Fe atom and surface magneto-crystalline anisotropy energy (MAE) for 15 ML thick Fe(001) slab [77].

(dashed) spin electrons in a Fe(001) slab under the influence of an external potential gradient. The spin-dependence of the process is obvious. As a result, the electron or hole accumulation depends on the spin channels, thus changing not only the occupation at and around the Fermi level, but, as a consequence, also changing the balance of majority and minority electrons. This leads, as a direct consequence, to a change of the magnetic moment of the interface atoms. Fig. 1.8 (b) shows the dependence of the magnetic moment of the interface atoms of the slab featuring in Fig. 1.8(a) on the applied EEF. A near-linear trend can be clearly observed. Not only the magnetic moment show a response to EEF, but also the orbital moment anisotropy [77, 78] and the magnetic anisotropy energy [see Fig. 1.8 (c)].

The effect of electric field is not restricted only to coexistence of magnetic layers but it can also influence the interlayer exchange coupling. For example, electric field has significant contribution in the process of switching of magnetization. Wang *et al.* revealed that electric field can possibly assist the reversible switching of magnetic tunneling junction (MTJ) which has perpendicular interfacial magnetic anisotropy [54].

The fields considered in this work are quite realistic. However, the change in the magnetic moment and magnetic anisotropy are not quite enough to use that particular system in technological solutions. One possible way to enhance the effect of the EEF is to use electrolyte to additionally charge the surface by EEF [69, 79]. This possibility shall be discussed in more detail in a later section.

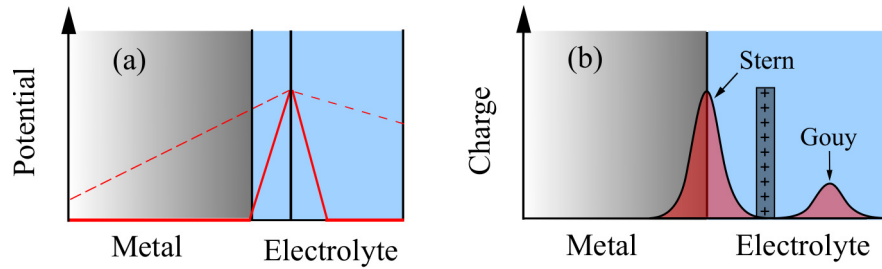


Figure 1.9: A model of the effect of the surface charging by an electrolyte. The (a) potential and the (b) charge re-distribution of the slab and the electrolyte when an external potential is applied are shown. The accumulation of negative charges is shown at the metal-electrolyte interfaces.

1.3.2 Charging of metallic surfaces

In a purely metallic system, as we have seen in the previous section, the charge is provided by the metal itself in the attempt to screen the EEF. However, the charge density redistribution obtained in that manner is relatively moderate. One way to provide additional charge is to add to the surface a layer of an ionic liquid [80] or electrolyte [69].

To create a perturbation in the electrostatic potential of the surface an EEF is not the only option. If a surface comes in contact with an electrolyte solution or ionic liquid (Fig 1.9), the so called electric double layer (EDL) is created due to the adsorption of electrolyte ions directly at the interface (Stern layer) and the consequent screening of that charge by the opposite charge carriers in the electrolyte (Gouy layer). The Gouy layer screens the Stern layer on the side of the liquid solution. Free electrons of the metal surface remain exposed to the Coulomb forces from the Stern layer. Since the ions are adsorbed directly at the interface, this is analogous to the surface being exposed to an extremely strong electric field (see the respective plots in Fig 1.9 and Fig 1.7) [69]. In addition to intense charge redistribution, the electrolyte solution has a direct chemical influence on all processes at the surface. Both the chemical action and screening can strongly affect magnetism of adsorbates on or in the surface [69, 81]. However, inside the surface the effect of the electrolyte might be considered analogous to the application of a strong electric field, *i.e.* of purely electronic character. Finally, since the EDL can be controlled by an external bias [69], the use of electrolytes can be seen as an enhancement of the EEF application.

Weisheit *et al.* have shown [69], that immersing a highly magnetically anisotropic Fe/Pt or Fe/Pd layer in electrolyte (see Fig. 10 for a sketch of the experiment) and applying a bias across such junction one can reversibly modify the MAE of the system, as is indicated by the change in the coercivity of the sample and the Kerr rotation angle [Fig. 1.11(a,b)]. The electric double layer (EDL) formed at the interface in that case acted as a donor of charge carriers (electron or holes) thus enhancing the bare EEF screening of the metal.

The experiment has been done on Pt and Pd based systems, in each case with two different thicknesses of the FePt or FePd films. The results presented in Fig. 1.11(a) show that thin layers are more susceptible to the carried density change. This makes sense if one considers that the charge density redistribution and the associated anisotropy change are concentrated at the interface, leaving the bulk of the system unchanged. In the case of thinner slabs the interface anisotropy dominates the system, allowing for more drastic changes of MAE at the same bias voltages or electric field strengths.

A similar effect has been observed on ultra thin Co layers by Shimamura *et al.* [80]

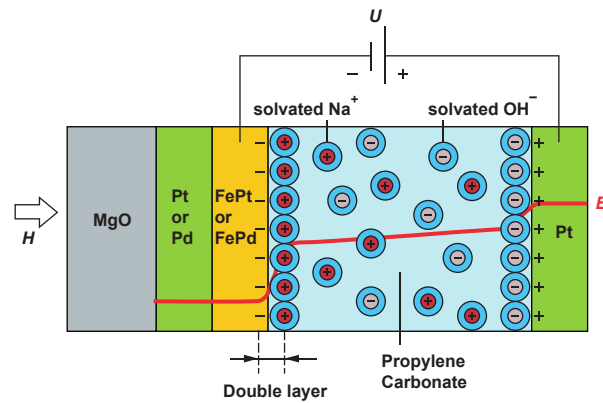


Figure 1.10: Schematic of the electrolytic cell containing the FePt or FePd film within an applied magnetic field. The potential profile E due to the applied potential U is indicated by the red line. The potential drop at the Pt electrode side is much lower (as compared to that of the sample surface) as a result of the Pt electrodes large surface area [69].

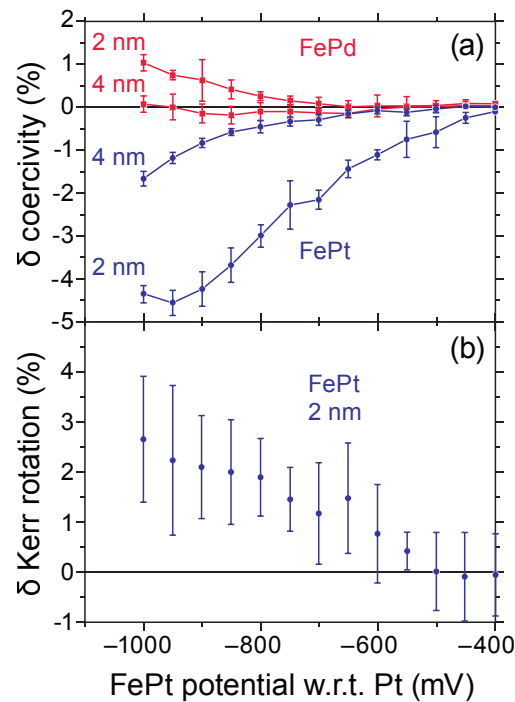


Figure 1.11: (a) Change of the film coercivity for FePt and FePd with external voltage at given thicknesses and (b) change of the Kerr rotation for the 2-nm-thick FePt film with respect to (w.r.t.) the value at -400 mV. Error bars indicate the statistical variation (σ) of the measurements [69].

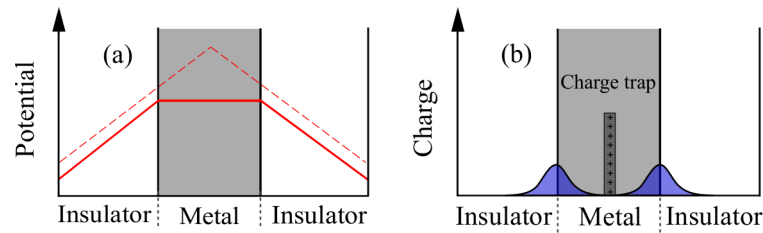


Figure 1.12: A model of the effect of the surface charging by an electrolyte. The (a) potential and the (b) charge re-distribution of the slab and the electrolyte when an external potential is applied are shown. The accumulation of negative charges is depicted at the metal-insulator interfaces.

The impact of the electric field was enhanced by coating the Co layer with a polymer film containing an ionic liquid. Applying just a small bias (not exceeding 2 V) to the sample at room temperature, Shimamura *et al.* has opened the magnetic hysteresis loop for the ultra thin Co film reenabling the magnetic anisotropy [80].

Apart from the use of EEF and electrolytes, there is also a promising option of charging the surface directly. If the surface slab is electrically decoupled from the substrate, *e.g.* by an insulating spacer (Fig 1.12, the charge, that is added to the surface slab shall remain trapped in the latter, effectively doping it with electrons or holes. Considering the Coulomb repulsion, the charge is expected to diffuse toward the interfaces of the metallic slab, forming an electron or hole excess cushion (Fig 1.12) which shall inevitably affect magnetic and electronic properties of the surface in a similar way as EEF or EDL does [82].

Objectives of the study

Experimental and theoretical studies covered in the first chapter have played a crucial role in the formation of the modern understanding of nanoscale systems. In this thesis, basing our arguments on *ab initio* techniques, we will further explore some novel fundamental aspects of magnetic nanostructures.

Keeping in mind the paramount goal of extending the scope of possibilities to tune magnetic properties of nanostructures we will concentrate on the following fundamental interrelations and mechanisms:

- dependence of magnetic anisotropy of linear metal-surface-supported chains on their geometry, relaxation and chemical composition
- magnetic properties of alloyed chains at vicinal stepped surfaces
- effect of electric field on magnetic moment and magnetic anisotropy of monatomic chains on metallic surfaces
- spin-polarized quantum well states (QWS) in alloyed metallic multilayers
- tailoring magnetic anisotropy by non-magnetic overlayers
- tuning and switching magnetic anisotropy with QWS and applied external electric fields
- controlling magnetic moments, anisotropy and interlayer exchange coupling in 1D systems with surface charging

Chapter 2

Theoretical framework of the study

This chapter covers the descriptions of the theoretical background of the methods that have been used for the exploration of various properties of the systems of interest. We will show the build up from concepts of the density functional theory (DFT) to a compact form of different formalisms that can properly describe non-collinear magnetism in density functional theory. The projector augmented wave technique (PAW) is also discussed. Finally, different ways of incorporating electric field and charging surfaces in the supercell approach will be presented.

2.1 Density functional theory (DFT)

The break-through work in many-body theory by Hohenberg and Kohn in 1964 gave birth to density functional theory (DFT) and its further developments [83]. In many body problem other than dealing with complicated many-body wave function, they propose to work with a function $n(\mathbf{r})$ which predicts the ground state energy. The DFT relies on the Hohenberg and Kohn theorems which state about the possibility of describing many body system with single particle electron density.[83, 84, 85]

Theorem 1 *For non-degenerate ground state ψ , the external potential $v(r)$ is uniquely determined by the density distribution $n(r)$.*

The theorem was formulated for non-degenerate ground state in scalar non-relativistic potential, one component and spinless particles, but later on these restriction were avoided and it was re-stated for general case.

Theorem 2 *For a given $v(r)$, the correct $n(r)$ minimizes the non-degenerate ground state energy, which is unique functional of $n(r)$*

In terms of the ground state charge density the quantity $E[n(\mathbf{r})]$ can be expressed as

$$E[n(\mathbf{r})] = F[n(\mathbf{r})] + \int V_{ext}(\mathbf{r})n(\mathbf{r})d\mathbf{r}, \quad (2.1.1)$$

where $V_{ext}(\mathbf{r})$ and $n(\mathbf{r})$ represent the electrostatic potential and charge density of the system. Whereas, $F[n(\mathbf{r})]$, known as the free energy functional, includes the kinetic energy,

classical Coulomb interaction of electrons and the exchange-correlation term. Even though the formalism is exact, in principle, the functional $F[n(\mathbf{r})]$, which doesn't depend on the system was not exactly described. Later on Kohn and Sham introduced a scheme to obtain the non-magnetic ground state energy of a system, by solving the non-interacting ground state charge density one-electron density [86],

$$n(\mathbf{r}) = \sum_i^N |\psi_i(\mathbf{r})|^2. \quad (2.1.2)$$

In addition, the $F[n(\mathbf{r})]$ functional is divided into three parts

$$F[n(\mathbf{r})] = T_s[n(\mathbf{r})] + E_H[n(\mathbf{r})] + E_{xc}[n(\mathbf{r})], \quad (2.1.3)$$

where $T_s[n(\mathbf{r})]$, $E_H[n(\mathbf{r})]$ and $E_{xc}[n(\mathbf{r})]$ are the kinetic energy, Hartree and exchange-correlation terms. The Hartree term is the classical Coulomb interaction of the ground state charge density, whereas $F[n(\mathbf{r})]$ is written as

$$F[n(\mathbf{r})] = \frac{\epsilon^2}{2} \int \int \frac{n(\mathbf{r})n(\mathbf{r}')}{|\mathbf{r} - \mathbf{r}'|} d\mathbf{r} d\mathbf{r}' + \frac{\hbar^2}{2m} \sum_{n=1}^N \int \psi_n^* \nabla^2 \psi_n d\mathbf{r} + E_{xc}[n(\mathbf{r})]. \quad (2.1.4)$$

2.1.1 The exchange correlation functionals

The exchange-correlation functional ($E_{xc}[n(\mathbf{r})]$) holds small part of the total energy, but most of the information about the complexity of electron-electron interaction is contained therein. However, the exact analytical description the exchange-correlation functional ($E_{xc}[n(\mathbf{r})]$) is not known. Hence, the delicate step in the DFT is describing the exchange correlation functional with proper approximation. Then the search for the ground state energy can be done by minimizing the electronic density, and this will lead us to the so called Kohn-Sham scheme [86],

$$H_{KS}\psi_i(\mathbf{r}) = \left[-\frac{\hbar^2}{2m} \frac{\partial^2}{\partial \mathbf{r}^2} + V_{KS}(\mathbf{r})\right]\psi_i(\mathbf{r}) = \epsilon_i \psi_i(\mathbf{r}), \quad (2.1.5)$$

and the Kohn-Sham potential and wavefunctions ($V_{KS}(\mathbf{r})$ and $\psi_i(\mathbf{r})$) are, respectively, represented by

$$V_{KS}(\mathbf{r}) = V_{ext}(\mathbf{r}) + \epsilon^2 \int \frac{n(\mathbf{r}')}{|\mathbf{r} - \mathbf{r}'|} d\mathbf{r}' + V_{xc}(\mathbf{r}), \quad (2.1.6)$$

and

$$V_{xc}(\mathbf{r}) = \frac{\delta E_{xc}}{\delta n(\mathbf{r})}. \quad (2.1.7)$$

Since $V_{KS}(\mathbf{r})$ depends on the charge density, the solutions of the Kohn-Sham equations are obtained by following self-consistent steps. As it was mentioned earlier, the exchange-correlation part, which doesn't have exact solution, has to be replaced with an approximation. The first approximation to E_{xc} was the local density approximation (LDA) [87, 88]. In this approximation the charge density is mapped from a homogeneous gas of non-interacting electrons to achieve the ground state of a non-homogeneous systems,

$$E_{xc}^{LDA}[n(\mathbf{r})] = \int \epsilon_{xc}^{hom}[n(\mathbf{r})]n(\mathbf{r})d\mathbf{r}. \quad (2.1.8)$$

On the other hand, for systems with strong bonding or when electrons are more localized, there might be a need of using other more complex approximation to overcome the shortcomings. One of such functionals introduced by Perdew and Wang is the general gradient approximation (GGA) which takes local variations of the charge density into account, *i.e.* the exchange correlation functional depends on the gradient of the charge density, in addition to the charge density itself [89],

$$E_{xc}^{GGA}[n(\mathbf{r})] = \int \epsilon_{xc}[n(\mathbf{r}), \vec{\nabla}n(\mathbf{r})]n(\mathbf{r})d\mathbf{r}. \quad (2.1.9)$$

GGA was found to improve some of the drawbacks of LDA, most importantly for systems with strong inhomogeneity. Many extended versions of GGA have been proposed through in the passed years [89]. Up to now the system under treatment is assumed to be non-magnetic, but, for magnetic system the spin density will be another variational quantity. The next part of this chapter deals with spin-polarized density functional theory.

2.1.2 Spin polarized systems

For systems with significant spin-polarization[90] the magnetization density $[\mathbf{m}(\mathbf{r})]$ augments the ground state charge density $[n(\mathbf{r})]$. In such description of the spin-polarized systems with DFT, the exchange correlation functional require highly non-local functional [91]. For the generalization of the the exchange correlation functional both charge density and spin-magnetization are involved. In this approximation the magnetization is fixed only in one direction, usually z -axis, *i.e.* the magnetization densities along x -axis and y -axis are set to zero.

Explicitly, the charge density is formulated using spin-up, $n_{\uparrow}(\mathbf{r})$, and spin-down densities, $n_{\downarrow}(\mathbf{r})$, as

$$n(\mathbf{r}) = n_{\uparrow}(\mathbf{r}) + n_{\downarrow}(\mathbf{r}). \quad (2.1.10)$$

In addition,

$$m(\mathbf{r}) = n_{\uparrow}(\mathbf{r}) - n_{\downarrow}(\mathbf{r}). \quad (2.1.11)$$

For spin polarized systems the general Hohenberg-Kohn theorem is re-stated as 'the ground state total energy is a variational functional of the magnetization densities' [90, 86], which is expressed as

$$E = E[n_{\uparrow}(\mathbf{r}), n_{\downarrow}(\mathbf{r})]. \quad (2.1.12)$$

The energy is decomposed according to equation 2.1.3 and the Coulomb term remains to be a functional of total charge density, whereas T_s and E_{xc} are functional of the two magnetization densities. The spin-polarized KS equations is described as

$$(T_s[n(\mathbf{r})] + V_H[n(\mathbf{r})] + V_{xc,\sigma}[n(\mathbf{r})])\psi_{i,\sigma}(\mathbf{r}) = \epsilon_{i,\sigma}\psi_{i,\sigma}(\mathbf{r}), \quad (2.1.13)$$

where σ (\uparrow or \downarrow) is the spin index, and

$$n_{\sigma}(\mathbf{r}) = \sum_i^{occ} \psi_{i,\sigma}^*(\mathbf{r})\psi_{i,\sigma}(\mathbf{r}). \quad (2.1.14)$$

For the spin-polarized case equation 2.1.7 is written as:

$$V_{xc}(\mathbf{r}) = \frac{\delta E_{xc}[n_{\uparrow}(\mathbf{r}), n_{\downarrow}(\mathbf{r})]}{\delta n(\mathbf{r})} \quad (2.1.15)$$

Spin polarized collinear approximation provides good descriptions for systems which are either collinear by nature or are well described by collinear spin treatment. However, magnetic systems can have multiple stable states that corresponds to variety of stable magnetic configurations. Indeed, many magnetic nanostructures are often non-collinear, hence, a method which treats such magnetic systems is required. The non-collinear spin treatment of magnetism in DFT is addressed in the next section.

2.1.3 Spin-orbit coupling and non-collinear magnetism

Naturally magnetic systems are non-collinear, implying that the orientation of the magnetization varies spatially. Non-collinearity could arise from a frustrated exchange interaction, Fermi surface effects which lead to spin-spirals [92], as well as the magnetic anisotropy energy which is the parameter responsible for magnetic stability, e.g. in nanomagnets, arises from spin-orbit coupling. Unlike for the case of the spin-polarized collinear magnetism, non-collinear representation does not depend the charge densities indices, equation (2.1.14) [93]. Alternatively, an internal artificial magnetic field, $m(\mathbf{r})$, [92, 94] is introduced in the form of an exchange correlation field which holds the three components of the magnetization density.

The implementation of spin-orbit coupling, *e.g.* in VASP-code, was done by Kresse and Lebacqz [94]. The relativistic Hamiltonian is described as basis of the total angular momentum eigenstates, $|j, m_j\rangle$, where $j = l \pm 1/2$, according to Kleinman [95] and MacDonald [96]. The relativistic corrections up to order of α^2 is presented in the form of 2x2 density matrix. Whereas, the eigenstates of the angular momentum are expressed in terms of the regular

angular momentum eigenstates $|l, m\rangle$ and eigenstates of the z -component of the Pauli spin matrices [94].

The relativistic effective potential consists of a term diagonal in spin-space, which contains the mass velocity and Darwin corrections. In addition, it has spin-orbit operator [97],

$$\mathbf{V} = \mathbf{V}^{SC} + \mathbf{V}^{SOC} = \sum_{l,m} [V_l \cdot \mathbf{1}_\sigma + V_l^{SO} \vec{\mathbf{L}} \cdot \vec{\mathbf{S}}] |l, m\rangle \langle l, m|, \quad (2.1.16)$$

where $\mathbf{1}_\sigma$ is unit operator in spin-space, and

$$\vec{\mathbf{L}} \cdot \vec{\mathbf{S}} = \begin{pmatrix} L_z & L_- \\ L_+ & -L_z \end{pmatrix} \quad (2.1.17)$$

For both the scalar V_l and spin-orbit V_l^{SO} potentials their l components are weighted averages over the $l \pm 1/2$ components, assuming that the magnetization is directed along the z -axis. The Hamiltonian is therefore 2x2 matrix in the spin-space. The non-diagonal elements originate from the spin-orbit coupling [97]. This implies that calculations including spin-orbit coupling should be done in the non-collinear mode, whereas the Hamiltonian is functional of 2x2 density matrix.

After Kubler *et al.*, non-collinear magnetism is expressed by 2x2 density matrix which constitute $n^{\alpha\beta}(r)$ [98]. The electron density $n(r)$ is described as trace of the density matrix, and the density matrix could be written as linear combination of unit matrix and the Pauli spin matrices,

$$Tr[n^{\alpha\beta}(\mathbf{r})] = \sum_{\alpha} n^{\alpha\alpha}(\mathbf{r}), \quad (2.1.18)$$

and the total density is given by

$$n^{\alpha\beta}(\mathbf{r}) = \frac{[n_{Tr}(\mathbf{r})\delta_{\alpha\beta} + \vec{m}(\mathbf{r}) \cdot \vec{\sigma}^{\alpha\beta}]}{2}, \quad (2.1.19)$$

with the magnetization density

$$\vec{m}(\mathbf{r}) = \sum_{\alpha\beta} n^{\alpha\beta}(\mathbf{r}) \cdot \vec{\sigma}^{\alpha\beta}. \quad (2.1.20)$$

The Pauli matrices $\sigma = (\sigma_x, \sigma_y, \sigma_z)$ are defined by

$$\sigma_x = \begin{pmatrix} 0 & 1 \\ 1 & 0 \end{pmatrix} \quad (2.1.21)$$

$$\sigma_y = \begin{pmatrix} 0 & -i \\ i & 0 \end{pmatrix} \quad (2.1.22)$$

$$\sigma_z = \begin{pmatrix} 1 & 0 \\ 0 & -1 \end{pmatrix} \quad (2.1.23)$$

The KS density functional becomes [94],

$$E = \sum_{\alpha} \sum_n f_n \langle \psi_n^{\alpha} | -\frac{1}{2} \nabla^2 | \psi_n^{\alpha} \rangle + E_H[n_{Tr} + n_z] + E_{xc}[n^{\alpha\beta}]. \quad (2.1.24)$$

The electrostatic energy for the electronic charge density (n_{Tr}) and point charge density of the nuclei (n_z), $E_H[n_{Tr} + n_z]$ is defined by

$$E_H[\varrho(\mathbf{r})] = \frac{1}{2} \iint \frac{\varrho(\mathbf{r})\varrho(\mathbf{r}')}{|\mathbf{r} - \mathbf{r}'|} d\mathbf{r}d\mathbf{r}', \quad (2.1.25)$$

where $\varrho(\mathbf{r}) = n_{Tr} + n_z$. The exchange correlation and orbital occupation numbers are assigned by $E_{xc}[n^{\alpha\beta}]$ and f_n , respectively. The exchange correlation energy is parametrized for homogeneous electron gas with charge density of n_{Tr} and magnetization density \vec{m} [94],

$$E_{xc}[n^{\alpha\beta}] = \int n_{Tr}(\mathbf{r}) \epsilon_{xc}[n_{Tr}(\mathbf{r}), \vec{m}(\mathbf{r})] d\mathbf{r}. \quad (2.1.26)$$

The exchange splitting in non-collinear systems is given by $b(\mathbf{r})\vec{n} \cdot \vec{S}$ [92], where

$$b(\mathbf{r}) = \frac{\delta E_{xc}[n^{\alpha\beta}(\mathbf{r})]}{\delta m(\mathbf{r})}. \quad (2.1.27)$$

In order to determine the local electronic and magnetic properties the plane wave component of the eigenstates is projected onto spherical waves within the atomic sphere. Then the spin and orbital magnetic moments are referred to the local spin quantization axis. It was noted that non-collinear treatment of spins and the spin-orbit coupling leads to a mixing of different spin-components [97].

2.2 The plane wave pseudopotential method

Based on various ways of representing magnetic systems within the DFT framework, one has to look for an effective way of solving the KS [equation (2.1.6)]. By using plane wave (PW) basis set one can easily control the accuracy of the solutions of KS equation, and it is also possible to determine physical parameters like Hellman-Feynman forces. However, the size of the basis set to represent a given system, including the core electrons, is very large compared to other basis set. Besides, the wavefunctions of the core electrons strongly oscillate near the nuclei of an atom and vary smoothly far away from the nuclei [99]. In order to describe such scenario the use of very high energy cut-off for the plane wave expansions unavoidable, which is assumed to include plane waves of short wavelength. Besides, most

of the space in the unit cell has smoothly varying electrons, so that using very high energy cut-off would be wasteful.

The alternative solution for this problem is using pseudopotential (PP) approach, in which the core electrons that are tightly bound to the nucleus are frozen to atomic like ground state, and would not be affected by the chemical environment in which the atom is placed [100]. In addition, the pseudopotential approach will drastically reduce the number of degrees of freedom to deal with, only the valence electrons, for solving the Kohn-Sham equations.

Basically, in the Kohn-Sham Hamiltonian, the nuclear potential is replaced by a new pseudopotential in such a way that the lowest one-electron energies coincide with the valence ones obtained by an all-electron calculation [86].

In norm-conserving pseudopotentials high number of plane waves are needed to represent orbitals of an atom. In order to generate a smooth pseudo-wavefunctions that correspond to the all-electron wavefunction outside the core region, it was mandatory to re-evaluate the condition requiring the conservation of the norm inside this region. Otherwise it will be computational very costly, where transition elements can be mentioned as an example. Vanderbilt [101] in 1990, proposed ultrasoft pseudopotential (USPP), by generalizing the eigen-problem in which each pseudowavefunction differs from the one found by using all electron calculation. Furthermore, the difference in the charge densities evaluated from the all-electron orbitals and pseudo-orbitals is minimized to small number of localized augmentation functions [102]. The shape of the pseudowavefunction could be made smooth, in comparison with norm-conserving pseudopotentials. USPP's have been incorporated in *ab-initio* molecular dynamics codes within the density functional formalism, e.g. *Vienna Ab-initio Simulation Package* (VASP) code [103, 102] and QUANTUM ESPRESSO [104].

In this thesis we employ the supercell approach using projector augmented wave method (PAW), [105] and the Kohn-Sham wavefunctions are represented by the plane-wave basis set as

$$u_{n\mathbf{k}}(\mathbf{r}) = \sum_{\mathbf{G}} c_{n\mathbf{k}}^{\mathbf{G}} e^{i\mathbf{G}\cdot\mathbf{r}}. \quad (2.2.1)$$

Since it is not realistic to consider infinite number of plane waves, the basis set of the plane wave is truncated in k_{cut} . This was done by using the respective free electron energy of k_{cut} ($\hbar k_{\text{cut}}^2/2m_e$), often referred as *cut-off* energy. There are two main advantages of using such plane wave codes, the first one is the proper control of the convergences of the ground state energy which is important for accurate calculation of , e.g. forces, stress. The second one is the possibility to calculate the forces on the atoms using the Hellmann-Feynman theorem which is useful for the advancement of studies about the time evolution of systems. Almost two decade earlier the generalization of pseudopotential method and linear augmented plane wave had lead to the projector augmented wave method which can perform with higher efficiency [106]. An extended description of the the PAW technique is presented in the next section.

2.3 The projector augmented wave (PAW) technique

In 1994 P. E. Blöchl proposed a technique which is a combination of the linearized augmented-plane-wave (LAPW) method and the plane-wave pseudopotential method (including its simplicities) [106]. Unlike the pseudo potential approach the PAW approach is all-electron method which properly describes the potential from full charge density [106]. It means that the valence electrons are kept orthogonal to the core states. Besides, it does provide us the most accurate way of calculating electronic structures of variety of systems, that includes the first row and transition metal elements [106, 94].

In the PAW method the all electron wave function is transformed from the pseudo-wave functions by using linear mapping operator, τ , [94]

$$|\psi_n^\alpha\rangle = \tau|\tilde{\psi}_n^\alpha\rangle = |\tilde{\psi}_n^\alpha\rangle + \sum_i (|\phi_i\rangle - |\tilde{\phi}_i\rangle)\langle\tilde{p}_i|\tilde{\psi}_n^\alpha\rangle, \quad (2.3.1)$$

$|\tilde{\psi}_n^\alpha\rangle$ is the pseudo-wavefunction, which is a variational quantity. $|\phi_i\rangle$ $|\tilde{\phi}_i\rangle$ are the partial pseudo and all electron (AE) wavefunction. The index i represents the ionic sites, angular momentum quantum numbers (l, m) , whereas index k is assigned to the reference energy ϵ_{kl} [94].

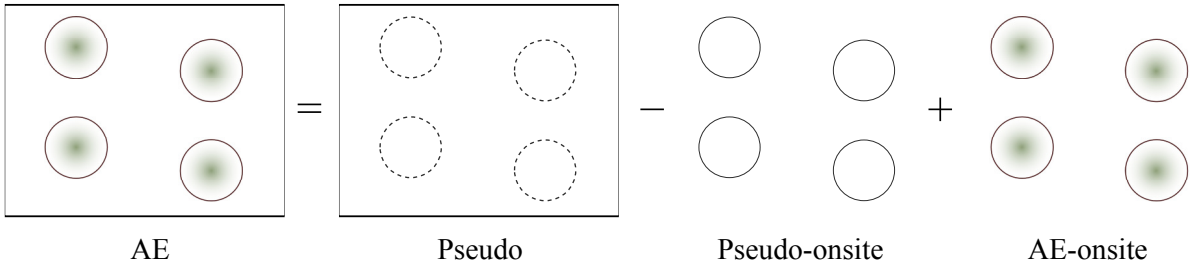


Figure 2.1: A model which illustrate the PAW method. It shows that by replacing the on-site pseudo wavefunction with the on-site AE wavefunction one can construct AE wavefunction. Similar scheme can be used for the charge density, total energy and Hamiltonian.

The pseudowave function in non-collinear magnetism is composed of $2N$ eigen-spinors when N is the total number of eigen values [94]. The pseudofunctions are expanded, in reciprocal space, into plane waves as

$$\langle\mathbf{r}|\tilde{\psi}_n^\alpha\rangle = \frac{1}{\Omega_{\mathbf{r}}^{\frac{1}{2}}} \sum_k C_{nk}^\alpha(\mathbf{r})e^{i\mathbf{k}\cdot\mathbf{r}} \quad (2.3.2)$$

where $\Omega_{\mathbf{r}}$ is the Wigner-Seitz cell volume. The AE partial waves (ϕ_i) are equivalent to the pseudo-partial waves ($\tilde{\phi}_i$) outside the core radius (r_c^l) [94]. The projectors fulfill the following conditions,

$$\langle p_i|\tilde{\psi}_n^\alpha\rangle = \delta_{ij}. \quad (2.3.3)$$

The projector functions are localized in a core region and the index i applies to all ionic sites. The all electron density matrix in the PAW technique is expressed as (See also Section 2.1.3),

$$n^{\alpha\beta}(\mathbf{r}) = \tilde{n}^{\alpha\beta}(\mathbf{r}) + {}^1n^{\alpha\beta}(\mathbf{r}) - {}^1\tilde{n}^{\alpha\beta}(\mathbf{r}), \quad (2.3.4)$$

starting with equation 2.3.1 [94]. The soft pseudo-density matrix calculated directly from the pseudo-wave functions on the plane wave grid as

$$n^{\alpha\beta}(\mathbf{r}) = \sum_n f_n \langle \mathbf{r} | \tilde{\psi}_n^\beta \rangle \langle \mathbf{r} | \tilde{\psi}_n^\alpha \rangle, \quad (2.3.5)$$

and the on-site density matrices are defined as

$${}^1n^{\alpha\beta}(\mathbf{r}) = \sum_{i,j} \rho_{ij}^{\alpha\beta} \langle \phi_i | \mathbf{r} \rangle \langle \mathbf{r} | \phi_j \rangle, \quad (2.3.6)$$

$${}^1\tilde{n}^{\alpha\beta}(\mathbf{r}) = \sum_{i,j} \rho_{ij}^{\alpha\beta} \langle \tilde{\phi}_i | \mathbf{r} \rangle \langle \mathbf{r} | \tilde{\phi}_j \rangle, \quad (2.3.7)$$

$\rho_{ij}^{\alpha\beta}$ are the occupancies of each augmentation channel, i, j , and they are evaluated by applying the projector function on the pseudo-wavefunctions:

$$\rho_{ij}^{\alpha\beta} = \sum_n f_n \langle \tilde{\psi}_n^\beta | \tilde{p}_j \rangle \langle \tilde{p}_j | \tilde{\phi}_n^\alpha \rangle. \quad (2.3.8)$$

2.4 Alteration of charge carriers in supercell approach

One of the many ways to impose a changes in the intrinsic properties of a functional material is to vary or re-distribute the charge carriers by external means. For example, by applying an external electric field or surface charging via medium (electrolyte) are some of the mechanisms. On the other hand, the tips of scanning tunneling microscopy (STM) [107, 108] and atomic force microscopy (AFM) [109] can be employed in order to control local charge or apply electric field in nanostructures. In this section we will present the way external electric field and charge injection are implemented in supercell approach.

2.4.1 External electric field

In the theoretical study of surfaces or interfaces, using supercell approach, it was usual to represent the geometry of the slab by few atomic layers. However, when we include

adsorbates on the surface the dipole induced by the adsorbates and the change in the work function makes it mandatory to include the adsorbates on the opposite sides of the slab [110, 111]. Still there exist an adsorbate-adsorbate interaction across the slab, and in order to minimize this interaction larger supercell is needed, e.g. ten atomic layer slab.

All these issues are addressed by adding planar dipole layer in the middle of the vacuum. The strength of the planar dipole is determined self-consistently in order to compensate adsorbate induced dipole. This will reduce the electrostatic interaction across the vacuum and the slab thickness can be reduced [111]. Besides, it should be stressed that the same method can be used to induce an artificial electric field by increasing (decreasing) the dipole strength. The total energy is modified by the introduction of the external electrostatic field [111],

$$\xi(\mathbf{r}) = -\vec{\nabla}\phi^{ext}(\mathbf{r}). \quad (2.4.1)$$

$$\Delta H = \phi^{ext} - \phi_o, \quad (2.4.2)$$

where ϕ_o is the interaction between ionic pseudopotential and ϕ^{ext} . The free energy ($F[n(\mathbf{r})]$) is re-written as

$$F[n(\mathbf{r})] = F[n(\mathbf{r})] + \Delta E[n(\mathbf{r})]. \quad (2.4.3)$$

The field-ion interaction is introduced without affecting the interaction between the ions [111]. Then energy functional is,

$$\tilde{F}[n(\mathbf{r})] = F[n(\mathbf{r})] + \Delta E[n(\mathbf{r})], \quad (2.4.4)$$

and the change in the energy [111, 110],

$$\Delta E[n(\mathbf{r})] = \int \Delta h(\mathbf{r})n(\mathbf{r})d\mathbf{r} = \int \phi^{ext}(\mathbf{r})n(\mathbf{r})d\mathbf{r} - \sum_J Z_J\phi^{ext}(\mathbf{R}_J). \quad (2.4.5)$$

There are also other techniques that are used to include external electric field effect in supercell approach. In this method it can be assumed as if the the slab is inserted in a parallel plate capacitors which are periodically repeated. [110] The potential of a constant field originate from the plates of the capacitor.

In metals the screening of the external field from penetrating into the bulk is accomplished by a surface charge build up, and it usually affects few atomic layers. During the charge build up on the surface the electronic charges interact via coulomb interactions, which depends on the net charge. When the metals are ferromagnetic, with significant exchange

interaction, the screening will also affect their magnetization. Hence, the screening in ferromagnetic metals could also affect the magnetic state or it is spin-dependent [72]. In Fig. 2.2 schematic representation of spin-dependent screening, for magnetic system on metal substrate, is presented. It shows the change in the charge distribution between the neutral system and the one exposed to an electric field of 1 V/\AA , along the axis perpendicular to the layer.

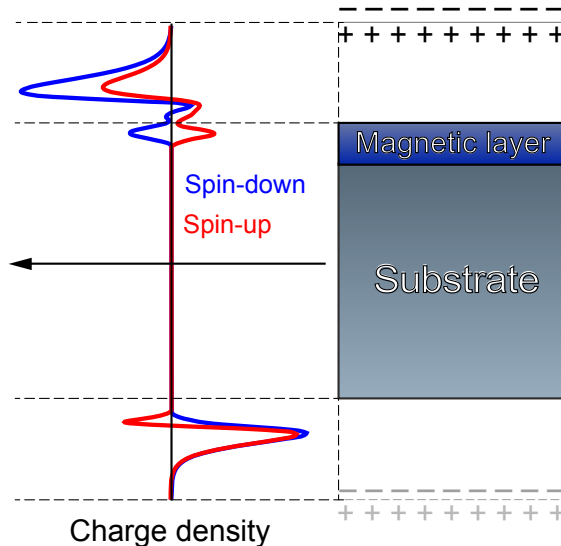


Figure 2.2: The sketch for the difference in the spatial distribution of charge density between the neutral system and when a system is exposed with an arbitrary non-zero electrostatic field. In the plot the difference in charge distribution for spin-up and spin down are shown.

2.4.2 Surface charging

The other technique that is used to alter charge carriers in supercell approximation is charge injection or removal. It is done by varying the number of electrons in the system and the charge neutrality of the supercell is kept by adding homogeneous charge background. The background charge is dependent on the number of extra electrons derived from the default system, and for zero number of atoms and non-zero electron number homogeneous electron gas (LDA-type) in the supercell is assumed. The schematic representation of these procedures is depicted in Fig. 2.3.

In this study we employ this technique in order to observe the variation of the magnetic properties of various multilayers. Most importantly we reveal the effect of surface charging on the magnetic anisotropy energy. However, it was suggested that one should include different kinds of corrections when dealing with charged supercell [112]. Meanwhile, we observe that quadrupolar corrections, [113] are not necessary for determining MAE. For charged systems having a large dipolar moment, quadrupolar corrections to the total energy are needed to be considered over dipolar ones [113, 114]. The corrected energy has the form

$$E(\vec{m}, q, Q) = E(\vec{m}, q) + \Delta E_{corr}(q, Q), \quad (2.4.6)$$

where \vec{m} , q and Q the magnetization, excess of charge and quadrupolar moment respectively. Assuming a scalar quadrupolar moment, $\Delta E_{corr}(q, Q)$ is independent of the direction of magnetization, hence MAE is independent of the quadrupolar corrections [82], *i.e.*

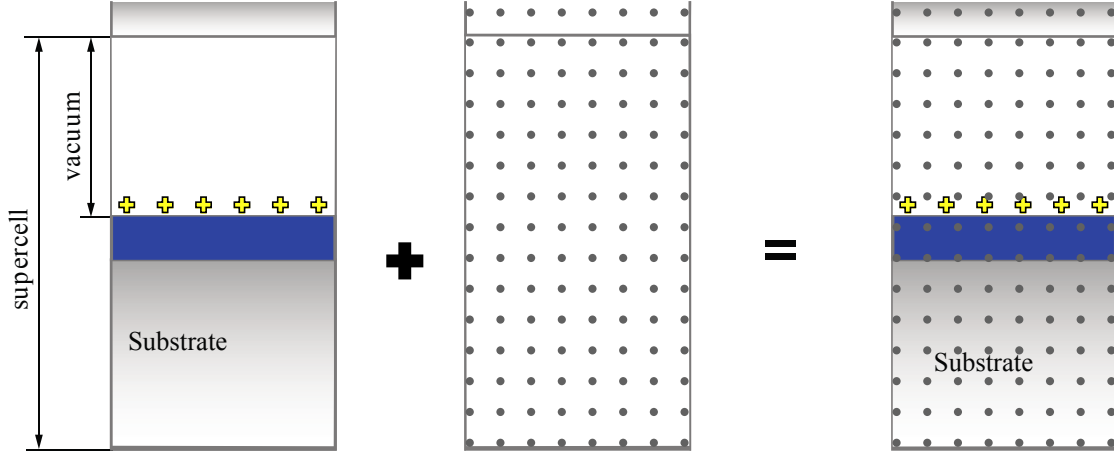


Figure 2.3: A model system of a charged slab (a) and the homogenous electron gas background (b). The compensating charge background added when the net charge in the supercell is different from zero.

$$MAE = E(m_{\perp}, q, Q) - E(m_{\parallel}, q, Q). \quad (2.4.7)$$

2.5 Current approaches to calculate magnetic anisotropy energy (MAE)

As was introduced in the first chapter the MAE is important parameters in magnetic systems for the understanding of the magnetic stability (against thermal fluctuations). Before we start discussing the main results in this thesis it is reasonable to introduce different approaches that are used to calculate the MAE in the magnetic systems. In order to investigate the MAE we need to go beyond collinear magnetism and connect the electron spin to the potential to reveal the magnetic anisotropy. This has been addressed by including spin-orbit coupling in the theoretical framework [96, 94, 115].

2.5.1 Force theorem

The force theorem treats the change in the band energy as a result of the variation of the angle of the magnetization axis with respect to the easy axis. Strictly, it is based on the assumption that the spin-orbit coupling (SOC) induced changes on either charge or spin densities to the total energy are negligible [116, 12]. Hence, to evaluate the MAE the SOC change in the band energies, summed over the occupied eigenvalues, is used for different quantization axes. MAE is written as

$$MAE = E_{\rightarrow} - E_{\uparrow} = \sum_{occ'} \varepsilon_i(\rightarrow) - \sum_{occ''} \varepsilon_i(\uparrow) + O(\delta\rho^n), \quad (2.5.1)$$

where the arrows represent the direction of magnetization and ε_i are the eigenvalues under consideration. In this method the contribution to the change in the energy from the Hartree and exchange correlation are not included, instead the contribution from the external potential is taken in to consideration. Normally, to calculate the MAE we relax the

geometry of the system using scalar relativistic methods, then in the next step we include SOC to the relaxed geometry with the frozen potential for different axis of magnetization, making a single iteration.

The advantage of evaluating the MAE from the difference in the band energies is that using the partial local density of states decomposed to layer and angular momentum, thus, atomic and layer resolved MAE can be determined, even if it is less accurate. [12] The fundamental problem of determining the MAE from the symmetry of the structure and the atomic species has been the main topic of discussion [116, 117, 118]. The model that explains the origin of the MAE from the anisotropy of the SOC energy of d atoms was demonstrated by Wang *et al.* [116] In this model emphasis was given to the SOC contribution to the MAE from spin-down and spin-up states. Within the relativistic theory the Hamiltonian perturbed by the SOC is described as

$$H = H^o + H^{SO} = H^o + \xi(\mathbf{r})\vec{\mathbf{L}} \cdot \vec{\mathbf{S}}, \quad (2.5.2)$$

where the SOC amplitude $\xi(\mathbf{r}) = (1/4c^2\mathbf{r})\partial V/\partial\mathbf{r}$. The integrated value of $\xi(\mathbf{r})$ for, e.g. $3d$ states of Fe, is 30 meV which is much smaller than the $3d$ bandwidth (few eV) [116, 117]. This justifies any perturbative treatment of the SOC for transition metals. Since the energy shift as result of the first order perturbation is identically zero (since the diagonal matrix elements of the H^{SO} are zero), the second order for the energy corrections is employed. It is expressed as [116],

$$E^{SO}(\sigma) = -(\xi)^2 \sum_{u,o} \frac{|\langle o|\vec{\mathbf{L}} \cdot \vec{\mathbf{S}}|u\rangle|^2}{\delta\epsilon_{uo}} \quad (2.5.3)$$

where o represents the occupied state and u is for unoccupied ones, $\delta\epsilon_{uo} = \epsilon_u - \epsilon_o$. The radial integral of the product of the SOC amplitude $\xi(\mathbf{r})$ is assigned with ξ which is assumed constant for all d -orbitals [116].

To understand the MAE mechanism it is helpful to differentiate the contribution of the SOC between parallel and opposite spin states. In order to study this Wang *et al.* considered the limiting case of strong exchange splitting where all the empty states belong to spin-down and all the spin up band is almost fully occupied [116]. Then the difference in the SOC energies or anisotropy between two axis of magnetization (x, z) has two terms. The contribution from occupied and unoccupied states of spin-down states (ΔE^{dd}) and contribution from opposite spins (ΔE^{ud}). Using Eq. 2.5.3 $\Delta E^{dd} = E_x^{dd} - E_z^{dd}$ is written as [116],

$$\Delta E^{dd} = MAE \sim (\xi)^2 \sum_{u,o} \frac{|\langle o|L_z|u\rangle|^2 - |\langle o|L_x|u\rangle|^2}{\epsilon_u - \epsilon_o}. \quad (2.5.4)$$

ΔE^{dd} strongly depends on the splitting between occupied and unoccupied states via the denominator. Indeed, both ΔE^{ud} and ΔE^{dd} are summed over the spin down empty states, and they depend differently on the band filling of the spin-down states. In comparison with ΔE^{dd} , the ΔE^{ud} has smaller dependence on the band structure. This method [equation (2.5.4)] can be used to understand the origin of the MAE and also the variation of the MAE with respect to different parameters.

2.5.2 Self consistent method

In this technique the MAE is calculated on the basis of the total energy which includes SOC induced changes to the spin-density. The SOC is incorporated according to the formulations given in Section 2.1.3 [94, 116, 115]. For the case of fully relativistic USPP the SOC is included in the nonlocal part [115], and by its nature this technique includes the contribution of the Hartree, exchange and correlation terms to the MAE. Basically, starting with an arbitrary magnetization direction the self-consistent steps should derive the system to the ground state where the magnetization is directed along the easy axis. This is accomplished by changing the resultant magnetization of the individual atoms in the system and the direction of the total magnetization, however, the very different energy scale of these two variables which is 10^{-1} and 10^{-3} eV, respectively makes it unrealistic. In the self consistent scheme the magnetization of the individual atoms converges faster than the direction of magnetization which can be time consuming [119].

Alternatively, different self consistent calculations are performed by fixing the direction of the individual atoms magnetization along various axis of symmetries. It can possibly be done by constraining the axis of quantization (reference axis) during the self consistent steps. Hence, one can determine the magnetic anisotropy energy (MAE) and easy axis from the energy difference of the systems with different axis of magnetization. aligned orthogonal to each other. Usually, the axis of magnetizations are chosen depending on the adsorption site with respect to the crystallographic axes of the substrate.

In most cases the self-consistent method and force theorem produce comparable MAE. Based on our calculations and assuming that all other parameters are well optimized the percentage difference in the MAE (per unit cell) between the two technique can be 12% (atomic chains), 4% (ultra-thin films) and 10% (thicker films), depending on the symmetry of the adsorbate.

Most of the investigations were performed within the density functional formalism as implemented in the *Vienna Ab-initio Simulation Package* (VASP) code[103]. The later is based on the supercell approach and employs projector augmented wave method (PAW) and a plane-wave basis set [105] for describing the Kohn-Sham wavefunctions. The exchange-correlation interactions was described by the local spin density approximation (LSDA) [87]. In addition, for the sake of comparison we have also employed similar codes, e.g. QUANTUM ESPRESSO [104], and other functionals for the exchange correlation part (GGA and LDA+U).

Technical details

The scheme for the calculation of the MAE is presented as follows; first, scalar relativistic calculations were carried out for the structural optimization of the systems. The force on each atom was minimized to be less than 5 meV/Å. It was found that the relaxations can not be neglected for the determination of magnetic anisotropy energy (MAE). For instance, considering the bulk Pt-interlayer distance, 1.95 Å, as a reference, geometrical optimization reduces the interlayer distance between adsorbates and the outermost Pt-layer of the substrate by $\sim 28\%$. Unless it is stated, all the results presented in the thesis are obtained from the relaxed geometries.

As a second step, in order to calculate the magnetic anisotropy energy (MAE), defined as ground state energy difference of the systems with x and z directions of magnetization ($E_x - E_z$), fully-relativistic self-consistent calculations including spin-orbit coupling were

performed. Since MAEs are usually relatively small (\sim few meV), a dense k -point mesh (depending on the geometry of the system) and large plane-wave energy cut-offs (400 eV) were employed in order to obtain an accurate MAE value. Larger number of k -point meshes and larger cut-off energies were tested for checking the reliability of the chosen parameters resulting in insignificant changes of the results. Therefore, the parameters considered in this study are a good compromise between accuracy and computational effort. It has to be mentioned that similar computational parameters are used for calculating MAE with force theorem.

The theoretical studies on magnetic multilayers (Co and Fe) are modeled by considering up to nine ($1 \leq N \leq 9$) layers supported by ten Pt layers, as the substrate. Whereas, for calculations of adatoms and chains we used six layers of Pt as substrate, for the reason of computational effort. These choices assure that the surface electronic structure in the layered-systems is properly described. We have used 12 Å of vacuum space in the supercell in order to avoid possible interactions between periodic images. The size of the vacuum layer has been converged with respect to surface energy, interlayer distance and most importantly with the MAE. For instance, for vacuum layer distance of 15 Å the MAE changes only by 4%, and such variation will not alter the conclusion or discussion made in our studies. When an external electric field was applied the dipole corrections were also taken into account [111].

Chapter 3

Magnetic properties of linear atomic chains on metal surfaces

This chapter deals with the magnetic properties of pure and alloy atomic chains supported by flat and vicinal metal surfaces. The discussion begins with the results on the inter-atomic exchange coupling of Co-Pt atomic chain on Pt substrate, with various Pt compositions. The effect of structural relaxation on magnetic properties of the atomic chains is also discussed. Investigation on the interplay between the chemical composition of the atomic wire and the magnetic anisotropy will be followed. Here we will show that alloying 3d chain with Pt enhances the magnetic anisotropy energy. Further study on 1-D chains on Pt(997) surface have shown that the in-plane magnetization of Fe chain can be re-oriented to out-of plane direction after alloying it with Co. These discussions are finally followed by the effect of external electric field on magnetic properties of linear atomic chains supported by Pt surface.

3.1 Overview

In the field of magnetoelectronics and spintronics controlling the magnetic properties of devices and their elements by means of the electric field is worthwhile in order to reduce the energy consumption.[120, 4, 68] The coupling between electric and magnetic properties of a material, *i.e.* magnetoelectric effect, has already been suggested as a new promising technology for magnetic data storage devices.[55, 56] Unfortunately, most of the candidate systems which manifest magnetoelectric effect, *f.e.* multiferroics, magnetic semiconductors, have a major drawback. The critical temperature, at which thermal fluctuations destroy magnetic order, is too low for most of magnetic semiconductors and multiferroics.[67] This problem of thermal instability can be solved by achieving a critical magnetic anisotropy energy (MAE) of (1.2 eV/bit) is [121] thus, of crucial importance and could be used to stabilize the magnetic moments against thermal fluctuations. For example MAE can be enhanced if magnetic structures of reduced dimensions are used. It was shown that 0D (adatoms)[13, 12] and 1D (chains and wires)[122, 2, 123, 124] nanostructures on metal surfaces exhibit larger MAE than that of bulk structures.

On the other hand, using Pd/Pt-3d metal compounds, which have critical temperature T_c far above the room temperature, can also be another solution for thermal stability problem.[69] High T_c of these compounds arises from their large magnetic anisotropy. A reduced dimensionality of Pt-3d metal nanochains and a large spin-orbit coupling of Pt could even lead to a large MAE. For such systems (atomic chains) experimental measurement was

undertaken which reveals long range magnetic order of Co chains on Pt(111) surface. The reason for such measurements is related to concept of blocking temperature, which is the temperature at which the relaxation time of the magnetic structure to be superparamagnetic is longer than the time of measurement [2]. The experimental study of Co clusters supported by Pt(111) surface showed that the MAE per Co atom increases while the cluster size decreases, indeed, for a single Co adatom a giant MAE of 9 meV was measured [13, 21, 12]. Large MAE of Co chains on the Pt(997) surface was observed [2].

From our calculation and other theoretical studies very high MAE of Co adatom on Pt(surface) has been confirmed [12, 119]. These studies were performed on a surface represented by 5x5 surface unit cell and the substrate consists of six to ten Pt layers. The slab is also periodically repeated which is separated with the vacuum layer. The corresponding monolayer coverage of the adatom, i.e. considering the adatom as submonolayer constituent, on such surface unit cell is 0.04 ML. This does not have strong impact on the MAE since experimental investigation have already shown that increasing the monolayer coverage of Pt(111) surface from 0.007 to 0.03 ML decrease the MAE only by 0.6 meV (from 9.2 meV to 8.6 meV) [27]. This shows a good compromise for the surface cell modeling of adatoms. It was found that the spin magnetic moments of magnetic adatoms agrees well with the experimental values, but not the orbital magnetic moment. The theoretical value of orbital magnetic moment is very small, $0.08 \mu_B$ for Co adatom on Pt(111), compared to the experimental value ($1.0 \mu_B$).

It was mentioned earlier that different magnetic orders could be affected by electric field, in fact, the MAE can be mentioned as one of these parameters [69, 70, 78]. In this chapter we will demonstrate the effect of electric field on the MAE of linear Co and Co-Pt chains on Pt(111).

3.2 Co and Co-Pt chains on Pt(111)

In this section we discuss structural and magnetic properties of the Co and the Co-Pt chains on the Pt(111) surface. In Fig. 3.1 the vertical distances to the substrate for both non-relaxed and relaxed geometries are shown. The atomic chains were initially placed at the height of the bulk interlayer distance of 2.25 \AA , with respect to the top-most layer of the Pt (111) surface. Starting from the ideal geometry, we relaxed the structure by minimizing the forces. In the relaxed geometry of the Co chain on Pt(111) surface, the Co atom lies at vertical distance of 1.71 \AA from the surface and its magnetic properties are changed.

First, we emphasize on the inter-chain exchange coupling of the Co and Co-Pt chains on Pt(111) surface. In Co-Pt chain the Co atoms are considered as second and third nearest neighbors, shown in Fig. 3.2, and all the values of the exchange coupling are calculated from relaxed geometries, as a difference in the energy between ferromagnetic and anti-ferromagnetic couplings. In all cases the Co atoms have ferromagnetic coupling, and the exchange coupling in Co, Co-Pt, Co-Pt-Pt-Co chains, respectively, are 112, 14.2 and 12 meV/Co atom. Indeed, when the Co atoms are configured as third-nearest neighbors, the inter-atomic coupling between the Co atoms reduces, as compared to the other arrangements.

3.2.1 Monoatomic Co chains on Pt(111)

The magnetic anisotropy of these systems have also been studied. The easy axes of the pure Co chain in non-relaxed and relaxed geometries are oriented perpendicular to the surface.

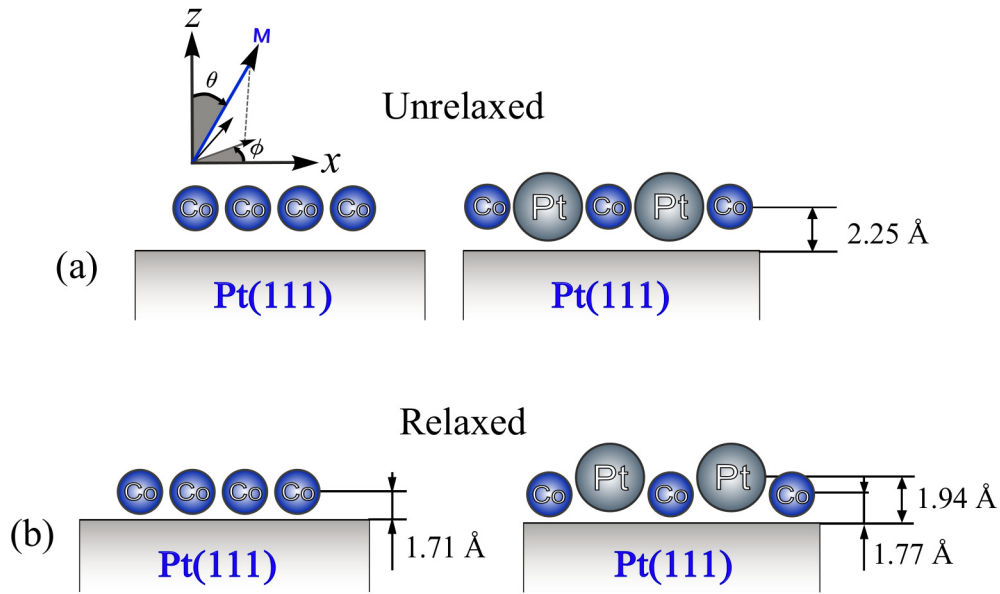


Figure 3.1: A sketch for linear Co and Co-Pt chains on Pt(111) surface. The vertical distances between the atomic chains and the Pt substrate for unrelaxed (a) and relaxed (b) geometries are given. All the distances shown in the figure are in units of Angstroms. The easy axes of relaxed structures of both systems are directed perpendicular to the surface ($\theta = 0$ and $\phi = 0$).

As shown in Table 3.1 the value of MAE in the relaxed geometry is 2.8 meV. The axes of magnetizations are also presented in terms of polar angles θ and ϕ , depicted in Fig. 3.1. Angle θ is measured from z -axis on zx -plane, whereas ϕ is spanned from x -axis on the xy -plane. The spin magnetic moment of Co atoms in the chain, for out of plane direction, shows small change of $0.1 \mu_B$ after relaxation, and the orbital magnetic moment decreases from $0.29 \mu_B$ to $0.16 \mu_B$. From Table 3.1 the higher value of the spin moment of the Pt substrate in the relaxed structure is explained by the shorter bond lengths [Fig. 3.1], which provide a stronger hybridization between d-states of Co and Pt. Additionally, the Pt atoms in the substrate have induced magnetic moment of $0.26 \mu_B$ in relaxed geometry.

Similar non-collinear calculations were performed using the GGA (PBE)[89] exchange-correlation functional, for relaxed pure Co chains on the Pt(111) surface. The equilibrium lattice parameter of bulk Pt is found to be 3.99 \AA . Subsequently, it was found that the MAE is 2.8 meV and the easy axis is unchanged. Compared to the LDA the spin magnetic moment of Co and Pt increases by $0.05 \mu_B$ and $0.01 \mu_B$, respectively. At the same time, the orbital moment of Co atoms in the Co chain is reduced in the case of the GGA. To address recent calculations [119] performed for Co chains on Pt(111), we also did similar studies by means of the PWscf code of Quantum-ESPRESSO [104] using LDA-fully relativistic ultrasoft pseudopotential (USPP). Employing bulk lattice parameter of Pt, 3.92 \AA , the MAE in the relaxed geometry was found to be 0.9 meV and the easy axis is in-plane along the direction of the chain (90,90); which agrees with Ref. [119]. Further studies have been done using LDA, VASP to see the change of MAE with respect to the variation in the lattice parameter. At 4.08 \AA we observe a decrease in the MAE (1.04 meV) and switch of the easy axis, from out of plane to into the plane (along the chain). This leads to the conclusions that the MAE strongly depends on the lattice parameter.

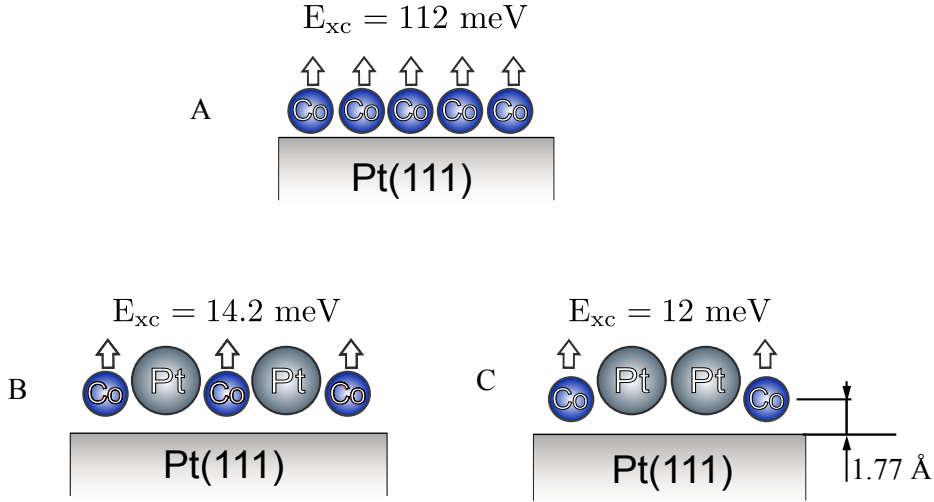


Figure 3.2: Inter-chain exchange coupling between Co atoms for different composition of Pt atoms in the chain. The value of the exchange coupling is evaluated as the difference in the ground state energy between ferromagnetic and anti-ferromagnetic orders, for all the cases ferromagnetic ordering is more stable. The pure Co chain is shown in (A) and Co-Pt chain which is separated by single Pt atom is depicted in (B), whereas Co-Pt chain separated by two Pt atoms is shown in (C).

Table 3.1: Spin magnetic moments (m_s), orbital magnetic moments (m_o) and the MAE of pure Co and the mixed Co-Pt chains in the Pt(111) surface. The two columns represent relaxed and unrelaxed geometries. Pt atoms in the mixed chain and Pt substrate atoms nearest to the chain are denoted by Pt₁ and Pt₂, respectively. All the magnetic moments presented are for the easy axis of magnetization.[74]

	<i>Pure Co chain</i>		<i>Mixed Co-Pt chain</i>	
	Unrelaxed	Relaxed	Unrelaxed	Relaxed
MAE (meV)	2.2	2.8	2.0	4.3
Co, m_s (μ_B)	2.1	2.0	2.22	2.03
Co, m_z^L (μ_B)	0.29	0.16	0.29	0.19
Co, $m_{x(y)}^L$ (μ_B)	0.16	0.07	0.14	0.1
Pt ₁ , m_s (μ_B)	—	—	0.23	0.18
Pt ₂ , m_s (μ_B)	0.13	0.26	0.15	0.08
Easy axis(θ, ϕ)	(0, 0)	(0, 0)	(90, 90)	(0, 0)
Hard axis(θ, ϕ)	(90, 0)	(90, 0)	(90, 0)	(90, 0)

3.2.2 Atomic Co-Pt chain on Pt(111)

We now discuss the Co-Pt atomic chains supported on the Pt(111) surface. The summary of the results on the interplay between magnetic properties and the geometrical relaxation of the Co-Pt mixed chain is presented in Table 3.1. The vertical distance of the chain atoms

from the surface and the length of the bonds are displayed in Fig. 3.1. The Co and Pt atoms in the chain are situated at the vertical distances of 1.77 and 1.94 from the Pt surface, respectively. The Co atom in the Co-Pt mixed chain lies by 4% higher compared to the vertical distance of the Co atom in the relaxed Co chain. The interaction between the Co and the Pt atoms is stronger than the interaction between Pt atoms, which is the reason for the stronger relaxation of the Co atom towards the Pt surface than the Pt atoms in the chain. This results in an oscillatory vertical distance of Co and Pt atoms along the chain which resembles a zig-zag-like shape. In addition, the Co atoms in the Co-Pt chain also interact with Pt atoms in the chain, which prefer to stay higher.

As shown in Table 3.1, the MAE in the Co-Pt chain increases from 2.0 meV for non-relaxed geometry to 4.3 meV for the relaxed one. The spin and orbital magnetic moments of the Co atom in the relaxed (non-relaxed) geometries are 2.03 (2.22) μ_B and 0.19 (0.29) μ_B , respectively. In non-relaxed geometry, the Pt atom in the chain has a spin magnetic moment of 0.23 μ_B , since Pt is suitable for element-specific Stoner criteria.[76] The induced magnetic moment of the Pt atom in the substrate is 0.15 μ_B . In the relaxed geometry the Pt atom in the chain and the Pt atom in the substrate have magnetic moments of 0.18 μ_B and 0.08 μ_B , respectively. For both relaxed and unrelaxed geometries the Pt atom in the chain has less coordination number than the one in the Pt(111) surface, which is the origin for the higher induced magnetic moments of Pt on the chain.

Obviously, the second quantization contribution due to the spin-orbit coupling between occupied and unoccupied eigenstates near the Fermi level affects the ground state energy at most.[117, 116] The orbital projected LDOS for the minority d states of Co atom in the Co-Pt chain, which are the most dominant states near the Fermi energy, are shown in Fig. 3.3. Relaxations split the degenerate d -levels in a close proximity to the Fermi energy providing, thus, the first contribution to the change of the MAE.

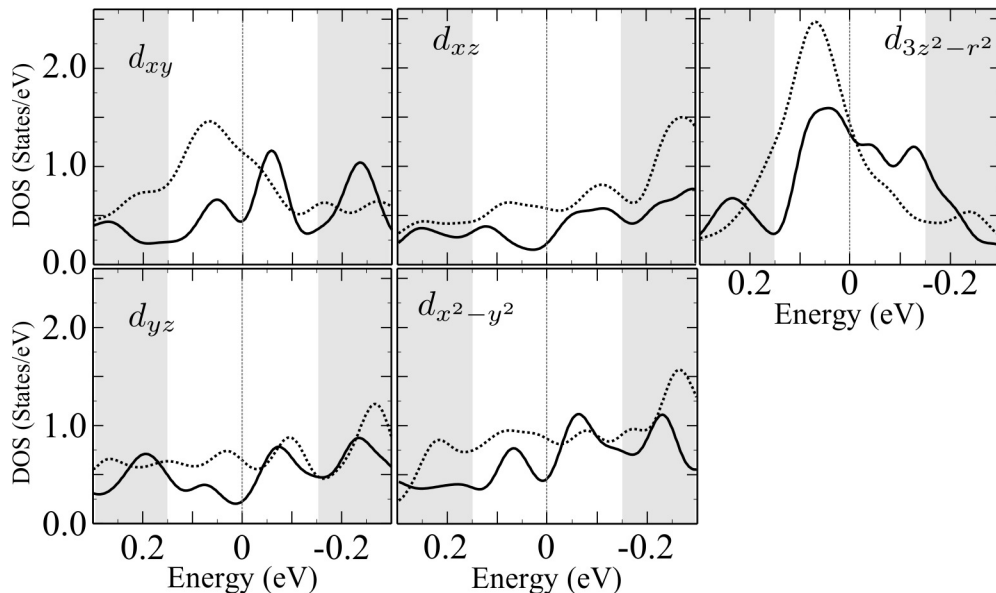


Figure 3.3: Orbital-projected minority d -LDOS of the Co atom in the Co-Pt chain, without the presence of external electric field, for relaxed (full lines) and unrelaxed (dashed lines), are represented. Only the minority density of states are considered, since the density of majority states is negligibly small at the Fermi level.[74]

In the non-relaxed Co-Pt chain the easy axis of magnetization is directed along the chain

direction ($\phi = 90$ and $\theta = 90$) and the MAE is 2 meV. Following geometrical relaxation the easy axis changes to normal to the surface ($\phi = 0$ and $\theta = 0$) and the MAE increases by more than two times. In the non-relaxed geometry there is a higher density of d_{xy} and $d_{3z^2-r^2}$ states just below the Fermi energy, however for relaxed geometry these states split and the density of states is shifted to higher energies (Fig. 3.3). The later effect which results in a re-distribution of $d_{3z^2-r^2}$ states around the Fermi energy, decreases the SOC between $d_{3z^2-r^2}$ states with d_{xz} and d_{yz} , *i.e.* $\langle d_{xz(yz)} | L_x | d_{z^2} \rangle$. Equation (2.5.4) is re-written as

$$MAE \sim \frac{(\xi)^2}{\epsilon_u - \epsilon_o} \sum_{u,o} |\langle o | L_z | u \rangle|^2 - |\langle o | L_x | u \rangle|^2. \quad (3.2.1)$$

Additionally, from the change in the spin-orbit coupling matrix element for the easy and hard axes, the coupling between occupied and unoccupied states of d_{xy} and $d_{x^2-y^2}$ (for the easy axis) through \vec{l}_z ($\langle d_{xy} | L_z | d_{x^2-y^2} \rangle$) increases, with an aggregate effect of enhancing the MAE in the relaxed geometry.

Similarly, the change of the easy axis can also be seen from the variation in the spin-orbit coupling matrix elements of the easy and the hard axis of magnetization. Analysis on the spin-orbit matrix elements of the Co atom in the non-relaxed and the relaxed Co-Pt chain reveal that the magnetization direction parallel to the surface is mostly determined by the spin orbit coupling of $\langle d_{xz(yz)} | L_x | d_{3z^2-r^2} \rangle$, see equation (3.2.1). In the non-relaxed geometry this firmly decides the spin-orbit coupling contribution to the ground state energy of the easy axis. The magnetization axis perpendicular to the surface is characterized by the SOC of $\langle d_{xy} | L_z | d_{x^2-y^2} \rangle$, in addition to the coupling already stated above. And these couplings play the main role here. Atomic relaxations decrease the interaction between $d_{3z^2-r^2}$ states with d_{xz} and d_{yz} , for the magnetization direction parallel to the surface. There is also an increase in the SOC between d_{xy} and $d_{x^2-y^2}$, which decreases the energy of the easy axis configuration for the relaxed geometry. From the variation stated above, the direction of the easy axis changes from parallel to the surface in non-relaxed geometry to normal to the surface in relaxed geometry.

It is worthwhile to study the magnetic properties of freestanding Co and Co-Pt chains, in order to point out the effect of substrate. The MAE per atom is evaluated for isolated chains of Co and Co-Pt chains with respective interatomic distance of 2.76 Å and 2.77 Å, which is the distance between the atoms on the Pt(111) surface. A very high MAE is found to be 31 meV and 22 meV, with an easy axis of perpendicular to the chain and parallel to the chain, for Co and Co-Pt chains, respectively. The relation between MAE and orbital anisotropy is only valid only for free-standing Co-Pt chain.

The approximation which correlates MAE and orbital anisotropy, known as Bruno's relation, is valid for all supported atomic chains that are considered in this study,[117, 11, 125]

$$MAE = \frac{\varepsilon}{4\mu_B} [m_z^L - m_{x(y)}^L], \quad (3.2.2)$$

where ε is spin-orbit coupling constant. For the validity of this approximation the easy axis should have higher orbital moment. For instance, the orbital anisotropy of Co atom in Co-Pt chain for relaxed and unrelaxed geometries is 0.08 μ_B and 0.1 μ_B , respectively. In addition, the higher orbital magnetic moment is oriented along the easy axis, parallel to

the chain (in-plane) for non-relaxed geometry and perpendicular to the surface for relaxed geometry.

An interesting properties of the Co-Pt alloy chains have been revealed by adding one more Pt atom to form Co atoms separated by two Pt atoms (Fig. 3.2). In this system the stable order of magnetization remains to be ferromagnetic, but the exchange coupling energy (12 meV per Co atom) much is smaller than pure Co chain. Meanwhile the MAE has reduced to 3.4 meV per Co atom and the easy axis of magnetization is still oriented perpendicular to the surface.

As summary, by considering different composition of Pt atoms in Co-Pt chain we found that ferromagnetic order is the most stable configuration. For all relaxed geometries the easy axis of magnetization is oriented perpendicular to the surface. Other than the composition of the atomic chains we have considered the effect of the surface morphology on their magnetic feature, in particular we have explored magnetic properties of 1-D atomic chains on Pt(997) surface and it will be described in the next section.

3.3 Co(Fe) chains on Pt(997) surface

Most of the atomic chains that have been realized, using STM manipulation [22, 126, 30, 24, 127] or atomic self assembly [25, 23, 26], are supported by vicinal surfaces.[27, 26] Consequently, using ab-initio technique we have investigated the magnetic properties of pure Co(Fe) chains and mixed Co-Fe chains on Pt(997) surface. Furthermore. it opens a venue to study the effect of surface roughness on magnetic properties. We also have been interested in finding out the magnetic properties of magnetic alloys (Fe-Co), which is a scheme implemented to get some peculiar magnetic properties nanostructures.[128]

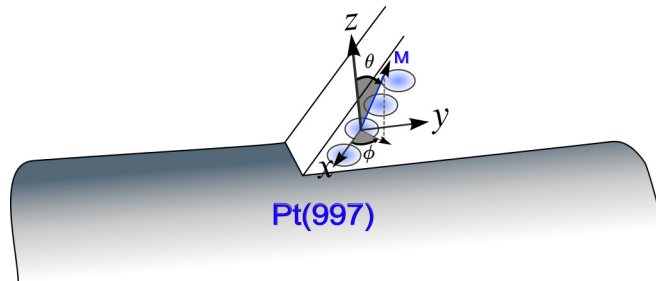


Figure 3.4: Pictorial representation of 1-D atomic chains on Pt(997) surface. The direction of magnetization \mathbf{M} with respect to the Cartesian coordinate is also depicted, and the z -axis and x -axis are parallel and perpendicular to the (111) plane, respectively. The axes of quantization are described by the polar angles θ and ϕ . The in-plane polar angle θ is spanned from the x -axis, whereas angle ϕ is measured from the z -axis.

In Table 3.2 the magnetic properties, namely the magnetic anisotropy energy, spin magnetic moment and orbital magnetic moments, of all linear atomic chains is presented. The values of spin magnetic moment and orbital magnetic moments are given for the easy axis of magnetization. These results are obtained by doing fully self-consistent non collinear calculation for different directions of magnetization. The magnetization axes are depicted using the polar angles θ and ϕ which are measured from the z and x , respectively (See Fig. 3.4). For the properties related to magnetic anisotropy, we have compared the ground state energy of different magnetization direction (Shown in Fig. 3.4); along z -axis (0,0), parallel to the

chain axis (90,0) and (in-plane) perpendicular to the chain axis (90,90). Strictly, the MAE is calculated from the energy difference between the easy and hard axes of magnetization.

Co atomic chains on Pt(997) surface has high MAE of 3.2 meV, and it is 0.6 meV higher than the MAE on flat Pt(111) surface, however, in both cases the easy axis of magnetization remain perpendicular to the chain axis. For Co chains the MAE presented in Table 3.2 is the difference between the magnetization along two orthogonal axis of magnetizations. The easy axis of magnetization for Co chains is in agreement with the experimental one [2, 27], *i.e.* in both cases the easy axis is perpendicular to the chain axis (x -axis). We have found that the hard axis of magnetization is oriented along y -axis. The theoretical value of the MAE is higher than the experimental one and the difference could be related to the way the MAE is evaluated; the polar angle (θ) in theoretical study and experimental measurement have respective value of 0° and 43° [2, 27] The STM topographic image of Co linear chains decorating Pt(997) surface is shown in chapter 1, [Fig. 1.3(a)]. In this measurement the easy axis of magnetization is oriented 43° towards the edge of the step,[2] *i.e.* $(-43,0)$ according to Fig. 3.4. In addition, the presence of long and short range magnetic orders depending on the temperature could be another factor.[2]. Theoretical description of the spin magnetic moment agrees with the experiment, but not the orbital magnetic moment which is far below the experimental value.

We have done similar investigation for Fe atom on vicinal Pt(997) surface, and the spin magnetic moment and orbital magnetic moments are found to be $2.9 \mu_B$ and $0.1 \mu_B$, respectively. Unlike the pure Co chains Fe chains have an easy axis oriented in-plane and parallel to the chain axis (90,0), and the hard axis of magnetization is along the y -axis. Additionally, the MAE is estimated to be 1.5 meV per Fe atom, but the energy difference between the easy axis (x -axis) and the intermediate axis (z -axis) is 0.5 meV. The easy axis of magnetization is in good agreement with experimental study based on XMCD and scanning tunneling spectroscopy (STS).[14]

Table 3.2: Spin magnetic moments (m_s), orbital magnetic moments (m_o) and the MAE of pure Co, Fe and Co-Fe linear chains on Pt(997) surface. All the results presented are for the relaxed geometry, and all the magnetic moments presented are for the easy axis of magnetization. The magnetic properties of Pt atoms in the nearest to the chain are also presented.

	Co chain		Mixed Co-Fe chain		Fe chain	
	<i>Theory</i>	<i>Expt.</i> [27]	<i>Theory</i>	<i>Expt.</i>	<i>Theory</i>	<i>Expt.</i> [14]
MAE (meV)	3.2	2.0	2.1	—	1.5	—
Easy axis(θ, ϕ)	(0, 0)	(-46, 0)	(0, 0)	—	(90, 0)	(80, 0)
Hard axis(θ, ϕ)	(90, 90)	-	(90, 0)	—	(90, 90)	(10, 0)
Co, m_s (μ_B)	2.1	2.1	1.66	—	—	—
Co, m_o (μ_B)	0.1	0.7	0.08	—	—	—
Fe, m_s (μ_B)	—	—	2.97	—	2.85	3.1
Fe, m_o (μ_B)	—	—	0.08	—	0.1	0.3
Pt ₁ , m_s (μ_B)	0.21	—	0.23	—	0.22	—

An interesting feature has been observed for Co-Fe alloy on Pt(997) surface, where it has 50% composition of each Co and Fe atoms, for example the MAE (2.1 meV/per magnetic atom) of Co-Fe chain is less than the MAE of pure Co chain (3.2 meV/Co atom), and the easy axis of magnetization is oriented perpendicular to the surface (0,0). Nevertheless, the least stable axis of magnetization for Co-Fe chain is parallel to the chain axis. Co and Fe atoms in the alloy have manifested a spin magnetic moment of $1.66 \mu_B$ and $3.0 \mu_B$, respectively. Meanwhile, it should be noted that mixed Co-Fe chain has an out-of plane easy axis of magnetization, as compared to pure Fe chain. The explanation for the switch of the easy axis from chain axis (in-plane), for Fe chain, to out of plane for mixed Co-Fe chain, is explained based on the second-order perturbation formula (Equation (3.2.1)), along with Table 3.3.

Table 3.3: The couplings between occupied and unoccupied states of different orbital symmetries and their contribution to the respective axis of magnetization. The vertical and horizontal arrows are assigned for in-plane and out-of plane direction of magnetization, respectively.

$\langle o_k u_l \rangle$	d_{xy}	d_{xz}	d_{z^2}	d_{yz}	$d_{x^2-y^2}$
d_{xy}	0	~ 0	~ 0	~ 0	\uparrow
d_{xz}	~ 0	0	\rightarrow	\uparrow	\rightarrow
d_{z^2}	~ 0	\rightarrow	0	\rightarrow	~ 0
d_{yz}	~ 0	\uparrow	\rightarrow	0	~ 0
$d_{x^2-y^2}$	\uparrow	\rightarrow	~ 0	~ 0	0

In Fig. 3.5 the orbital resolved density of states for Fe atom, namely d_{yz} and $d_{x^2-y^2}$, is presented, where dashed lines and full lines are assigned for Fe chains in the Co-Fe chain and pure Fe chain, respectively. Other symmetries of the d-orbitals of Fe have been analyzed and have not shown noticeable change by mixing Fe with Co. In Table 3.3 a summary of the spin-orbit coupling matrix elements of Fe atom is presented. Most importantly the spin-orbit coupling among different d -orbitals of Fe and the direction of magnetization they tend to favor is described. The elements of the matrix which favor in-plane or out-of plane magnetization axis are assigned by horizontal and vertical arrows, respectively.

For Fe atom in the Co-Fe chain the overlap with d-orbital of Co reduces the DOS of d_{yz} and $d_{x^2-y^2}$ near the Fermi-energy. Hence, from Eq. (3.2.1) the coupling $\langle d_{yz} | L_x | d_{x^2-y^2} \rangle$ favors in-plane direction of magnetization. Besides the from Fig.3.5 the Fe atom in Co-Fe chain has reduced DOS of d_{yz} and $d_{x^2-y^2}$ orbitals, and hence $\langle d_{yz} | L_x | d_{x^2-y^2} \rangle$ coupling. As a result of this effect mixing linear Fe atoms with Co switches the easy axis of magnetization from in-plane to out-of plane.

In this section we have seen the route to alloy magnetic elements in 1-D chains, which has significant difference from the case of alloy monolayers.[128] The effect of mixing 3d-elements on the magnetic properties depends on the dimension of the nanostructure, and this is related to the coordination number. Moreover, we have explicitly revealed that the in-plane easy axis of magnetization for pure Fe chain on Pt(997) surface can possibly be re-oriented to out-of plane by alloying it with Co.

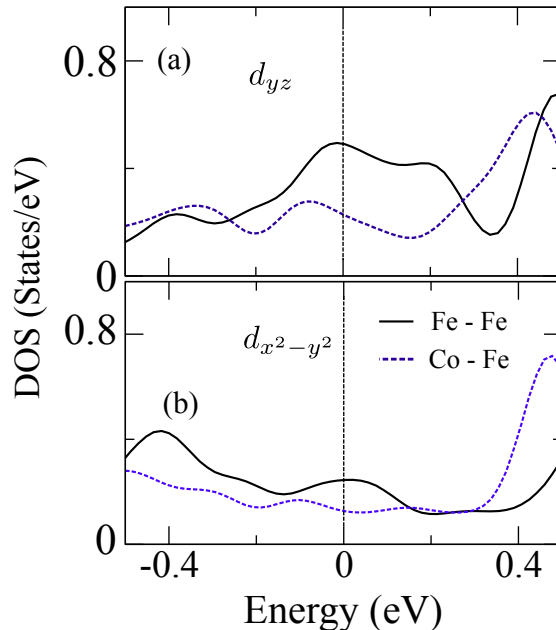


Figure 3.5: Orbital-projected minority states of the Fe atom in the Fe chain (full lines) and Co-Fe chain (dashed line). We have considered the d -orbitals of Fe which are degenerate near the Fermi energy, and showed significant change as result of alloying with the Co. In this plot (a) d_{yz} and (b) $d_{x^2-y^2}$ orbitals are shown.

3.4 The impact of electric fields on linear atomic chains

In this section we discuss the influence of the electric field on magnetic properties in the Co and the Co-Pt chains on Pt(111) substrate, The strength of the electric field varying from -1.0 V/\AA to 1.0 V/\AA is used. The positive electric field is directed towards the surface, which supports the atomic chains as shown in Fig. 3.6. Here we particularly analyze the tuning of the MAE ($E_{xz} = E_x - E_z$; $E_{yz} = E_y - E_z$) [Fig. 1(c)] of the Co and the Co-Pt chains on the Pt(111) surface by means of the electric field. The MAE of the Co chain and the Co-Pt chain as a function of the electric field is presented in Fig. 3.7.

For both Co and Co-Pt chains the MAE shows linear-like dependence as a function of the electric field, and the MAE is enhanced when the strength of the electric field, directed outwards from the surface, increases. The relative variation of the MAE (E_{xz}), when the electric field changes from 1.0 V/\AA to -1.0 V/\AA is 67 % and 57 %, for the Co chain and the Co-Pt chain, respectively. Whereas E_{yz} increases by 34 % and 39 %, in the same electric field range.

The change of MAE in the absolute value is as large as 1.2 meV for the Co chain and 1.4 meV for the Co-Pt chain. Above discussed results suggests that for higher electric field one can switch easy axis, from out of plane to into plane along the chain (intermediate axis). The origin of the change in the MAE is related to the spatial redistribution of the electronic density in response to the electric field, and the corresponding changes of the density of states near the Fermi energy. Furthermore, the surface screening phenomena in ferromagnetic metals are found to be spin-dependent.[72] Fig. 3.8 (a) shows the density of states for p -orbital (majority and minority) of the Co atom in different external electric fields. The majority and minority p -electrons screen the electric field differently, in which the minority states show higher variation to the change of the electric field. This phenomenon

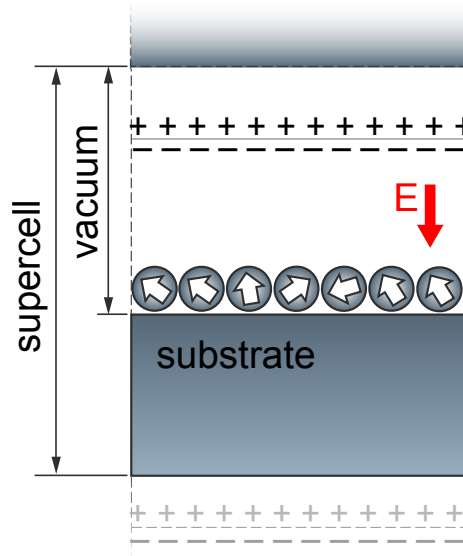


Figure 3.6: Characteristic model for atomic chains supported by Pt(111) surface and their interaction with electric field. Along z -axis the slabs are separated by $\sim 12 \text{ \AA}$ and the dipoles are located in of the vacuum which simulates the external electric field.

has once more revealed in the spin-polarized charge distribution on vertical cross-sectional area above the Co-Pt atomic chain. Fig. 3.9 shows the difference in the charge distribution when the system is exposed to the electric field of -0.8 V/\AA and 0.8 V/\AA [$\rho_{\uparrow(\downarrow)}(E = -0.8) - \rho_{\uparrow(\downarrow)}(E = 0.8)$] for both (a) the majority and (b) the minority spin channels. In this figure it is clearly seen that the effect of the external electric field on the minority states is stronger than on the majority ones. It is associated with the screening by the de-localized p -states [Fig. 3.8 (a)], which in turn affects d states in the Co atom and alters the magnetic properties.

In Fig. 3.8 (b) the orbital projected density of states for d -orbitals of the Co atom (d_{yz} and $d_{3z^2-r^2}$) in the Co-Pt chain is presented, for the electric field of -0.8 V/\AA , 0.0 V/\AA and 0.8 V/\AA . No significant changes are observed in d_{yz} , d_{xz} , and $d_{x^2-y^2}$ states near the Fermi energy. Depending on the direction and the magnitude of the electric field, the density of states near the Fermi level changes. In particular, when the electric field is changed from 0.8 V/\AA to -0.8 V/\AA , the density of $d_{3z^2-r^2}$ states just below the Fermi energy decreases and the density of d_{yz} states above the Fermi energy rises.

As it was mentioned in section 3.2.2, in the Co-Pt chain the interactions of d_{xz} and d_{yz} with $d_{3z^2-r^2}$, through \vec{l}_x operator ($\langle d_{xz(yz)} | L_x | d_{z^2} \rangle$), are responsible for the hard-axis configuration. For the electric field of -0.8 V/\AA there is significant decrease of $d_{3z^2-r^2}$ states just below the Fermi level, compared to these states at 0.8 V/\AA . The coupling $\langle d_{xz(yz)} | L_x | d_{z^2} \rangle$ for the field -0.8 V/\AA also decreases, compared to the couplings for the field 0.8 V/\AA . This increases the energy of the hard-axis configuration. Recalling the second order perturbation equation (3.2.1), one can see that the operator \vec{l}_x couples the occupied and unoccupied states of d_{xz} and d_{yz} with $d_{3z^2-r^2}$, and the coupling is stronger for 0.8 V/\AA than -0.8 V/\AA . This has an effect of decreasing the second term in the numerator at -0.8 V/\AA , which obviously gives higher MAE. Displacement of the atomic chains due to the electric field, *i.e.* 0.6 m\AA per 1 V/\AA in Co-Pt chain, is negligibly small.[74] In this chapter it was also shown that chemical composition of $3d$ ($5d$) strongly varies the magnetic anisotropy, sometimes by more

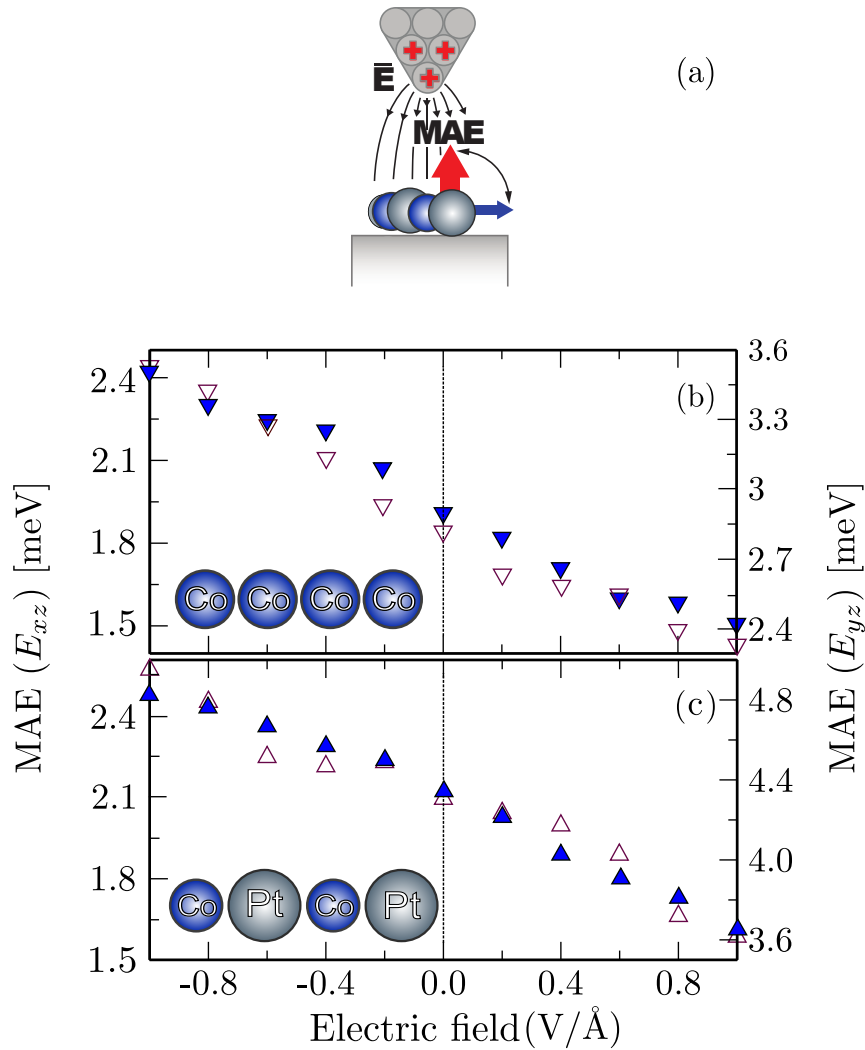


Figure 3.7: (a) Pictorial representation of atomic chains being exposed to an external electric field from STM or AFM tip. The effect of the electric field on the MAE of (b) the Co chains, and (c) the Co-Pt chain. In both cases [(a) and (b)] E_x , E_y and E_z are intermediate, hard and easy axes, respectively. The shaded triangles represent E_{yz} and unshaded triangles are for E_{xz} . [74]

than two fold. It was clearly depicted that geometrical relaxation has significant impact on the magnetic properties of the adsorbates.

The results we get for different atomic chain on vicinal surface of Pt manifest are comparable with the experimental values. For various quantization axis we analyze the change in the spin-orbit contribution, based on the variation in the spin-orbit matrix elements of d-states for the magnetic atoms. Finally, we have shown that the MAE of linear atomic chains can be tuned by using the modest strength of electric field.

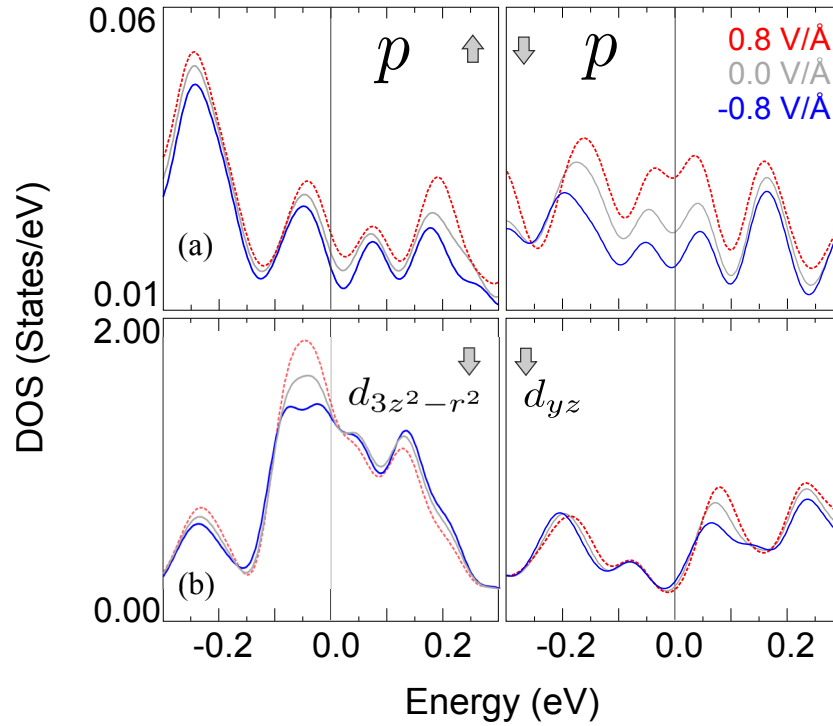


Figure 3.8: The density for p states of Co atom in the Co-Pt chain for spin up and spin down is presented (a). Orbital projected d-LDOS of Co atom in Co-Pt mixed chain for minority states of d_{xy} , $d_{3z^2-r^2}$ (b). The grey line, full line and dashed line represent density of states at -0.8 V/\AA , 0.0 V/\AA and 0.8 V/\AA electric fields, respectively.[74]

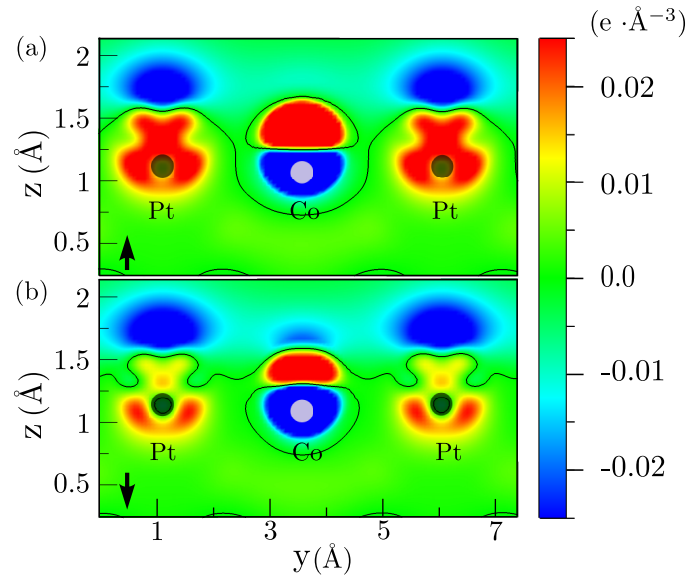


Figure 3.9: The difference in the charge distribution at -0.8 V/\AA and 0.8 V/\AA plotted over vertical section which crosses the atomic chains, for (a) the majority and (b) the minority states. The contour lines represent zero charge difference. The dimensions z and y measure the vertical and the horizontal distances of the cross-section. [74]

Chapter 4

Tailoring magnetic properties of thin films with quantum well states

Association of the 1-D quantum well states in thin films with magnetic properties is covered in this chapter. More specifically, the correlation of magnetic anisotropies and spin-polarization as function of the thickness of Fe and Co thin films will be discussed. The other field of concern is the dependence of the magnetic anisotropy on the thickness of the non-magnetic overlayers. In addition, emphasis will be given to the influence of external electric field on the spin-dependent quantum well states, and hence on the magnetic properties.

4.1 Quantum size effect and magnetic properties of thin films

Potential applications in nanotechnology often utilizes thin films. When such components of electronic devices are reduced to nano-scale quantum size effect becomes important and many properties of the nanostructure can be related to its presence [129, 75]. Following the prediction of the quantum-size effects, [33] it was confirmed that confinement of electrons at this scale leads to the formation of discrete energy levels, *i.e.*, quantum well states (QWS). One-dimensional (1D) QWS in thin adsorbate films can affect the electronic structure and spin polarization of the surface, [130, 131, 132, 39] and thus the MAE of the system [31]. Basically, the physics of QWS is well understood: QWS exist as a result of delocalized electrons, being confined in a potential well [33]. In thin adsorbate films, the bounding potentials of the substrate and vacuum determine the confinement state that affects the properties mentioned above. If the potential or the band structure of the delocalized electrons is spin polarized, then the QWS will manifest spin-dependent character [129, 72]. In prototype metal films, e.g Ag/Fe(001), the existence of QWS with *s, p* character spin-polarization originating from the spin-dependent boundary conditions of the magnetic substrate has been demonstrated [46].

Further investigations of low-dimensional magnetic systems, which are major candidates for spintronics technology, revealed noticeable quantum confinement features [27, 133, 46]. For instance, an oscillatory magnetic anisotropy dependence was measured as result of the variation of the Cu overlayer deposited on Co thin films suggesting that the *s, p* QWS modulate the magnetic properties of the Cu/Co(001) interface [134]. Spin-polarized QWS were also found in similar systems which could play a role in a possible transmission of

magnetic information between two magnetic layers [47]. As a particular example, it has been demonstrated that in the spin-dependent transport properties of magnetic tunneling junctions based on Fe thin films, the contribution from the QWS to the resonant tunneling through the iron-films is significant [135]. From atomic orbitals perspective, QWS are usually comprised of quasi-free (s,p -like) electrons, however, the existence of d -QWS has also been revealed [45, 43]. Basically, the momentum of the QWS within the potential of the thin film at the interfaces varies as a consequence of the variation of the film-thickness [46, 34]. The potential mismatches at the boundaries of the thin film determine the confinement state that affects the properties mentioned above. If the bounding potential or the band structure of delocalized electrons are spin-polarized, then QWS is expected to be spin-dependent. For instance, spin-polarized QWS of electron gas, [48] and spin-split dispersions in Co thin films on Mo(110) have been measured [32]. Further experimental studies on ferromagnetic Fe,[136] and Co [137] films show an oscillatory uniaxial anisotropy having a period of few monolayers. It has been found that in strongly correlated oxide ultra-thin films such as $SrVO_3$, orbital-selective QWS with d -character also exist [45].

The electronic-structure modeling of nano-sized systems encompasses the interplay between quantum size effects and the magnetic properties of different superlattices as well [138, 139, 123]. Alloying of supported Fe and Co layers with large spin-orbit coupling substrates,[140, 44] *e.g.* Pt, often leads to an enhancement of MAE, [141] as shown by Oda *et al.* Moreover, not only the magnetic anisotropy can be affected, but also the exchange interaction between ferromagnetic layers through a non-magnetic medium [142, 143, 144, 145].

The above mentioned examples essentially take into account only two parameters, the chemical composition and the size of magnetic nanostructures in order to modify the magnetic properties. As already mentioned in the first chapter, alternatively, one can manipulate the electronic and magnetic properties of the nanostructures by using external electric fields which change the charge carriers of the nano-sized systems [120, 55, 73, 146]. For tuning the spin degrees of freedom of such systems, electric fields are preferred over the magnetic ones, due to their ability to control the magnetic properties in a local way [55], resulting in the reduction of energy consumption in the magnetic data-storage mechanisms involved [120]. Such magneto-electric coupling in complex alloys is essentially mediated either by the hybridization between the orbitals of the magnetic atoms and the non-magnetic ones having large spin-orbit coupling [141], or directly with the atoms of the surface [147]. In such systems, the variation of the magnetic properties is commonly attributed to the screening of the electric field by the adsorbate. Moreover, an applied external electric field may not simply involve the screening of surface charges, but the confined electrons in the thin films are also affected.

In the next sections we reveal how the magnetic properties of the Fe(Co) thin films deposited on a Pt(001) substrate are related with QWS of the magnetic thin films having d -character. For both capped and uncapped Fe multilayers, we observe a strong thickness-dependence of MAE and, simultaneously, the switching of the easy axis from out-of plane to in-plane as the metallic-layer thickness is increased, while for the Co-systems the axis of magnetization remains mostly in-plane. These changes in the magnetic properties can be explained in terms of spin-dependent quantum well states in the magnetic thin films. In addition, for the case of Fe multilayers, a significant enhancement in MAE has been observed as a result of Pt-capping.

4.2 Fe multilayers on Pt(001) surface

In order to study the dependence of the magnetic properties with respect to the magnetic film thickness, we calculate the magnetic anisotropy and orbital anisotropy for different number of Fe multilayers deposited on Pt(001). For the case of a single Fe monolayer on Pt(001), we have found a MAE of 0.8 meV/magnetic atom having an out-of plane axis of magnetization, as shown in Fig. 4.1 (represented in circles). For larger Fe-layers ($2 \leq N \leq 9$), $[\text{Fe}]_N/\text{Pt}(001)$, MAE significantly reduces to roughly ~ 0.3 meV in average. In addition, MAE varies exhibiting an oscillatory behavior in the axis of magnetization, from out-of plane to in-plane direction. A similar behavior in MAE has been already observed in Fe films supported on Au(001) [148], and Ag(001)[136].

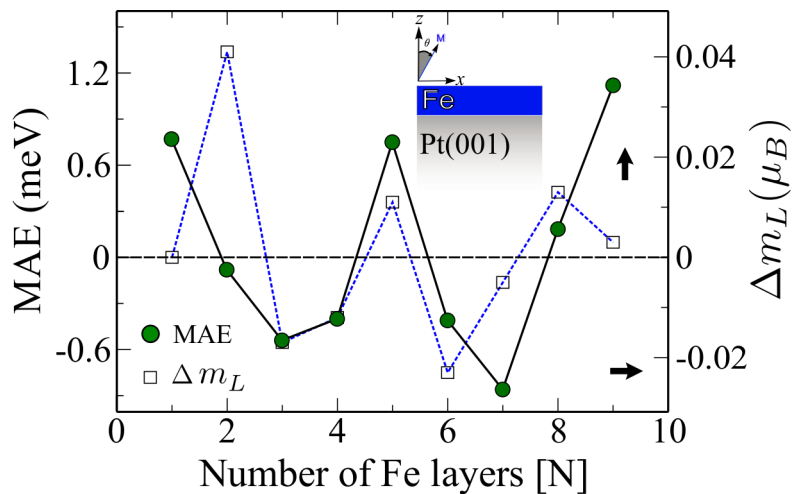


Figure 4.1: Magnetic anisotropy energy (circles), defined as $\text{MAE} = E_x - E_z$ in meV, for $[\text{Fe}]_N/\text{Pt}(001)$ multilayers as a function of the Fe-thickness for $1 \leq N \leq 9$, being N the number of Fe layers, is shown. A positive (negative) sign in MAE indicates an out-of plane (in-plane) axis of magnetization (easy-axis), respectively. The orbital moment anisotropy (rectangles), $\Delta m_L = m_z^L - m_x^L$, thickness-dependence is also presented [149].

Commonly, for ferromagnetic thin films of Co and Fe multilayers, MAE can be understood in terms of the variations of the orbital moment components. In general, the highest orbital moment component lies in the easy-axis. The link between MAE and orbital anisotropy (OMA) [$\Delta m_L = m_z^L - m_x^L$] is known as the Bruno's relation, $\text{MAE} = \xi/4 (m_z^L - m_x^L)$, where ξ is the spin-orbit constant of the magnetic layer [117, 116]. In Fig. 4.1, the relation between the orbital moment anisotropy, the orbital magnetic moment difference between out-of plane and in-plane quantization axes, as function of Fe-thickness is also plotted and compared with the MAE behavior. Clearly, one can observe that OMA exhibits a similar oscillatory trend like that of the MAE. In other words, the Bruno's relation is fulfilled. Furthermore, the changes in MAE and OMA can be related to the occurrence of spin-polarized quantum-well states in the iron thin films. But, let's first illustrate QWS from the band energy perspective using Bohr-Sommerfeld quantization conditions, Eq. 1.2.2 [37, 38]. The phase shift of the confined states at the interface with the substrate (ϕ_s) is function of the Fe band mismatch with Pt, and ϕ_v depends on the vacuum energy level, which is deduced from the Fermi energy and work function of Fe [38]. Thus, the nature of the QWS is defined by the band mismatch between Fe and Pt, which mainly involves minority bands, and the vacuum energy level.

Hence, the confined states within the magnetic films, bounded by the interfaces Fe/Pt and Fe/vacuum are expected to lead to a shift in the occupation number of the spin-polarized density of states (DOS) as the size of the film varies.

In Fig. 4.2 we have plotted the electronic band dispersion of *fcc* Fe (a) and Pt (b) along high symmetry points ($\Gamma \rightarrow X$ and $\Gamma \rightarrow M$). The dispersion for Fe are spin-split in which the majority and minority bands are represented by dashed (red) and dotted (blue) lines. There exist a band mismatch between minority bands of Fe and Pt along Γ -M, and this band just above the Fermi energy is mainly composed of $d_{xz(yz)}$ orbitals. It is also shown that the band mismatch is higher along $\Gamma \rightarrow M$ direction. It could be a hint that in thin films of Fe on Pt substrate these orbitals have high probability to be confined within a potential Fe/Pt and Fe/vacuum.

Coming back to the thickness dependence of the MAE, in Fig. 4.3 we plot the spin-resolved d and total DOS of the Fe slabs of different thicknesses (3 to 8 monolayer). A substantial change can be observed near the Fermi level for all the considered Fe-thickness in the minority band, in contrast with the majority one. It is worth to mention that for both spin channels there is strong contribution of d_{xz} and d_{yz} orbitals (dotted curves). The spin-up band, n_{\uparrow} , (majority band) is less sensitive to such variations since the majority band mismatch between Fe and Pt hardly exist (Fig. 4.2) As the magnetic film thickness increases the shift in the minority band (n_{\downarrow}) is enhanced, as shown in Fig. 4.3.

Meanwhile, the shift of the minority bands when the thickness of Fe increased (shown in triangles), which is a typical characteristics of QWS, is mainly driven by states of $d_{xz(yz)}$ and $d_{x^2-y^2}$ symmetries. In addition, we also observe s, p QWS which are highly dispersive bands and have small effective masses. We believe that the variation of $d_{x^2-y^2}$ orbitals is assisted by s, p QWS via $sp - d$ hybridization. It should be also noted that the rest of the orbitals that are not presented in Fig. 4.3 have not shown a significant size-dependent effect.

The variations of the DOS can be directly associated with changes in MAE through the second order perturbation formula [117, 116], re-writing equation (2.5.4) as

$$MAE \sim \frac{(\xi)^2}{\epsilon_u - \epsilon_o} \sum_{u,o} |\langle o|L_z|u\rangle|^2 - |\langle o|L_x|u\rangle|^2, \quad (4.2.1)$$

where o and u are occupied and unoccupied states. It is already clear that the states close to the Fermi level are the ones which give the main contribution to MAE. Insights about the changes in the spin-orbit coupling among d -orbitals of magnetic layers can be inferred directly from features of the DOS. Hence, one would expect to explain the trends in MAE in terms of the variations of the density of states. After analyzing all the d -orbital matrix elements in Eq. 4.2.1, which give the magnetic properties in the magnetic multilayers, we found that the main contributions to MAE are made by the coupling between the occupied and unoccupied states of d_{xy} with $d_{x^2-y^2}$, by \vec{L}_z operator ($\langle d_{xy}|L_z|d_{x^2-y^2}\rangle$), whereas the coupling of $d_{xz(yz)}$ with d_{z^2} and $d_{x^2-y^2}$ states ($\langle d_{xz(yz)}|L_x|d_{x^2-y^2}\rangle$) contribute to the second part of Eq. 4.2.1. From Fig. 4.3, one can see, for almost all the considered Fe-thickness, a depletion in the d_{xz} and d_{yz} unoccupied states above the Fermi level and smaller density of $d_{x^2-y^2}$ orbitals close to the Fermi energy. Hence, decreasing the coupling $\langle d_{xz(yz)}|L_x|d_{x^2-y^2}\rangle$, which favors an in-plane magnetization. Such reduction of the second term in Eq. 4.2.1 is particularly observed for the case of Fe multilayers having 5 and 8 Fe-monolayers which show a perpendicular magnetization. Similarly, for $[\text{Fe}]_{4(7)}/\text{Pt}(001)$ systems, the DOS near the Fermi energy is mainly described by $d_{xz(yz)}$ and $d_{x^2-y^2}$ orbitals, which also strongly favor an in-plane magnetization axis.

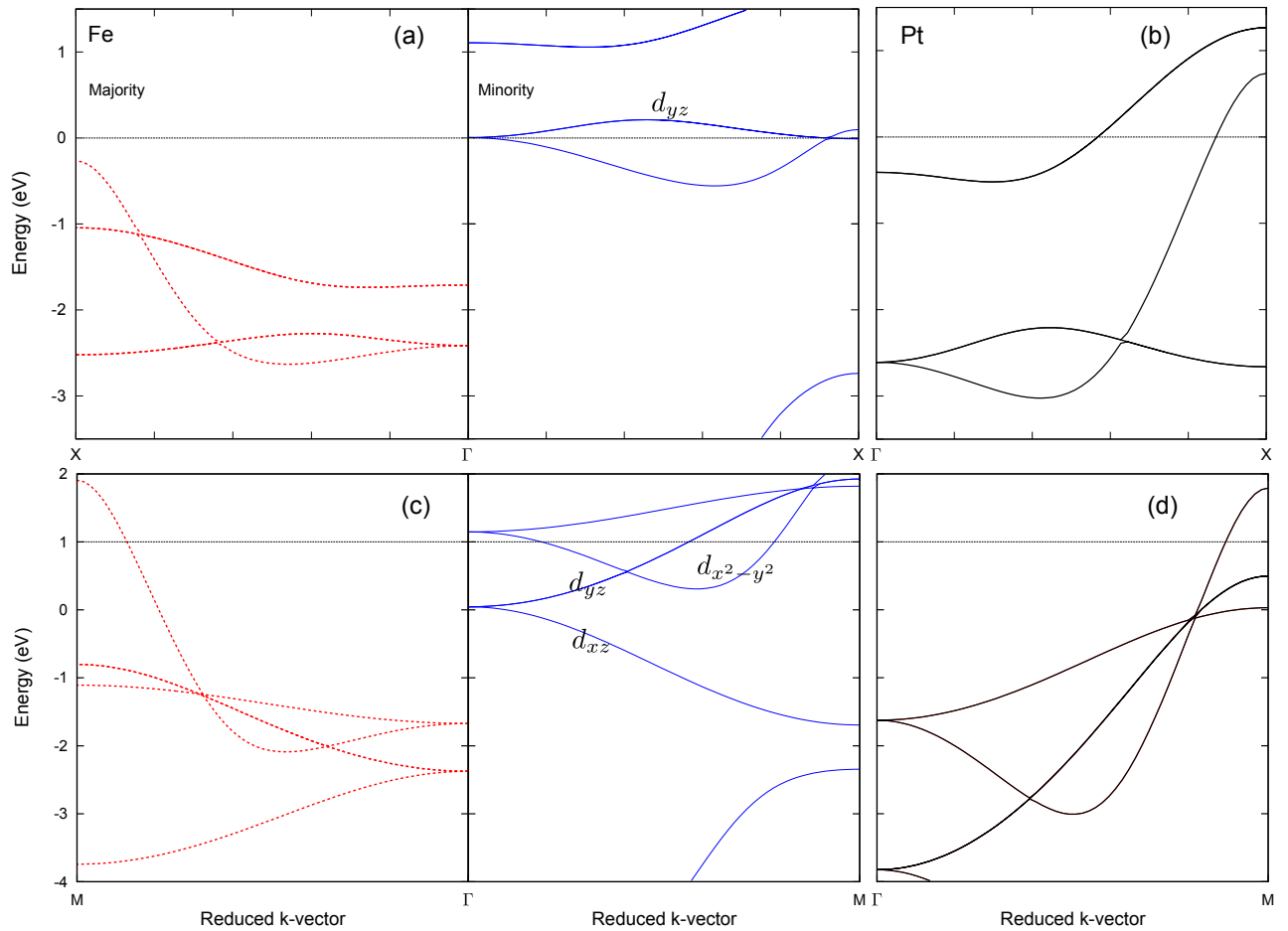


Figure 4.2: Electronic band dispersion of *fcc* Fe (a and c) and *fcc* Pt (b and d), along high symmetry points in the Brillouin zone. The minority and majority bands of Fe are represented by full (blue) and dashed (red) lines. The band dispersion is drawn along high symmetry directions of $\Gamma \rightarrow X$ (higher panel) and $\Gamma \rightarrow M$ (lower panel).

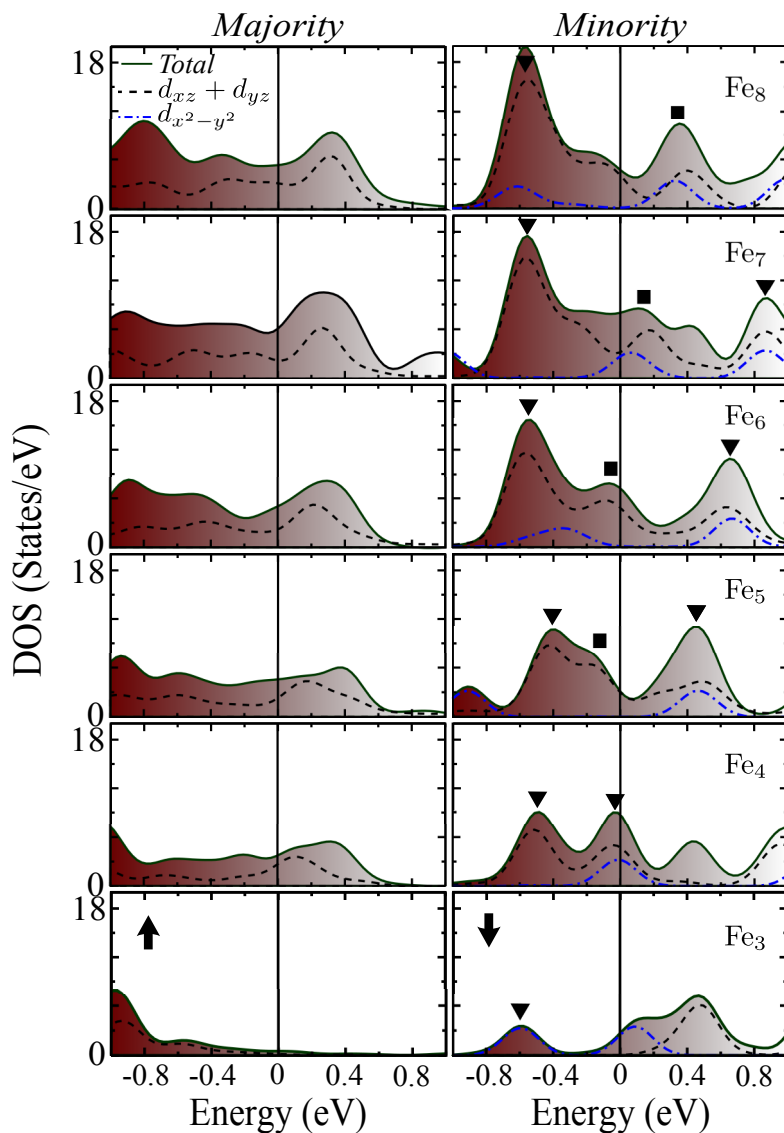


Figure 4.3: Majority (minority) density of states, DOS, (solid lines) for $[\text{Fe}]_N/\text{Pt}(001)$ with $3 \leq N \leq 8$, close to the Γ is plotted. The dotted lines represent the contribution from both the d_{xz} and d_{yz} orbitals and the projection on $d_{x^2-y^2}$ orbital is assigned by dotted and dashed line. The triangle and rectangle arrows guide the shift in DOS as the Fe-film thickness is increased[149].

4.3 Capping $[\text{Fe}]_N/\text{Pt}(001)$ with a Pt-monolayer

In order to obtain further understanding of the MAE behavior in Fe multilayers, we now explore the effect of capping such layered-systems with a Pt-monolayer, i.e., $\text{Pt}/[\text{Fe}]_N/\text{Pt}(001)$. It has been predicted that capping Fe monolayer with non-magnetic ones usually yields in a significant enhancement of the MAE [141, 150]. X-ray magnetic circular dichroism (XMCD) measurements at low temperature report a perpendicular magnetization for Pt-capped Fe-monolayers on Pt [151]. In agreement with these previous results [141, 151], we also found a large MAE for $\text{Pt}/\text{Fe}/\text{Pt}(001)$. For this particular system, MAE reaches ~ 5 meV having an out-of plane axis of magnetization. Such strong enhancement in MAE, in comparison with the uncapped Fe monolayer on Pt (0.8 meV/atom) is attributed to a depletion in the minority d_{xz} and d_{yz} Fe-orbitals near the Fermi energy, as consequence of a strong hybridization of Fe with the capping Pt layer [141]. For larger Fe-thickness, namely, $2 \leq N \leq 9$, the magnetic properties in the $\text{Pt}/[\text{Fe}]_N/\text{Pt}(001)$ multilayers are strongly modified, as can be seen in Fig. 4.4. For instance, when a second Fe-layer is added, i.e., $\text{Pt}/[\text{Fe}]_2/\text{Pt}(001)$, MAE abruptly decreases from 5 to ~ 2.5 meV per atom exhibiting magnetization reversal from out-of plane to in-plane. For $N \geq 4$, MAE has a value of 3 meV/atom in average and the in-plane axis of magnetization always remains to be the easy axis. In this particular case, the variations in MAE can be explained as the result of a variation in the DOS near the Fermi level for the d_{xz} and d_{yz} orbitals which is not present in the case of $\text{Pt}/\text{Fe}/\text{Pt}(001)$, since for this capped system, the Fe-layers are partially hybridized between each other.

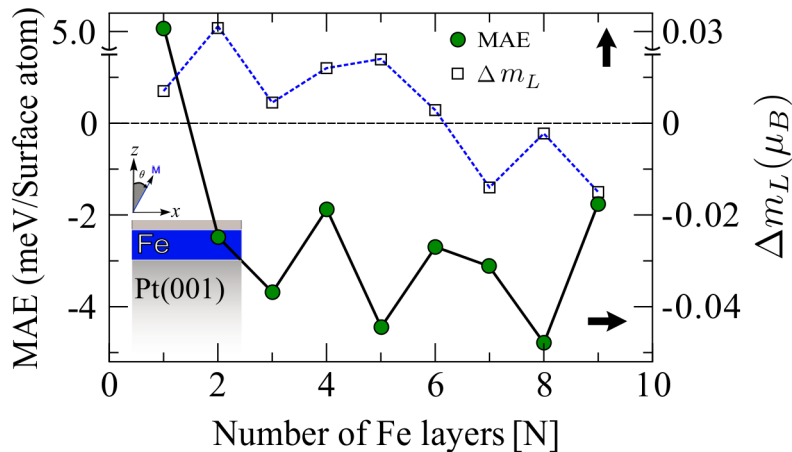


Figure 4.4: Magnetic anisotropy energy (MAE) in meV for $\text{Pt}/[\text{Fe}]_N/\text{Pt}(001)$ multilayers as a function of the Fe-thickness, $1 \leq N \leq 9$, where N is the number of Fe-layers is plotted. A positive (negative) sign of their MAE stands for out-of plane (in-plane) magnetization axis, respectively.[149]

One would expect that by capping $[\text{Fe}]_N/\text{Pt}(001)$ system with a single Pt-layer, the phase shift at the vacuum side (ϕ_v) tends to be altered as a result of the change in the vacuum energy level being replaced by Fe/Pt interface. It causes a difference in the work function of Fe and Pt terminated multilayers [Eq. 1.2.2]. This could hint that for $\text{Pt}/[\text{Fe}]_N/\text{Pt}(001)$ systems there exist similar scattering pattern at the two boundaries, since there are Pt-layers in both sides of the interface. Nevertheless, in both cases, the onset of QWS in the magnetic films is supposed to be present due to the quantum confinement conditions. Indeed, the MAE variations can be analyzed in terms of the spin-polarized QWS, finding a

similar behavior for both the capped and uncapped Fe multilayers. Furthermore, we have also analyzed the behavior of the orbital moments for the magnetic thin films in the capped-multilayer systems, finding in almost all the cases, that MAE and orbital anisotropy have not a direct correlation as in the uncapped systems. As an example, for Pt/[Fe]_N/Pt(001) having $2 \leq N \leq 6$, the higher orbital moment component is perpendicular to the surface (z -direction), while for the other cases, the higher orbital moment is directed along the easy-axis of magnetization.

The non-direct correspondence between MAE and OMA could be explained by using a more generalized second-order perturbation treatment of the spin-orbit coupling, which also takes into account all the atomic species (magnetic and non-magnetic) [117, 152]. The formulation for all atomic species were made using similar approach in Ref. [117], i.e. the energy contribution to the magnetic anisotropy and orbital moment of specific magnetization axis in second order perturbation of the spin-orbit coupling, $\mathbf{H}_{so} = \xi \mathbf{L} \cdot \mathbf{S}$. The energy difference between the two magnetization axes can be written as a sum over the atomic species (q) [152],

$$\Delta E_{soc} = \sum_{qss'}^n \{E_q^{ss'}(x) - E_q^{ss'}(z)\}, \quad (4.3.1)$$

where s and s' correspond to the spin indices of occupied, and unoccupied states which are included as double sum. Similarly, the orbital anisotropy can be expressed as sum over spin index. In these formulations, orbital anisotropy and magnetic anisotropy, the sum over all sites have an off site contributions ($q' \neq q$), through spin-orbit on different sites. Obviously, these contribution become significant for species which are strongly hybridized with high spin-orbit coupling at the other site. On the other hand, the spin diagonal anisotropy energy term and the spin-dependent ($s=\pm 1$) orbital anisotropy contribution have direct relation [152],

$$\Delta E_q^{ss'} = s \frac{\xi}{4\mu_B} \Delta m_{L,q}^s. \quad (4.3.2)$$

For instance, for Fe atoms the difference in the anisotropy between spin-up bands ($\Delta E_{Fe}^{\uparrow\uparrow}$), as well as between spin-up and spin-down bands ($\Delta E_{Fe}^{\downarrow\uparrow}$) are avoidable, due to low density of unoccupied (majority) states of Fe close to Fermi energy, see Fig. 4.5. If one ignores the off-site spin-orbit coupling, the spin-flip term, Eq. 4.3.2 leads to Bruno's relation. However, for the case where Fe atoms are strongly bonded with the high SOC elements (e.g. Pt), the spin-flip contribution term ($\Delta E^{\downarrow\uparrow}$) is not negligible, such as in the case of strong SOCs (e.g. Au/Co/Au).

It is interesting to investigate how the spin-polarization of the QWS depends on the Fe-thickness, for both capped and uncapped thin films, since the various properties of the multilayers are mainly determined by the electrons near the Fermi energy. The spin-polarization (SP) of the confined states in iron thin films can be defined as follows:

$$SP(E) = \frac{n_{\downarrow}(E) - n_{\uparrow}(E)}{n_{\downarrow}(E) + n_{\uparrow}(E)} \quad (4.3.3)$$

where $n_{\downarrow(\uparrow)}(E)$ stands for the minority (majority) states, respectively. In Fig. 4.6 the average spin-polarization of the QWS all magnetic layers at, and around the Fermi energy, namely the average $SP(E_f)$ and $SP(E_f \pm 0.1\text{eV})$, is presented as a function of the Fe-thickness

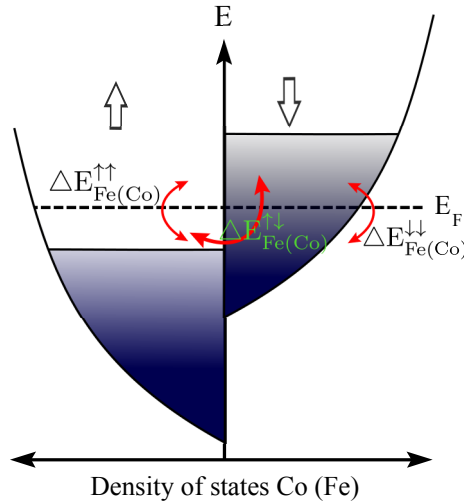


Figure 4.5: Schematic model for majority and minority density of states of $\text{Fe}(\text{Co})$. The possible contribution to the specific magnetization axis in the second-order treatment of the spin-orbit coupling. The coupling between minority and majority density of states is shown by $\Delta E_{\text{Co}(\text{Fe})}^{\uparrow\uparrow}$ and $\Delta E_{\text{Co}(\text{Fe})}^{\downarrow\downarrow}$ respectively. Whereas, the spin-flip term is represented by $\Delta E_{\text{Co}(\text{Fe})}^{\downarrow\uparrow}$.

for both capped and uncapped Fe multilayers. First, similar trend in the behavior of SP is observed in both capped and uncapped Fe multilayers. Nevertheless, the SP is strongly sensitive to the Fe-thickness, for instance, in the case of uncapped Fe-multilayers having a single Fe monolayer SP varies from having $\sim 40\%$ minority polarization to $\sim 60\%$ majority polarization after capping the system with two more Fe-layers, i.e., $[\text{Fe}]_3/\text{Pt}(001)$, as can be seen. Indeed, it is a manifestation that the SP can be switched from minority to majority polarization as the thickness of Fe layer increases. Additionally, for states above the Fermi level, an oscillating SP behavior was also observed [Fig. 4.6] as the number of Fe-layers is increased. For higher thickness the oscillations are damped showing a reduced SP for $N \geq 4$. The fact that SP varies for different Fe thickness is a clear evidence for the existence of spin-dependent QWS.

The above results suggest that SP of the QWS can affect the tunneling magnetoresistance (TMR). The TMR can be expressed by using the tunneling current of for parallel and anti-parallel alignments of the the tip and monolayers layers [153].

$$TMR = \frac{I_{\uparrow\uparrow} - I_{\uparrow\downarrow}}{I_{\uparrow\downarrow}}. \quad (4.3.4)$$

The relation between TMR and SP can be found by using thr Julliere's formalism [154]. The magnetization of each layer that form the TMR sandwich as function of SP can be written as

$$\vec{m}_{1(T)} = (n_{\downarrow} + n_{\uparrow})SP_{1(T)}\vec{\mu}_{(1)T}, \quad (4.3.5)$$

$\vec{\mu}_{(1)2}$ are the unit vectors that define the direction of the spin moments. In terms of the SP the tunneling current can be expressed as

$$I(E) = I_0(E)(1 + SP_1(E)SP_T(E)\vec{\mu}_1 \cdot \vec{\mu}_T). \quad (4.3.6)$$

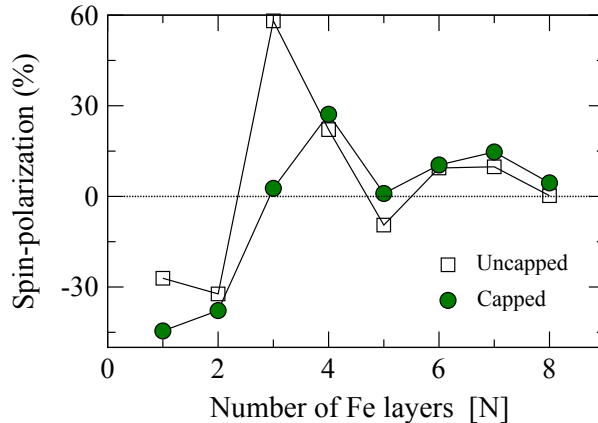


Figure 4.6: Spin-polarization of QWS in $[\text{Fe}]_N/\text{Pt}(001)$ (rectangles) and $\text{Pt}/[\text{Fe}]_N/\text{Pt}(001)$ (circles) as a function of Fe-thickness, averaged from the SP at the Fermi level (E_f), above the Fermi level ($E_f + 0.1$) and below the Fermi level ($E_f - 0.1$) [149].

Employing Eq.(4.3.4), the TMR is described as function of $SP_1(E)[SP_T(E)]$,

$$TMR(E) = \frac{2SP_1(E) \cdot SP_T(E)}{1 - SP_1(E) \cdot SP_T(E)}, \quad (4.3.7)$$

$SP_1(E)$ and $SP_T(E)$ are the spin-polarization of each magnetic layers and the STM tip. Actually, experimental investigation on the SP of Fe and Co thin films could be done by using scanning tunneling spectroscopy (STS) [49], since the DOS profile for the top two layers of Fe is similar to the DOS presented in Fig. 4.3. In other words, the TMR of tip and sample should be affected by the SP of the QWS. In order to confirm the argument, in Fig. 4.7 we have plotted the spin-polarization, only for the top two layers, of the Fe multilayers supported by Pt(001) substrate. It is clearly shown that the SP for the top two Fe layers resembles the SP of the whole Fe multilayers, i.e. the SP in the two cases are comparable. Assuming all other parameters are well optimized, based on Eq. 4.3.6 two and four layers of Fe are expected to have high TMR.

As summary, the spin polarization of the Fe films is rather sensitive to the film thickness. Experimentally the SP of magnetic multilayers can be studied with scanning tunneling spectroscopy (STS) [49, 155]. Our investigations on QWS and SP also suggest that spin-dependent transport in similar systems should also be influenced by quantum size effect phenomena [155].

4.4 Co multilayers on Pt(001) surface

In this section we present the results concerning Co-multilayers on Pt(001). First the MAE as a function of the Co-thickness is presented in Fig. 4.8. The values of MAE for a single and two Co-layers on Pt(001) was predicted to to be 0.83 meV and 0.78 meV per atom respectively, having an in-plane direction of magnetization. Experimental study of one and two monolayers of Co supported by Pd(001), at low temperature, have also an in-plane axis of magnetization[156].

The calculations for larger Co-thicknesses show an in-plane axis of magnetization for all the cases except $[\text{Co}]_7/\text{Pt}(001)$, which has a perpendicular axis of magnetization but a very

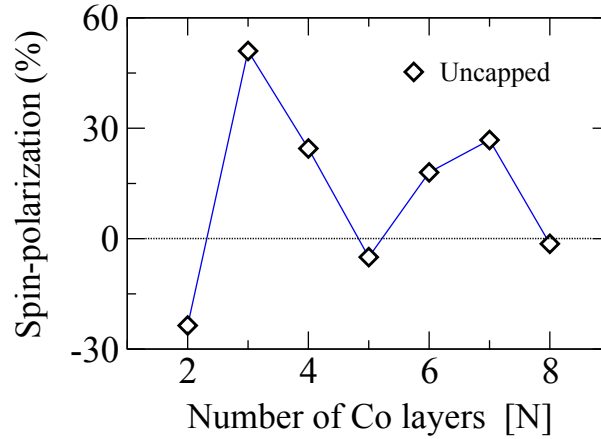


Figure 4.7: The spin-polarization of the QWS, only for the top two Fe layers, in $[\text{Fe}]_N/\text{Pt}(001)$ systems as function of different number of Fe layers is plotted. The SP is averaged from the SP at the Fermi level (E_f), above the Fermi level ($E_f + 0.1$) and below the Fermi level ($E_f - 0.1$).

small MAE value (~ 0.1 meV). Experimental studies employing different techniques, have been done on Co layers grown in layer-by-layer mode, and magnetic properties were also measured. Our results are in accordance with experimental results of Co-films on Pt(001), specifically, in both cases the easy axis of Co layers, with thickness $N \geq 5 \text{ \AA}$, lies in-plane of the surface [157]. The orbital moment anisotropy as a function of Co-thickness is also calculated and shown in Fig. 4.8. As in the uncapped Fe multilayers, here, we also find a direct correspondence between MAE and OMA, which can be explained in terms of the Bruno's formula [117].

Once again we can explain the correlation between the MAE and the spin-polarized QWS of the Co thin films. Similar to the case of uncapped Fe multilayers the variation of the DOS have been analyzed and the change in the MAE is attributed to the redistribution of the DOS of d orbitals close to the Fermi energy.

4.5 Capping $[\text{Co}]_N/\text{Pt}(001)$ with Pt monolayer

This section discuss the results for Pt capped Co films on Pt(001) substrate. The relation between MAE and the number of Co layers is provided in Fig. 4.9, and it is shown that capping Co multilayer with Pt strongly increases the value of the MAE for all layers, except for a monolayer of Co (as compared with Fig. 4.8). For the Co monolayer on Pt(001) surface, the capping layer strongly reduces the magnitude of the MAE from -1 meV to -0.2 meV. For $N \geq 2$ the MAE has an oscillatory behavior, in which a highest value of the in-plane anisotropy have been observed at four layers of Co. These results are in agreement with magneto-optical Kerr effect (MOKE) and x-ray measurements which show in-plane easy axis for Pt capped Co multilayer [157].

In addition, the orbital moment differences $[\Delta m_L = m_z^L - m_x^L]$ of Pt/ $[\text{Co}]_N/\text{Pt}(001)$ system is presented in Fig. 4.9. The interesting feature in the MAE plot of Pt/ $[\text{Co}]_N/\text{Pt}(001)$ system is that for the MAE (circles) and OMA (rectangles) are inversely symmetric. Additionally, the higher value of the orbital moment is perpendicular to the surface plane (z -axis), except one monolayer of Co. Such incompatibility of orbital anisotropy with magnetic

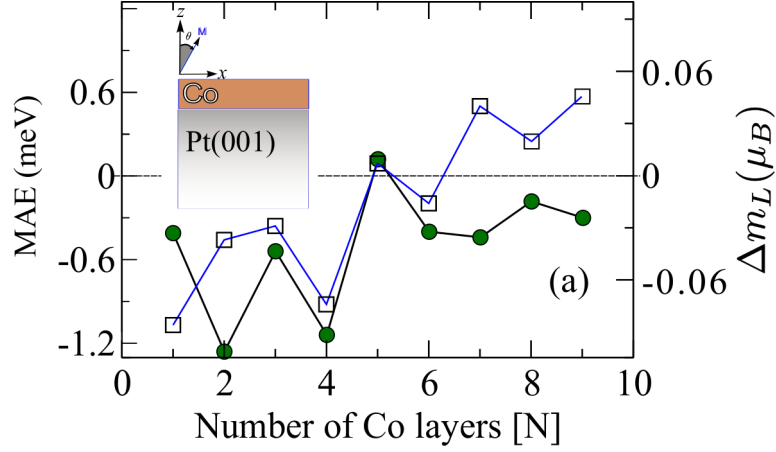


Figure 4.8: Magnetic anisotropy energy (circles), in meV as defined previously, of $[\text{Co}]_N/\text{Pt}(001)$ multilayers as a function of the Co-thickness for $1 \leq N \leq 9$, being N the number of Co layers, is shown. A positive (negative) sign of the MAE indicates an out-of plane (in-plane) easy-axis, respectively. Thickness-dependence of the orbital moment anisotropy (rectangles) in μ_B , is also presented [149].

anisotropy, unlike that of the uncapped Co multilayers, are well explained by emphasizing the spin-flip contribution ($\Delta E_{\text{Co}}^{\downarrow\uparrow}$). This term should be taken in to consideration for atomic species which are hybridized with high spin-orbit coupling elements.

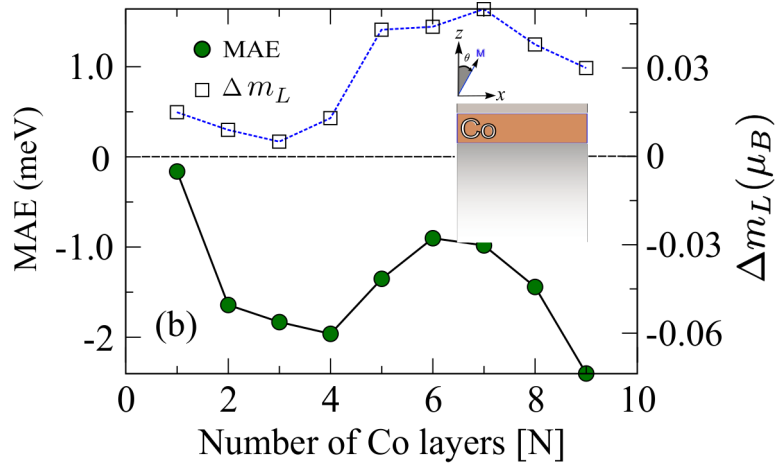


Figure 4.9: Magnetic anisotropy energy (circles) of $\text{Pt}/[\text{Co}]_N/\text{Pt}(001)$ multilayers as a function of the Co-thickness for $1 \leq N \leq 9$ is shown, where N is assigned for the number of Co layers. A positive (negative) sign in MAE indicates an out-of plane (in-plane) easy-axis, respectively. Thickness-dependence of the orbital moment anisotropy (rectangles) in μ_B , is also presented [149].

We have also investigated the correlation between MAE and spin-polarized QWS for Co thin films capped with Pt. In Fig. 4.10 the majority and minority DOS for Co multilayers ($3 \leq N \leq 8$) on Pt(001) and the d -orbitals which give the high contribution to DOS, namely, $d_{xz(yz)}$, $d_{x^2-y^2}$ and d_{z^2} are plotted. As in the case of Fe multilayers the majority band show insignificant variation, and the QWS of the minority carriers are driven by $d_{xz(yz)}$, (dashed lines) and $d_{x^2-y^2}$ (dotted lines) orbitals, which shifts towards the Fermi energy. However,

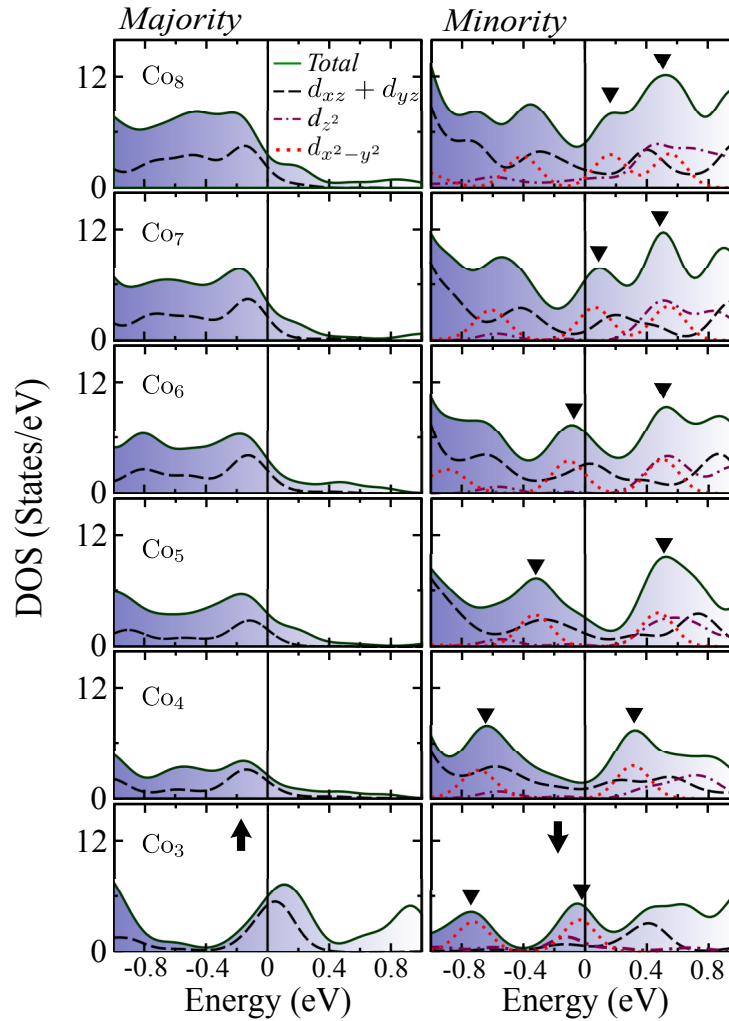


Figure 4.10: Majority and minority DOS of Pt capped Co multilayer on Pt(001) for $3 \leq N \leq 8$, close to the Γ point, are plotted. The dashed, dashed-dotted, and dotted lines represent the contribution from, $d_{xz(yz)}$, d_{z^2} and $d_{x^2-y^2}$ orbitals, respectively. The triangle arrows guides the shift in the DOS [149].

for $N \leq 4$ the minority d_{z^2} (dashed and dotted lines) component also provides contribution to the QWS moving towards the Fermi energy from unoccupied states. Here we point out that the magnetic layers undergo strong changes in the occupation numbers (Fig. 4.10, dashed lines) if the thickness of the film is modified. It should be mentioned that the projection of majority d_{z^2} is negligibly small and has thus been omitted.

For the understandings of the thickness dependence of MAE, we have analyzed the spin-orbit matrix elements. It turns out that the coupling between occupied and unoccupied states of d_{xz} (d_{yz}) with d_{z^2} and $d_{x^2-y^2}$ orbitals dominates couplings. These couplings favor an in-plane axis of magnetization [second term in Eq. 4.2.1], which is the case for most Co-layers in $\text{Pt}/[\text{Co}]_N/\text{Pt}(001)$ system. From Fig. 4.10 one can see a remarkable correspondence between the MAE plots, and the DOS plot close to the Γ point. For example, in Co multilayer of $3 \leq N \leq 8$ the high values of MAE are observed at 3 and 8 monolayers of Co, and from Fig. 4.10 for three layers of Co there are both $d_{xz(yz)}$, ($d_{x^2-y^2}$) and d_{z^2} orbitals, close to the Fermi energy. This will enhance the magnitude of an in-plane MAE, which is the second matrix element in Eq. 4.2.1. For Co trilayer ($[\text{Co}]_3$) the presence of d_{z^2} orbitals

close the Fermi energy could be related to hybridization effect of the Co layers with the interfaces. Further increase of Co layers shifts d_{z^2} orbitals to the higher unoccupied energy levels, however once again d_{z^2} orbitals can be found in a close proximity to the Fermi energy at $Pt/[Co]_8/Pt(001)$.

As summary, both occupied and unoccupied QWS are mainly driven by $d_{xz(yz)}$, $d_{x^2-y^2}$ and d_{z^2} states, and the presence of these orbitals near the Fermi energy established the connection between the enhanced in-plane MAE and the QWS. The magnetic anisotropy of the magnetic thin films originate not only from the surface anisotropy or top atomic layers but the the spin-dependent QWS have the strong contribution to it.

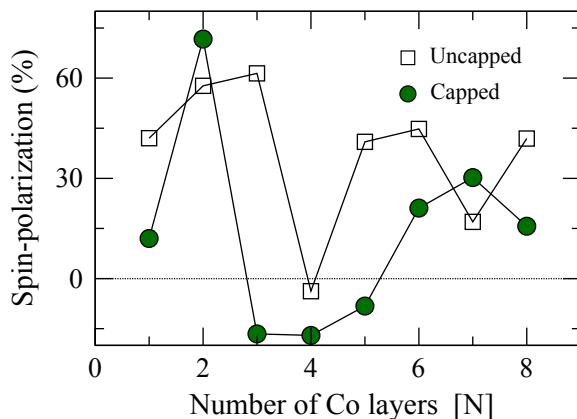


Figure 4.11: The spin-polarization of the QWS in $Pt/[Co]_N/Pt(001)$ (rectangles) and $Pt/[Co]_N/Pt(001)$ (circles) systems for different number of Co layers is plotted. It is averaged from the SP at the Fermi level (E_f), above the Fermi level ($E_f + 0.1$) and below the Fermi level ($E_f - 0.1$) [149].

Regarding the spin polarization near the Fermi energy for Co multilayers, in Fig. 4.11 we plot the average SP of the QWS with respect to the film thickness. For both capped and uncapped Co multilayers, the SP strongly varies when the thickness changes. For instance, the SP for three and four layers of Co can be as large as 60% and 5%, respectively. In almost all Co multilayers, the SP is positive with an exception of four monolayers of Co (Co_4). The transition of the polarization from majority to minority as the thickness of the Co layers increase agrees well with an experimental investigation of Park *et al.* on Co thin films [32]. Different from the results of Fe multilayers, here, capping thin films of Co with Pt strongly affects the SP. As an illustration, capping of three and five $[Co_3(5)]$ layers of Co with Pt induces a switch in the spin polarization. From Fig. 4.11 one can see that thicker films of Co ($N \geq 5$) have higher tendency to be polarized, as compared to Fe thin films.

Up to now the effect of thickness and capping on SP of the QWS is discussed for both Fe and Co thin films. In contrast to the SP of ultra-thin Fe films, $N \leq 2$, the first few Co thin films is oppositely polarized. This distinguishable difference can be seen in Fig. 4.11 (Co) and Fig. 4.6 (Fe). The other possibility to study the correlation between magnetic properties and quantum size effect phenomena in such alloyed multilayers is to alter the thickness of the non-magnetic overlayer. This relation will be discussed in the following section.

4.6 Influence of non-magnetic capping layers

It was mentioned earlier in section 4.1 materials which constitute Co(Fe)Pt alloys are indispensable candidates for hardening of perpendicular magnetic anisotropy [158, 159, 160, 8]. Large value of magnetic anisotropy in these systems is caused by the high spin-orbit coupling element (Pt) which is mediated by $5d-3d$ hybridization. In an experimental investigation it was shown that capping of Co clusters with Pt (Pd) strongly affects the magnetic order, *i.e.* the paramagnetic state of the cluster can be changed to ferromagnetic by capping the Co nanoparticles with thicker Pt layers [161]. Indeed, magnetic properties of Co(Fe) can be tailored by bringing it in contact with Pt. For example, it has been shown that the magnetic anisotropy energy of *hcp* Co is sensitive to the concentration of the Pt [162].

Experimentally the concentration of each of the components of such alloys could be controlled by irradiating the sample with proper energetic ions, hence one could control the magnetic properties of the alloy [163, 164]. Here we concentrate on a more manageable and controllable structure - capping layers.

4.6.1 Pt overlayers on Co ultra-thin films

Let us consider a magnetic heterostructure taking Fe(Co) ultra-thin films capped by a non-magnetic Pt or Cu layers. In Fig. 4.12 a sketch of this system is shown. We first start with the effect of the capping Pt multilayers, looking for the overlayer-thickness dependence of the system's magnetic properties. Similar to the structures in the past section, the Pt substrate is modeled by ten layers and we consider 1-6 Cu and Pt capping layers, and all the results are obtained in the relaxed geometry. The Co atom has magnetic moment of $1.8 \mu_B$, and the nearest Pt neighbors have an induced magnetic moment of $0.3 \mu_B$.

In Fig. 4.13 we have plotted the MAE of the $\text{Pt}_N/\text{Co}/\text{Pt}(001)$ system with respect to the size of the capping layer of Pt. As it was discussed in section 4.4 one layer of Co on Pt(001) surface has an in-plane MAE of ~ 0.4 meV. When this system is capped with one or two Pt layers the absolute value of the MAE decreases.

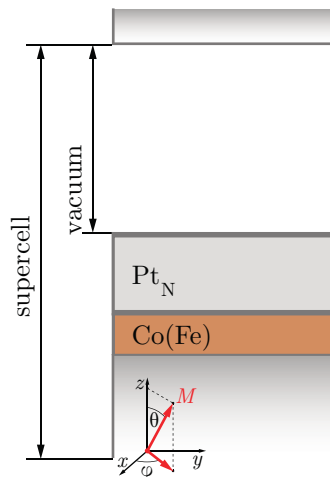


Figure 4.12: A model of Fe or Co monolayers capped with non-magnetic capping layers of Pt and Cu. The Fe(Co) is supported by Pt(001) surface and 1-6 layers of Pt(Cu) have been considered.

A peculiar effect is observed when the thickness of Pt overlayer increased. That is, cap-

ping the Co/Pt(001) with more than two layers of Pt, switches the easy axis of magnetization from in-plane to out-of plane direction. Additionally, the MAE is enhanced to ~ 2 meV for Pt₄/Co. For six capping Pt layers the MAE tends to decrease. In Fig. 4.13, the values of the MAE of Co monolayer embedded in an infinite slab of Pt(001) is also presented, and the value of MAE is found to be ~ 2 meV, whereas the easy axis is directed perpendicular to the Co-Pt interface plane.

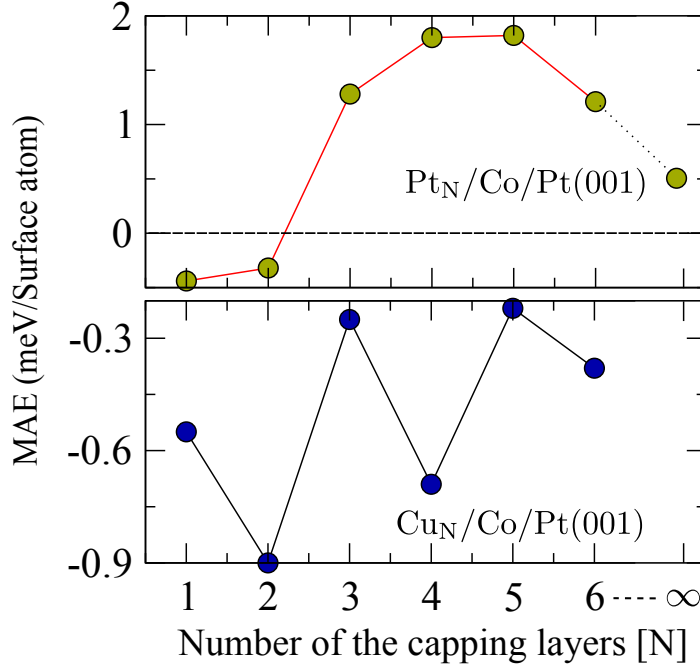


Figure 4.13: The magnetic anisotropy energy of (a) Pt_N/Co/Pt(001) and (b) Cu_N/Co/Pt(001) systems as function of the number of the capping layers is plotted. The negative and positive values of MAE represent in-plane and out-of plane magnetization axis, respectively.

For all layers of Pt in Pt_N/Co/Pt(001) the magnetization directed in the z -axis has higher orbital moment (for Co layer), and the orbital moment difference with respect to the in-plane axis is $0.02 \mu_B$, on average. This implies that for $N > 2$ the Pt_N/Co/Pt(001) system qualifies for Bruno's relation (Eq. 3.2.2), between MAE and orbital anisotropy. The induced spin and orbital magnetic moments of Pt could be up to $0.3 \mu_B$ for Pt atom at the interface and $0.05 \mu_B$ for the top Pt, *i.e.* it decays for Pt layers far away from Co-Pt interface (see Fig. 4.15). Such characteristic induced by non-magnetic capping on the ferromagnetic layer is also observed in other studies [165, 166]. For $N > 5$ the easy axis of magnetization remains out of plane but the value of MAE reduces.

To understand these changes in the MAE from the variation of the electronic structure near the Fermi energy, in Fig. 4.14 we have plotted the DOS of Co atoms capped with two and four layers of Pt. Most of the orbitals have not shown significant changes as the thickness of the Pt capping layer changes from two to four layers. Specifically, when the system is capped by four Pt layers the unoccupied states of d_{xy} and occupied states of d_{z^2} , near the Fermi energies, have shown an increase in the density of states. But the unoccupied states of d_{z^2} orbital of Co atom capped with two layers of Pt is also enhanced. From the spin-orbit coupling matrix element and DOS plot we have observed strong change of the $\langle d_{xz(yz)} | d_{z^2} \rangle$ and $\langle d_{xy} | d_{x^2-y^2} \rangle$ couplings, following the variation of the thickness of the Pt overlayer. By

referring equation (4.2.1) the former and later couplings, respectively, favor in-plane and out-of plane direction. This implies that the increase in the DOS of unoccupied d_{xy} orbitals, for $\text{Pt}_4/\text{Co}/\text{Pt}(001)$, will enhance $\langle d_{xy}|d_{x^2-y^2}\rangle$, favoring out-of plane direction of magnetization, as shown in Fig. 4.13. Meanwhile, the $\langle d_{xz(yz)}|d_{z^2}\rangle$ coupling has been increased, which is related to the high density of d_{z^2} states just below the Fermi energy.

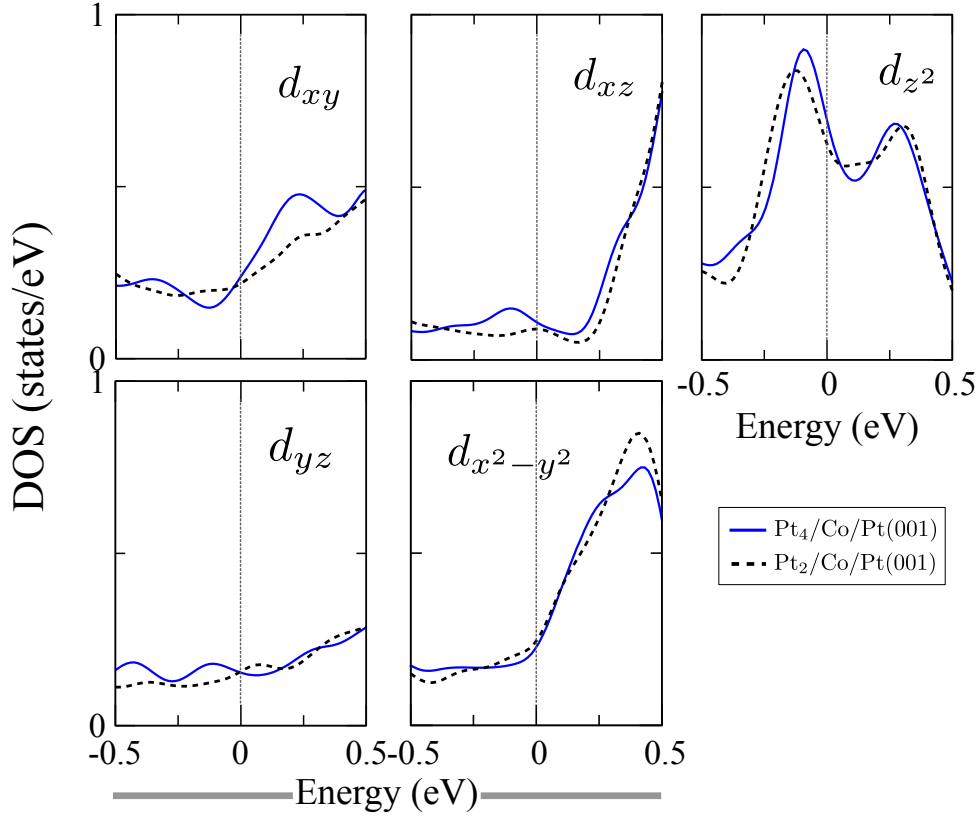


Figure 4.14: The orbital resolved density of states for Co under-layer in $\text{Pt}_N/\text{Co}/\text{Pt}(001)$ system, for the case of two (dashed-lines) and four (full-lines) capping layers of Pt. The DOS of each orbitals of Co are depicted as a ligand in their respective curves.

Moreover, the contribution from the capping Pt layer is also considerable since the induced magnetic moment of capping Pt layers ranges from $0.3 \mu_B$ to $0.07 \mu_B$, respectively, for Pt atom interfaced with Co and surface Pt atom. Since Pt almost fulfills Stoner's criteria and it can be magnetized when it is adjacent to ferromagnet.

In Fig. 4.15 the spatial polarization of the charge density for $\text{Pt}_4/\text{Co}/\text{Pt}(001)$ on a plane of $y = 0.7 \text{ \AA}$. The largest and smallest charge polarization are depicted with white and black colors. The highest charge polarization is observed for Co and the neighboring Pt layers and it decays far away from the Co-Pt interface. This observation supports the argument mentioned above. In Fig. 4.15 the spatial polarization of the charge density for $\text{Pt}_4/\text{Co}/\text{Pt}(001)$ on a plane of $y=0.7\text{\AA}$. The largest and smallest charge polarization are depicted with white and black colors. The highest charge polarization is observed for Co and the neighboring Pt layers and it decays far away from the Co-Pt interface. This observation supports the argument mentioned above.

The total induced magnetic moment of interface Pt layer ($0.37 \mu_B$) is comparable to the experimental value which is $0.61 \mu_B/\text{atom}$ [165]. The effects mentioned above from the

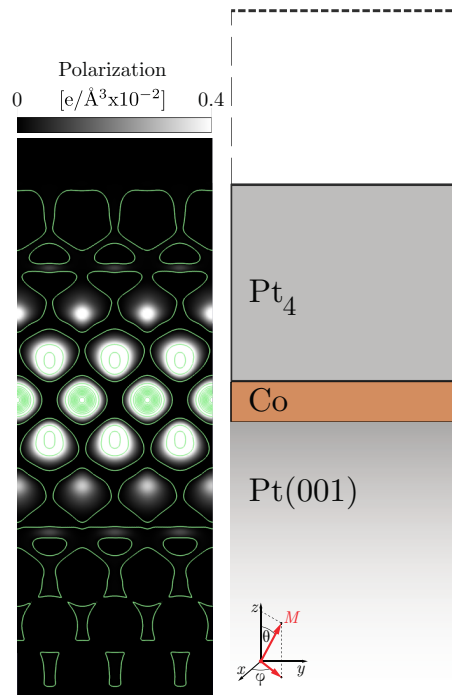


Figure 4.15: Polarization of the charge density on $x=0.7 \text{ \AA}$ plane of Pt₄/Co/Pt(001) system where the maximum and minimum polarization are depicted with white and black colors. The model on the right column is a guide that can be used to compare the vertical position of the atoms with respect to the charge polarization. The contour lines represent zero charge differences.

magnetic layer (Co) and the capping layers lead to an increase in the MAE and reversal of the easy axis, for thicker capping layers, from in-plane to out-of plane.

Fowley *et al.* have done experimental studies on the modification of local magnetic properties of Co/Pt multilayers by partially removing the capping Pt layer. They use various doses of He^+ ion per cm^2 to remove substantial amount of Pt that can induce spin reorientation transition [167]. Explicitly, small doses for the ion milling process which results in thicker Pt capping layers shows high coercivity and higher doses (thinner capping layers) lead to a vanishing coercivity or loss of perpendicular magnetic anisotropy. In other words by removing the Pt overlayers the authors were able to close the magnetic hysteresis loop. The physics of these experimental investigations could possibly be explain by the results and discussions above.

As matter of fact, the effect of Pt overlayers on thicker magnetic films has also been observed, Pt_N/Co₃/Pt(001). For instance, by changing the size of the Pt capping in Pt_N/Co₃/Pt(001) structure, it is possible to increase the absolute value of the MAE of the system from 1.7 meV to 3.6 meV by capping it with one and two layers of Pt. But further increase of the number of Pt layers decreases the MAE, and for Pt₅/Co₃/Pt(001) system the MAE decreases to 0.6 meV.

On the other hand, the MAE versus the number of Cu capping layers [Fig. 4.13(b)] of Cu_N/Co system has shown oscillatory behavior of the MAE with respect to the thickness of the capping layers. For $N \geq 5$ capping layers Cu_N/Co/Pt(001) has on average MAE of 0.5 meV with an in-plane easy axis of magnetization. Such oscillatory behavior of the MAE is originated from the quantum well states in Cu overlayer which are spin-dependent as result of

the Co-Cu interface [134]. The orbital moment difference between the two quantization axes is $\sim 0.02 \mu_B$ on the highest orbital moment corresponds to the out-of plane magnetization.

4.6.2 Pt(Cu) multilayers on Fe monolayer

Similar investigation on the effect of capping Pt(Cu) multilayers on Pt_N/Fe system supported by Pt(001) substrate have been done. The spin magnetic moments of Fe atom can be as large as $2.8 \mu_B$, whereas the nearest Pt neighbor has an induced magnetic moment of $0.3 \mu_B$. The magnetic moment of Fe decreases by $0.14 \mu_B$ when the thickness of the Pt capping layer varies from one to five. The plot for the MAE of $Pt(Cu)_N/Fe/Pt(001)$ system against different layers of Cu and Pt is presented in Fig. 4.16. For different number of capping layers, the MAE of both $Pt(Cu)_N/Fe$ systems behave in similar way, *i.e.* the capping layers tend to decrease out-of plane axis of magnetization (in case of Pt) and increase in-plane axis of magnetization (in case of Cu) until four layers, favoring an in-plane axis of magnetization.

In contrast to Pt capped Co monolayer (in Fig. 4.13), one can observe that the capping Pt layer has opposite effect on Fe monolayers. But the easy axis of Pt_N/Fe always remains out-of-plane. The very large MAE of Fe monolayer capped with one Pt layer (5 meV) reduces to 0.2 meV when it is capped with five layers of Pt. Further increase of the Pt layer increases the MAE once again. In all the cases considered the higher orbital magnetic moment of the Fe atom is always directed to out-of plane. Similar density of states analysis can be used to explain the change in the magnetic anisotropy, like the case of Pt capped Co layer.

Meanwhile, for two Cu capping layers [$Pt(Cu)_2/Fe/Pt(001)$] the easy axis of magnetization switches from out-of plane to in-plane directions. The value of the in-plane MAE can be as large as 0.8 meV for Cu_4/Fe system.

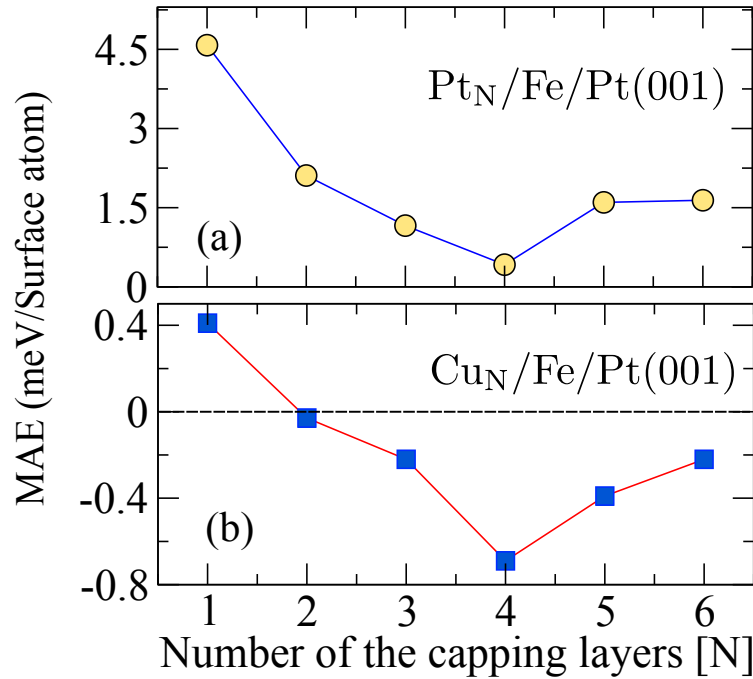


Figure 4.16: The magnetic anisotropy energy of (a) $Pt_N/Fe/Pt(001)$ and (b) $Cu_N/Fe/Pt(001)$ systems as function of the number of the capping layers is plotted. The negative and positive values of MAE represent in-plane and out-of plane magnetization axis, respectively.

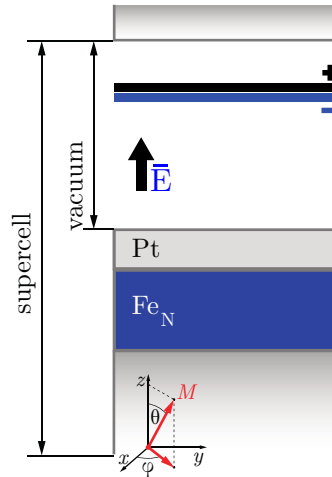


Figure 4.17: The schematics which illustrates the unit cell employed for the calculations on the influence of external EF on the magnetic anisotropy of Fe multilayers.

As summary, variety of experimental investigation on magnetic thin films could involve non-magnetic capping layers. Hence, one should take into consideration that the thickness of paramagnetic capping layers can strongly affect the magnetic properties of the hetrostructure, via QWS in the capping layer or magnetic proximity effect. Besides, one can even further increase the magnetic anisotropy energy by a special alignments of Co(Fe)-Pt alloys. This could have higher perpendicular magnetic anisotropy that can enhance the thermal stability of magnetic units.

The next section is the venue for the interaction between the QWS in magnetic thin films and external electric fields.

4.7 Effect of electric field on magnetic thin films

Once we have investigated the interplay of size and chemical composition of Fe(Co) multilayers on Pt with QWS, MAE, and SP, we draw our attention to the possibility of controlling QWS (and hence the MAE) with the external electric field. In this section we would like to demonstrate the effect of the external electric field on the QWS and the magnetic properties of thin films. Basically, when the electric field is introduced, the electrostatic potential near the capping layer is strongly modified and causes a charge redistribution at the interface. As explained in Sec. 4.3, the Pt atoms which have high spin-orbit coupling hybridize well with the magnetic atoms, and this determines the magnetic features of the film. Hence, for Fe layers in Pt/ FeN/Pt(001) structure the external electric field affects the hybridization of Fe(Co) and Pt, and such variation on the Fe(Co)-Pt interface will change the magnetic properties of the film or monolayer. In order to determine these properties we have chosen Pt capped Fe(Co) multilayers as a sample model. A schematics representation of the external EF applied on the alloy multilayers is shown in Fig 4.17. But first, we reveal the effect of electric field on Fe and Co monolayers and in the next part thicker films will be exposed to external electric field.

4.7.1 Effect of electric field on Fe and Co monolayers Pt(001)

We have determined the MAE of Fe and Co monolayers on Pt(001) surface for different magnitude of electric field. We have already established that FePt alloys have high magnetic anisotropy energy (5 meV/per Fe atom) [141]. For both Fe and Co monolayers the MAE has approximately linear behavior with respect to the external electric field and the change of the MAE is 0.2 meV on average, as shown in Fig. 4.18(a). The variation for Fe monolayer is almost analogous with other ab-initio studies of such systems [141]. In addition, the electric field seems to have opposite effect on Fe and Co monolayers, but the fact is that the electric field tends to favor in-plane magnetic anisotropy, i.e. positive electric field decreases and increases the values of the MAE oriented out-of plane (Fe) and in-plane (Co), respectively.

In these systems the overlap of $3d-5d$ orbitals due to alloying of Fe(Co) atoms with Pt atoms, which have high spin-orbit coupling, has significant impact on the magnetic properties of the compound. Hence, for Fe layers in Pt/ Fe_N/Pt(001) structure the external electric field affects the hybridization of Fe(Co) and Pt, and such variation on the Fe(Co)-Pt interface will change the magnetic properties of the monolayers. We have investigated the orbitals responsible for the screening of the external electric field, and the variation of the magnetic properties. As an example we have plotted [See Fig 4.18(b)] the density of states for different orbitals of Co and Pt that have played a significant role in the process of screening the electric field. Other than surface dipole formation [168], the screening of the electric field directly involves s and p , mainly p states, of the capping Pt layer. This leads to the variation in the d -orbitals of the Pt via $sp - d$ hybridization, and the overlap among d orbitals of Co(Fe) and Pt will affect the magnetic properties. Since their delocalized nature, sp states of Co are also involved.

The changes of the MAE are explained by the second-order perturbation formalism [Eq.4.2.1]. First splitting of d_{z^2} and $d_{x^2-y^2}$ orbitals as result of spin-orbit coupling will lower the energy of the system. Besides, the coupling between occupied and unoccupied states of d_{z^2} and $d_{xz(yz)}$ ($\langle d_{xz(yz)} | L_x | d_{z^2} \rangle$) favors in-plane anisotropy, whereas $\langle d_{xy} | L_z | d_{x^2-y^2} \rangle$ contributes to the out-of plane anisotropy. For Co monolayer in the capped system the later coupling is enhanced by positive electric field, higher density of $d_{x^2-y^2}$ orbitals near the Fermi energy, and it decreases the absolute value of the MAE which has in-plane easy axis.

4.7.2 Effect of electric field on quantum well states

Basically, when an electric field is introduced the electrostatic potential near the capping layer strongly alters, and causes a charge re-distribution on the interface. The Pt atoms which have high spin-orbit coupling hybridizes well with the magnetic atoms, and it determines the magnetic features of the film. Hence, for Fe layers in Pt/ Fe_N/Pt(001) structure the external electric field affects the hybridization of Fe(Co) and Pt, and such variation on the Fe(Co)-Pt interface will change the magnetic properties of the film. In order to quantify this effect an electric field is applied for all thicknesses of Fe in the capped system.

The response of the MAE to the external electric field is found to follow nearly linear behavior, is presented in Fig. 4.19(a), for the case of four layers of Fe in Pt/ Fe_N/Pt(001) system. Meanwhile, in order to investigate how sensitive the MAE of metallic thin films reacts to an external electric field, in Fig. 4.19 (b) the rate of change of the magnetic anisotropy energy (Δ MAE) with respect to electric field is presented for all thicknesses of Fe in Pt/Fe_N/Pt(001). We generally quantify the rate of change of MAE as

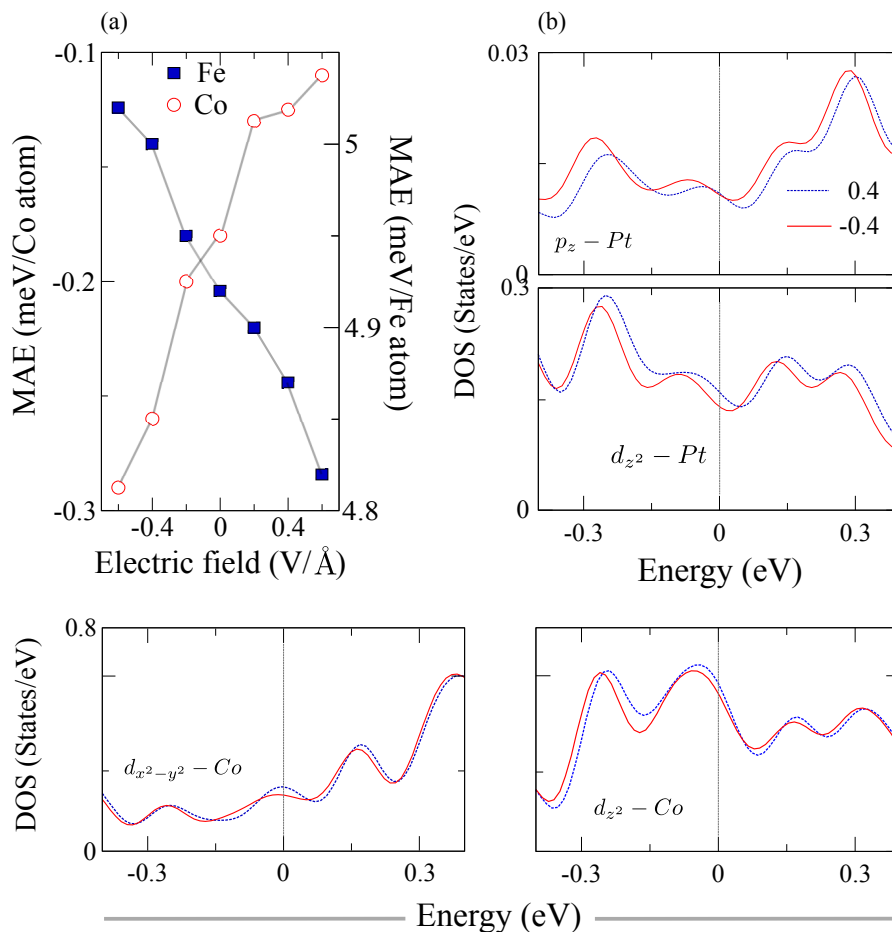


Figure 4.18: The effect of the electric field on the MAE of Pt capped Co (circles) and Fe (square) monolayer on Pt(001) surface. (b) LDOS of the capping Pt layer for the z -components of p and d orbitals. (c) LDOS for the d orbitals of the underlying Co layer that have been indirectly affected by the external electric field. The LDOS for electric field of 0.4 and -0.4 V/\AA are represented with blue dashed and full line red lines, respectively.

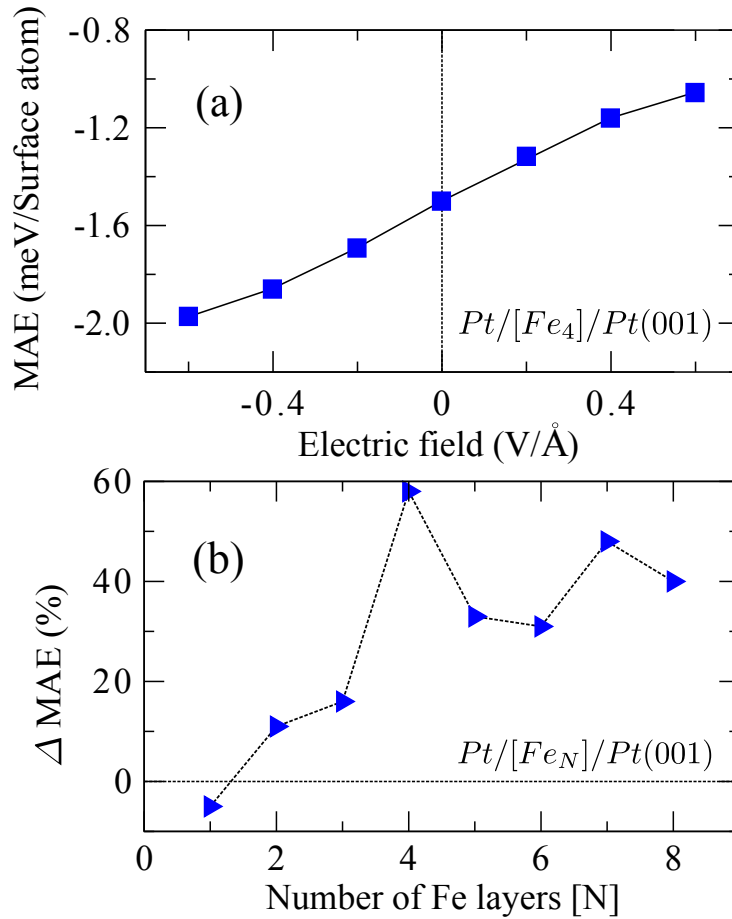


Figure 4.19: (a) The rate of change of the MAE (in percentage) as result of an external electric field normalized by the MAE of the neutral system, for different number of Fe layers of Pt/[Fe]_N/Pt(001) system. (b) The MAE as function of external electric field for Pt/[Fe]₄/Pt(001) supercell in the capped system [149].

$$\Delta\text{MAE} = \left[\frac{\text{MAE}(E_-) - \text{MAE}(E_+)}{|E_- - E_+|(\text{MAE}(0))} \right] \times 100\%, \quad (4.7.1)$$

where $[\text{MAE}(E_-)]\text{MAE}(E_+)$ are the magnetic anisotropy energies at [negative] positive electric fields.

Whereas $\text{MAE}(0)$ is the value of MAE for the neutral system, see Eq. (4.7.1). As an example we discuss the rate of change of the MAE (ΔMAE) per $\text{V}/\text{\AA}$ (in percents) for $E_+ = 0.4$ and $E_- = -0.4$, shown in Fig. 4.19(b). Our calculations reveal that for all Fe layers, except for one layer of Fe, a negative electric field increases the MAE. The plot for the MAE of four layers of Fe versus the external electric field is presented in Fig. 4.19(a). Additionally, from Fig. 4.19(b) the ΔMAE strongly depends on the thickness of the Fe thin film. One layer of Fe, Pt/Fe₁/Pt(001), exhibits different response to the electric field, i.e. positive. The value of ΔMAE is $\sim -5\%$, which is normalized by the high MAE of the neutral system (~ 5 meV). For all other multilayers ($2 \leq N \leq 8$) the rate of change of MAE is positive in sign, and shows oscillatory behavior as the thickness of Fe layers is increased.

Generally, when a negative electric field is applied it has a tendency to favor in-plane magnetization axis, i.e. negative electric field decreases out-of plane MAE ($N = 1$) and

increases the absolute value of in-plane MAE ($2 \leq N \leq 8$), compared to the neutral system. Besides, as can be seen in Fig. 4.19, the change in the MAE has the highest value of 60% for $N=4$, and oscillates as the number of Fe layer increases. In other words the four layers of Fe is the most susceptible to the external electric field. The high ΔMAE for thicker thin films (e.g. Pt/Fe₄₍₇₎/Pt(001)) can be associated with the influence of the external electric field on QWS, other than the contribution only from Fe-Pt interface. On the other hand the SP of the QWS is also affected by the electric field, and it was found that the change in the SP by electric field varies at and around the Fermi energy. For example, five and six Fe layers exhibit an increase in the SP(E_f) by 14 % and 11 %, respectively, upon exposure to an electric field of 1 V/Å. In relation to the above discussion, i.e. variations of the MAE and SP by electric field, the Kohn-Sham levels close to the Γ point for four layers of Fe are plotted in Fig. 4.20 as a particular example. The Kohn-Sham levels (close to the Fermi energy) which have non-zero occupation (occupations ≥ 0.04) by the orbitals, namely $s + p$, $d_{xz(yz)}$ and $d_{x^2-y^2}$, are presented. The eigenenergies are plotted for external electric field of -0.4 V/\AA and 0.4 V/\AA . Both the majority and minority states are shifted as result of external electric field which resembles a Stark shift. Moreover, one can see that the shift of the $d_{xz(yz)}$ and $d_{x^2-y^2}$ band energies are correlated to $s + p$ ones, and thus it is an evidence that the effect of electric field on d -states is mediated by $s + p$ states via the mixed orbitals.

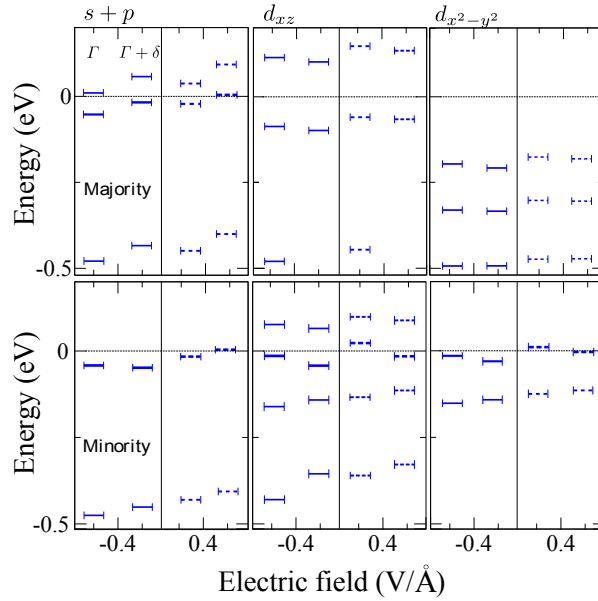


Figure 4.20: The Kohn-Sham energy levels close to the Γ point for which the $s + p$, d_{xz} and d_{xy} orbitals of four layers of Fe [Pt/[Fe]₄/Pt(001)] have high contribution. The energy of the electronic levels (relative to the Fermi energy) are presented for an electric field of 0.4 V/\AA and -0.4 V/\AA , and two k-points, Γ and $\Gamma + \delta$ points, have been considered [149].

A robust correlation between rate of change of MAE and the DOS for $d_{x^2-y^2}$ orbitals has occurred. i.e. the high ΔMAE for Pt/[Fe]₄₍₇₎/Pt(001) system is caused by the high density of $d_{x^2-y^2}$ orbitals, shown in Fig. 4.3, that are affected by sp QWS. Specifically, the response to the electric field mainly involves the sp QWS, and it modifies the d -states by $sp - d$ hybridization, and from the orbital resolved DOS a pronounced overlap between sp and $d_{x^2-y^2}$ states has been observed. Since the capped and uncapped Fe multilayers have similar profile these DOS (in Fig. 4.3) can be used for comparison.

The variations of the MAE and SP can be explicitly associated with the shift of the Kohn-Sham energy levels, reminding that the minority DOS of Fe multilayers near the Fermi energy are dominated by $d_{xz(yz)}$ and $d_{x^2-y^2}$ states. Hence, for positive electric field we observe the shift of the Kohn-Sham band energies towards higher energy levels, and even a crossing of the Fermi energy. Furthermore, as result of positive electric field the increase in the density of states of unoccupied $d_{xz(yz)}$ and $d_{x^2-y^2}$ orbitals near the Fermi energy affects the coupling of $\langle d_{xz(yz)} | L_x | d_{x^2-y^2} \rangle$ and $\langle d_{xy} | L_z | d_{x^2-y^2} \rangle$, where the former and later couplings favor and in-plane and out-of plane MAE, respectively. Recalling the second-order perturbation theory, the decrease in the value of the MAE for positive electric fields is attributed to the higher number of bands for $d_{x^2-y^2}$ orbital near the Fermi energy, which enhances the contribution to the first term of Eq. 4.2.1. Besides, since both orbitals are affected by the electric field, the $\langle d_{xz(yz)} | L_x | d_{x^2-y^2} \rangle$ coupling remains unaffected. The two contributions mentioned have collective effect of decreasing the magnitude of the in-plane MAE.

Similar investigation on the effect of electric field on the MAE and SP of Co multilayers have been performed and the results show that the MAE of Pt/[Fe]_N/Pt(001) ($N \geq 2$) linearly increase when a negative electric field is applied. From the analysis on Fe multilayers, using the DOS profile near the Fermi we have figured out the route to strongly enhance the MAE of Co multilayers. Hence, we have selected Pt/[Co]₆/Pt(001) system as model, since there is high density of $d_{xz(yz)}$ and $d_{x^2-y^2}$ orbitals, and it was found that the MAE could be tuned by 56 % with 1 V/Å of electric field compared to the neutral system of 0.16 meV.

To sum up the concepts that are covered in this chapter; spin-selective quantum well states in magnetic thin films and magnetic anisotropy energy have been related. The investigations establish the possibility of controlling the MAE of Fe(Co) thin films by changing the thickness of either magnetic thin films or the non-magnetic overlayer. These variations in most cases are mediated by the the spin-dependent-quantum well states. These variations are qualitatively explained in terms of the coupling between the occupied (unoccupied) d -orbitals of the magnetic layer with the angular momentum operators within the framework of second-order perturbation theory. For almost all magnetic thin films capping strongly enhances the MAE. Additionally, a transition of the SP of the QWS was observed as the size of the thin film increases. The MAE and SP are sensitive to the external electric field, and substantial change of MAE can be achieved therewith. We believe that the results presented in this part of the thesis can be additional ingredients for the understanding and engineering of spintronic and magnetoelectric devices.

Chapter 5

Surface charge tuning of magnetic anisotropy and interlayer exchange coupling

In the previous two chapters it was shown that high magnetic anisotropy can be achieved by employing Fe-Pt alloys and its dependence on the thickness of the thin films was revealed. In this chapter we turn to surface charging in the hope to find yet another way to efficiently tailoring magnetic properties of multilayers. Indeed, it is found that surface charging can not only change the value of MAE, but even leads to a reversal of the easy axis of magnetization. Additionally, the interlayer exchange coupling in Fe-Cu alloy multilayers is investigated. It is revealed that interlayer exchange coupling is sensitively linked to the excess charge introduced into the system.

5.1 Surface charging of alloy multilayers

As it was mentioned in the introductory part of this thesis (Chapter 1) large values of MAE are often preferred in order to stabilize the orientation of magnetization in a sample against thermal fluctuations, reducing the probability of magnetization reversal. In section 1.1.1 it has been shown that alloying 3d elements with high spin-orbit coupling elements is one of the route to increase the magnetic anisotropy [13, 169]. Such large MAE in 3d-5d alloys arises as a result of the large intra-atomic spin-orbit (SOC) interactions [13]. Strong magnetic materials, 3d-transition metals (TM), usually display weak SOCs in contrast to the heavy elements (4d/5d elements) which are paramagnetic but highly polarizable. From all the possible 3d-5d alloys, Fe-Pt compounds are particularly attractive for technological application such as magnetic recording media [69]. Indeed, previous theoretical studies on Pt-Fe ultrathin films report anisotropy energy values of ~ 5 meV/magnetic atom [141].

Yet, having large MAE values is not sufficient. It is also important to be able to dynamically tune the anisotropy. The external electric field has been used to tailor magnetic anisotropy of adsorbates [54, 77, 147]. It has also been thoroughly investigated, particularly in ultra-thin films [54, 141, 150, 77], or in low-dimensional systems such as aggregates and atomic chains deposited on substrates [73, 74]. The basic physics behind all these effects is the redistribution/change of the charge carrier density in an attempt of the system to screen the electric field. There is, however, a much more direct way of affecting the intrinsic charge carriers in the systems; charge-doping. It is widely used in electrochemistry [170],

where the charge carriers in solution are either driven by externally applied voltage or by the chemical reaction within the solution. This scheme has been less investigated in the field of spin-electronics. Remarkably, it has been shown that charge doping can be used to tailor most of the properties mentioned above, and these properties are extremely sensitive to the excess electrons (holes). One of the schemes used to introduce charge(hole) injection in nano-sized systems is by electrolyte (insulator) charging [69, 170]. Nevertheless, this method usually requires the use of liquid electrolytes or an insulator to induced a change in the carrier density, see section 1.3.1.

Such an effect has been proven to exist on ultra thin Co layers by Shimamura *et al.* [80]. To enhance the effect of the applied external electric field Co layers have been coated with a polymer film containing an ionic liquid. The Curie temperature of the system was found to change by as much as 100K upon application of an external bias of 2 V. With no bias applied, the T_C of the system was estimated to be $\sim 324\text{K}$, being much lower than the bulk value due to two-dimensionality of the system [80]. Applying just a small bias (not exceeding 2 V) to the sample at room temperature, the authors were able to increase the coercive field of the ultra thin Co film re-enabling the magnetic anisotropy (see Fig. 5.1). At a bias of 2 V the T_C of the system could be enhanced to 380K and the coercivity of the film reached 15 Oe.

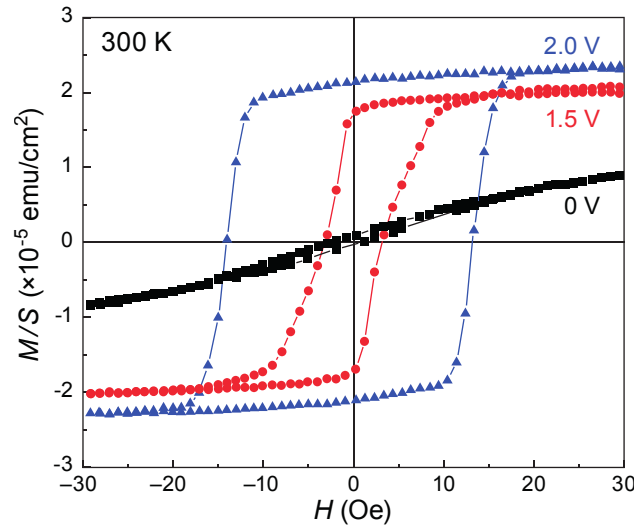


Figure 5.1: Magnetization (M) versus external magnetic field (H) curves at 300K under different gate voltages (V_G): 0, 1.5 and 2.0 V. The vertical axis represents M divided by the total area of the sample (S). H was applied perpendicular to the sample plane. Adapted from [80].

More advanced methods of achieving local charge injection in nanostructures involve the usage of Scanning Tunneling Microscopy (STM) [107, 108], and Electron Force Microscopy (EFM) tips [109]. In the next sections we will discuss interesting results on the effect of both alloying and charge-doping effects in $3d/5d$ layered structure. Specifically, it was shown that the stable magnetization axis of ultra-thin films of Fe(Co)-Pt alloy can be reversed by surface charging, and the value of the MAE can be enhanced strongly.

5.2 Surface charging and magnetic anisotropy

Motivated by the interesting studies illustrated above we turn our attention to tailor the magnetic anisotropy of Fe and Co thin films with charge doping. First the discussion of one and two Fe (Co) layers supported by ten layers of Pt-substrate will be presented, where the Fe(Co) layers are also capped with Pt. Charging the surfaces of these heterostructures is controlled by the number of valence electrons of the system, and majority of the net charges are expected to spill over the surfaces or interfaces. Thus a true surface-charging in the slabs can be simulated (shown in Fig. 5.2). In order to simulate a negative (positive) charging-doping in a supercell approach, one needs to add (remove) charges of the order of $1.2 e$ per unit cell to the neutral system.

In practice, the highest concentration of charge is placed on the opposite sides (surfaces) of the slab with very small charge oscillations inside due to the relative reduced atomic-thickness. But as the thickness of the slab is increased, the excess charge will lie only on the surface and the usual metallic-like behavior is recovered. To reduce the influence of the extra charge interactions across the slab, we have increased the size of the slab from ten to twelve Pt layers and have not seen significant change on the value of the magnetic anisotropy. Meanwhile, to avoid interaction between lateral periodic supercells as result of the extra charges a compensating homogeneous background-charge is also assumed to neutralize the supercells, and it scatters over the dotted area of the model shown in Fig. 5.2.

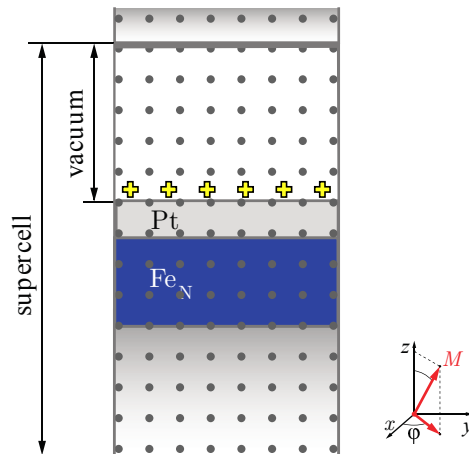


Figure 5.2: A model of charged slab which includes a Pt substrate and Fe layers capped with Pt. The extra charges of the slab will be spilled over the surfaces and it will be compensated by the homogeneous background-charges (dotted area) spread over the supercell, for the sake of computational effort.

The MAE, taken as the energy difference between systems with magnetization aligned in two orthogonal crystallographic axes *i.e.*, $E[100] - E[001]$ ($E_x - E_z$) is obtained self-consistently. For ultra-thin films both techniques, the force theorem and self consistent, gave comparable results. Hence, only the values of the MAE for self-consistent method are discussed in the present work. The charge-doping influence on the structural relaxation of the multilayers was found to be insignificant in the magnitude of MAE. The effect is a modest interlayer expansion of less than 2%, compared to the bulk interlayer distance, leading to the variations of the MAE by less than 1% [82].

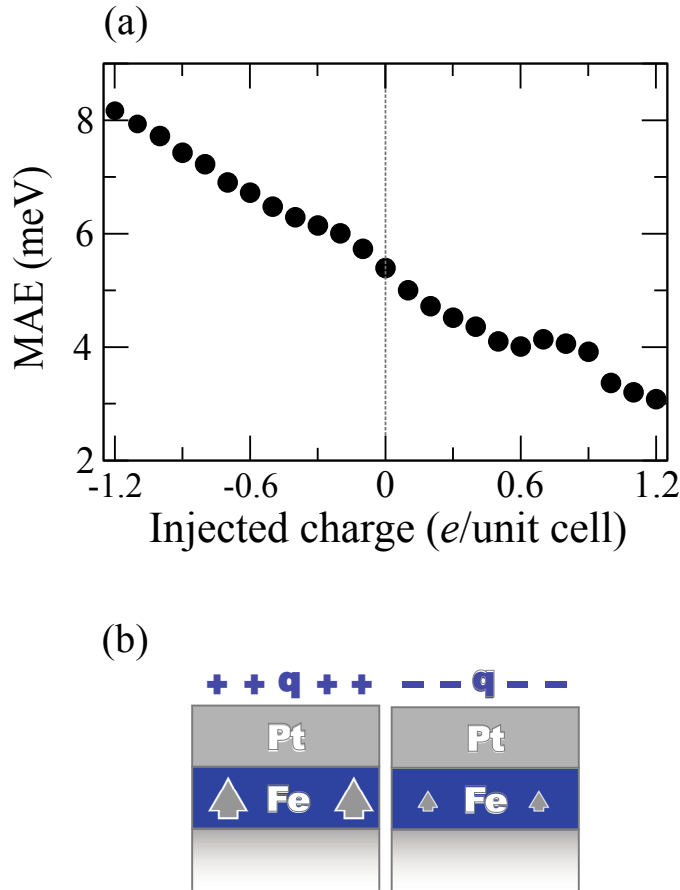


Figure 5.3: (a) The magnetic anisotropy energy (in meV) for Pt/Fe/Pt(001) as a function of the injected charge(holes). The charge-doping scale (in units of $e/\text{unit cell}$) is referred to the neutral system. Positive (negative) values stand for an excess (lack) of electrons [82]. (b) Schematic representation of the reduction of the magnetic anisotropy for two opposite charging scenarios.

5.2.1 Fe(Co) monolayers capped with Pt

We first begin with the results about Fe monolayer capped with Pt [Pt/Fe/Pt(001)], which has relatively large MAE (5.12 meV) and out-of-plane axis of magnetization. In section 4.7.1 for this particular system of Fe monolayer a linear dependence of the MAE with respect to the external EF is observed. In fact a change of $\sim 8\%$ on MAE has been predicted in the presence of an external electric field (EEF), which is similar with Ref. [141]. Its origin is often attributed with the small variations of the number of the valence electrons near the Fermi level induced by the EEF [141, 69]. Nevertheless, the charge-doping was found to have a stronger effect on MAE than the EEF.

The relation between MAE and charging of Pt/Fe/Pt(001) system, shown in Fig. 5.3(a), has shown a linear-like behavior. A remarkable MAE enhancement for positive charging (excess of holes) of $\sim 50\%$ (8.2 meV for 1.2 holes/unit cell) and a considerable reduction for negative charging (excess of electrons) of $\sim 40\%$ (3 meV for 1.2 e) with respect to the neutral system. Therefore, the observed changes in the magnitude of MAE as a function of the charge injection (removal) reveals a net variation in the anisotropy energy of nearly $\sim 95\%$ (5 meV/magnetic atom), which is comparable with the MAE for the neutral system.

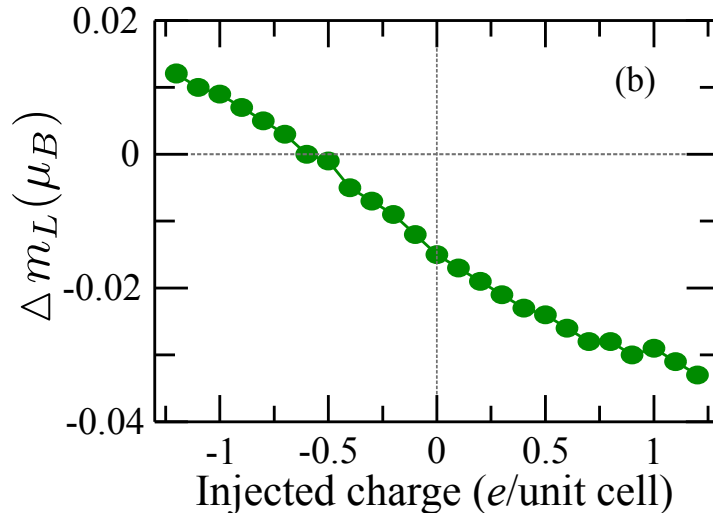


Figure 5.4: The orbital moment difference ($\Delta m_L = m_L^x - m_L^z$ in units of μ_B) as function of injected charges in which the charge-doping scale (in units of $e/\text{unit cell}$) is referred to the neutral system. Orbital moment differences Positive (negative) values stand for an excess (lack) of valence electrons [82].

Not only the MAE depends on the surface charging but also the orbital anisotropy, the orbital moment difference between two different quantization axes (z and x) of the Fe layer in Pt/Fe/Pt(001) system. The orbital anisotropies are plotted in Fig. 5.4. The magnitude of the orbital anisotropy can be as large as $0.04 \mu_B$, and it is clearly seen that orbital anisotropy and MAE have direct relation regardless of the magnitude of the charge doping.

The MAE behavior with respect to surface charging is not only observed for this particular alignments of multilayers. By adding a second Pt layer, a similar linear dependence on MAE as a function of the charge doping is revealed. This leads to the conclusion that the capping with a second non-magnetic layer can significantly affect the local electronic environment exhibiting the robustness of MAE against hybridization and spin-orbit interactions. In addition, by alternating the Pt-Fe layers twice, Pt/Fe/Pt/Fe/Pt(100) a large value of MAE (~ 5.6 meV) is found but still the effect of surface charging is maintained. Moreover, for both systems due to the large MAE, the out-of plane axis of magnetization is unchanged [82].

In order to further explore the effect of surface charging on magnetic properties of other chemical compositions, we have also done similar studies for Pt capped Co monolayers, Pt/Co/Pt(001). The value of the MAE for Co monolayer is predicted to be 0.2 meV, and the easy axis points in-plane, see section 4.7.1. Using technique of surface charging one can reverse the stable direction of magnetization to out-of plane by doping the system with only 0.2 electrons per unit cell. The value of MAE can be as large as 0.5 meV when the system is charged with extra electrons of 0.6 $e/\text{unit cell}$, where the easy axis of magnetization is oriented perpendicular to the surface.

5.2.2 Fe bilayers capped with Pt

Following the strong tuning of the MAE for Fe(Co) monolayers with electron (hole) doping, we are interested to modify the MAE of other FePt hetrostructure with high MAE. Explicitly, we have added one more Fe layer on Fe/Pt(001) and then capped it with one or two Pt

layers. Here we observe a remarkable feature in the magnetic properties. First, it should be mentioned that for the two configurations, Pt/Fe₂/Pt(100) and Pt₂/Fe₂/Pt(100), the total MAE of the neutral systems is relatively small roughly 2.7 and 1.0 meV, respectively, in contrast with Fe monolayer system [Pt/Fe/Pt(001)]. But it is very high relative to the MAE of Pt/Co/Pt(001). The easy axis of magnetization of (Pt₂)Pt/Fe₂/Pt(100) system is oriented to in-plane, making them preferable candidates that could manifest spin-reorientation, if the local electronic environment is strongly modified.

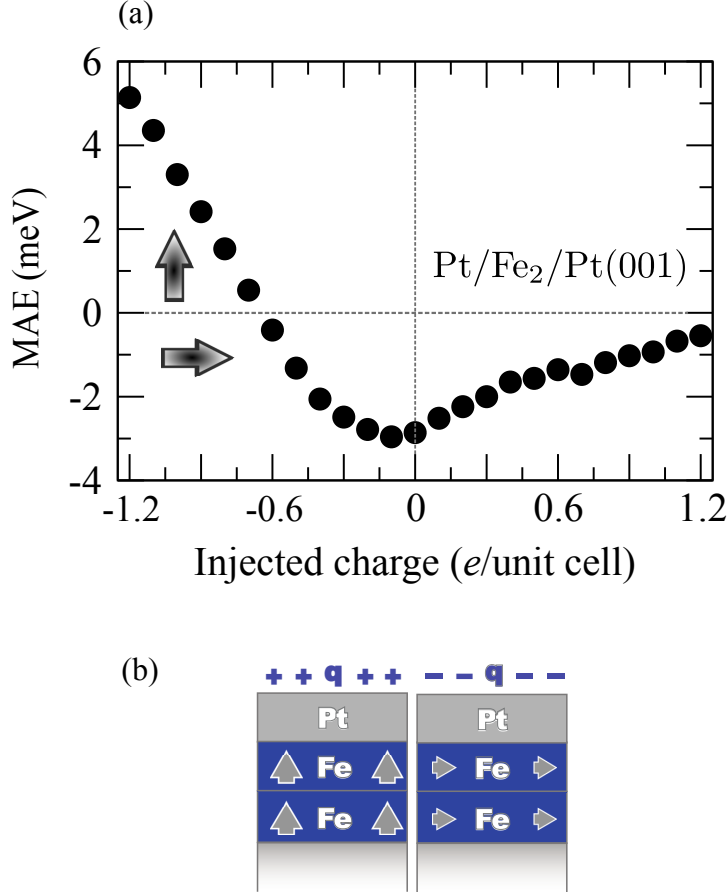


Figure 5.5: (a) Magnetic anisotropy energy for Pt/Fe₂/Pt(100) system. The charge-doping (in units of $e/\text{unit cell}$) has the same meaning as in Fig 5.3. The positive (negative) values of MAE stands for out-of plane (in-plane) axis of magnetization. (b) Schematic representation of the the magnetization reversal for two opposite charging scenarios.

Moreover, the linear relationship between MAE and the charge-doping vanishes for both systems, unlike for the case of Fe monolayers, showing a more complex dependence. The MAE behavior as a function of the injected charge is shown in Fig. 5.5, for Fe bilayer capped with one Pt layer. MAE shows small variation for electron-doping, the net changes in MAE for positive charging, $\Delta\text{MAE} = |\text{MAE}(-1.2)| - |\text{MAE}(0)|$, are estimated to be 8 meV with respect to the neutral value for Pt/Fe₂/Pt(100). However, for negative doping a considerable variation in MAE is found to follow a partial linear behavior. On the other hand we have observed similar behavior for Pt₂/Fe₂/Pt(100) system where the MAE varies by 6.5 meV with respect to the uncharged system, see Fig. 5.6.

Simultaneously, a transition in the axis of magnetization from in-plane to out-of plane is observed for both systems above 0.6 holes. The manifestation of such peculiar feature has

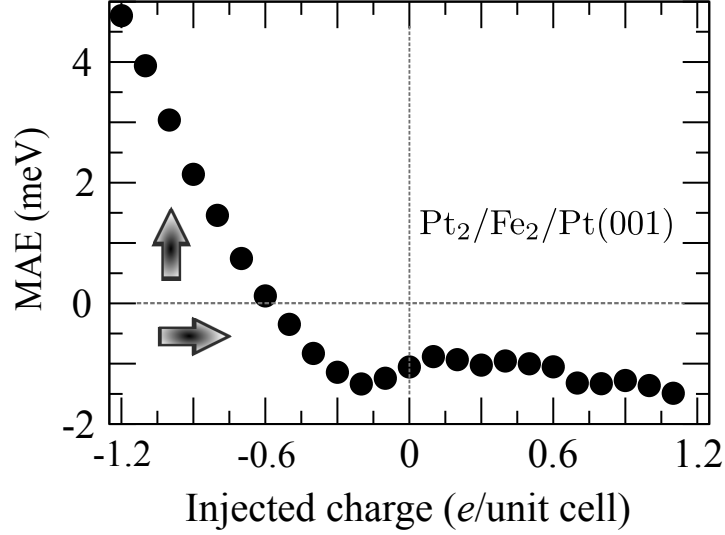


Figure 5.6: Magnetic anisotropy energy for $\text{Pt}_2/\text{Fe}_2/\text{Pt}(100)$ system. Positive(negative) MAE values stand for an out(in-plane) axis of magnetization [82].

many possible implications. After the easy-axis switching, MAE rises to high values of ~ 2.5 meV/magnetic atom, indicating the stability of the magnetization reorientation. Thus, the charge-doping can possibly tune the magnetization of Fe bilayers between the two stable axes [82]. Furthermore, from our analysis we conclude that the interaction of the double Fe-layer with the capped Pt-layer and the substrate is essential in the magnetization reversal.

In order to understand this intricate behavior found in the Fe-Pt multilayers, we analyze the d -orbital-resolved local density of states (LDOS) of the magnetic layer in Pt/Fe/Pt(100), which is expected to give the main contribution to MAE [141], through the second-order perturbation formula [116]. Equation (2.5.4) can be re-written as

$$MAE \sim (\xi)^2 \sum_{u,o} \frac{|\langle o|L_z|u\rangle|^2 - |\langle o|L_x|u\rangle|^2}{\epsilon_u - \epsilon_o}, \quad (5.2.1)$$

where o and u are occupied and unoccupied states. Ignoring the spin-flip terms between up and down states, as for Fe the majority d -band is fully occupied, the predominant changes in MAE can be only attributed to the coupling between states in the minority band close to the Fermi energy. After analyzing the spin-orbit coupling matrix elements between the different d -orbitals, we found that the d_{xy} and d_{xz} orbitals have the highest contribution to MAE. These orbitals are coupled with each other through the L_x operator ($\langle d_{xy}|L_x|d_{xz}\rangle$) leading the variations in MAE to arise from the second term in equation (5.2.1). Insights about the nature of this coupling can be qualitatively inferred from LDOS features, which provide a direct information of the local structure, particularly about MAE behavior.

For instance, as can be seen in Fig. 5.7, for hole-doping (positive charging) the d_{xz} orbitals remain unchanged, while the d_{xy} orbitals undergo a depletion near the Fermi level decreasing the spin-orbit coupling between them. According to equation (5.2.1), the reduction of the $\langle d_{xy}|L_x|d_{xz}\rangle$ coupling results in an enhancement of MAE. Such reduction is monotonous (due to the gradual depletion of d_{xy} orbitals as the number of holes is increased) and this might explain the observed linear enhancement in MAE. On the other hand, for electron injection (negative charging), the coupling between the d_{xz} and d_{xy} orbitals, $\langle d_{xy}|L_x|d_{xz}\rangle$, rises up fast increasing the SOC interaction which leads a reduction of MAE. The analysis

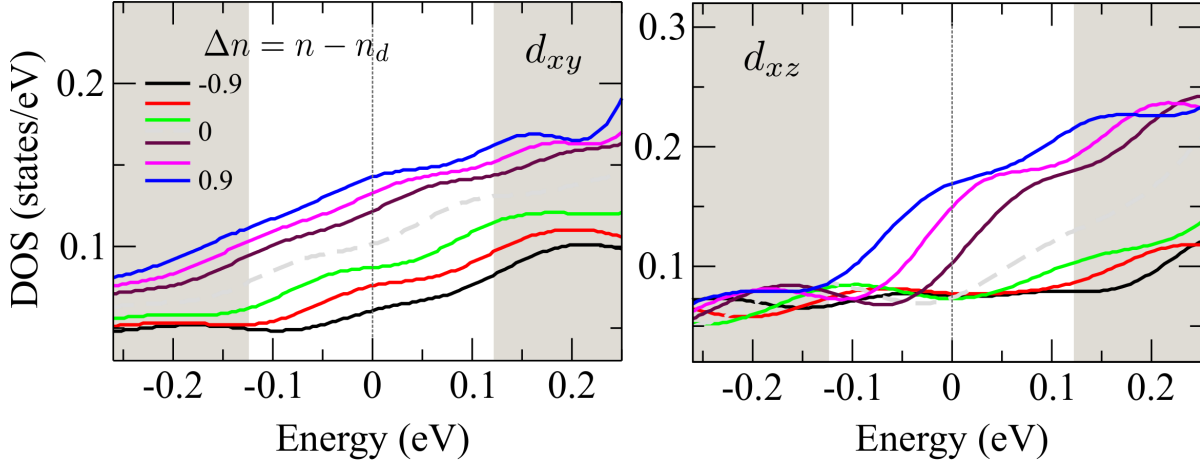


Figure 5.7: Orbitaly decomposed minority d local density of states (LDOS) for the Fe monolayer capped with one Pt layer. $\Delta n = n - n_d$ where $n(n_d)$ refers to the number of electrons in the charged (neutral) system respectively [82].

of explaining MAE trends through the second-perturbation formula can be extended to other samples. As an example, for Pt/Fe₂/Pt(100), the main contribution to MAE comes from the coupling between the d_{xy} and $d_{x^2-y^2}$ orbitals. However, in this case, the coupling between the d_{yz} and $d_{x^2-y^2}$ orbitals, $\langle d_{x^2-y^2} | L_x | d_{yz} \rangle$, which favors an in-plane magnetization, has also an important contribution to MAE. Therefore, the interplay between these two couplings determines the direction of the easy-axis. Moreover, one can relate MAE to the orbital moment anisotropy (OMA) which is found to partially follow the Bruno's relation ($\Delta E_{\text{SOC}} = -\frac{\xi_{\text{Fe}}}{4\mu_{\text{B}}} \Delta m_{l,\text{Fe}}$) [117], since the highest orbital moment lies in the easy-axis only in the range of -0.6 to 1.2 e /unit cell (see the inset of Fig. 5.7).

For Pt/Fe₂/Pt(100) it is also possible to associate MAE with OMA. Here, the total orbital moment of the Fe-bilayer goes along with a linear dependence of MAE following in part the Bruno's criterion as well since in this case, the highest orbital moment does not lie at any charge value in the easy-axis as it always points out-of plane.

In section 4.3, based on the generalization of second-order perturbation theory and experimental evidence [152, 117], it was suggested that Bruno's formula is valid for special cases when only the on-site contributions to MAE are taken into account and the exchange splitting is large enough. Apart from that, if the hybridizations become important and the spin-flip terms are not vanished, a more general relationship between MAE and OMA, which considers all the atomic species and off-site spin-orbit terms, needs to be taken in to account [152]. Since Bruno's relation seems to be partially fulfilled for such systems, it is interesting to explore its limitations by investigating the relationship between MAE and OMA as a function of the charge-doping. This kind of relation between orbital anisotropy and MAE has linear like behavior for Fe monolayer in the capped structure, section 5.2.1.

Taking Pt/Fe₂/Pt(100) as example (illustrated in Fig. 5.5), one can find that a linear dependence is preserved for positive charging while the stronger deviations to this linear behavior are observed at high charge density concentrations (~ 1 e /unit cell). From these results, one infers that the electronic environment significantly changes beyond certain charge threshold, enhancing the hybridizations and the spin-orbit coupling between the Fe 3 d and Pt 5 d -orbitals.

When SOC is strong enough or when the hybridizations are dominant, even at moderate

charge concentrations, no direct relationship between MAE and OMA is observed. This assumption is more clear in the case of $\text{Pt}_2/\text{Fe}_2/\text{Pt}(100)$, when the two capped Pt-layers boost the spin-orbit coupling leading in a non-linear correspondence between MAE and OMA. The interplay between the SOC strength and d - d hybridizations will determine the magnitude of MAE and the direction of magnetization at once and hence, whether or not Bruno's formula can be used. In our calculations we model the Fe-Pt multilayers by a slab in vacuum splitting the charge over both faces of the slab. Nevertheless, due to the strong effects that cause the charge-doping, one would not expect significant changes in the trends and main conclusions discussed in the present work.

Indeed, in a more detailed investigation of other Fe based ultra thin films, *e.g.* Fe-Pd(Pt) with two Fe-layers such as $\text{Fe}_2/\text{Pt}(100)$, $\text{Fe}_2/\text{Pd}(100)$, $\text{Pd}/\text{Fe}_2/\text{Pd}(100)$ and $\text{Pd}_2/\text{Fe}_2/\text{Pd}(100)$, an easy-axis switching is always observed. For an illustration the effect of charge injection on the magnetic properties of Fe bilayers in $\text{Pd}/\text{Fe}_2/\text{Pd}(100)$ is presented. The relation between MAE and the net injected (removed) electrons from the system is plotted in Fig. 5.8. The slope of this plot is opposite to the one for FePt, besides, the MAE is almost one order of magnitude less than that of Fe-Pt alloy thin films. Unlike that of FePt multilayers here high amount of electrons per unit cell ($1.2 e/\text{unit cell}$) is needed in order to induce spin reorientation transition.

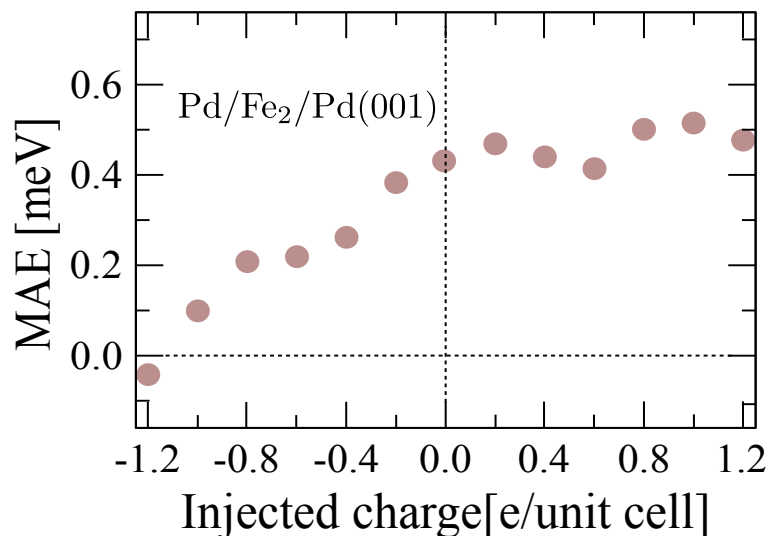


Figure 5.8: Magnetic anisotropy energy for $\text{Pd}/\text{Fe}_2/\text{Pd}(100)$ system. Positive (negative) MAE values stand for an out of plane and in-plane axis of magnetization, respectively.

Up to now the strong alteration of the MAE by surface charging in ultra-thin films, including reversal of magnetization axis, has been thoroughly investigated. We believe that extending such intriguing phenomena to thicker magnetic thin films would lead to similar outcomes. Certainly, the impact of surface charging on magnetic properties of thicker magnetic films is related with the spin-dependent quantum well states therein (See Sec. 4.2). Indeed, the fascinating features obtained as result of surface charging on magnetic anisotropy lead us to evaluate its impact on interlayer exchange coupling of pseudo-TMR structures, which will be discussed in the next section.

5.3 Switching of interlayer exchange coupling by interface charging

Interlayer magnetic interaction is another important parameter in nano-magnetism and controls the mutual magnetization orientation between the magnetic layers interspaced by metallic films [117, 142, 144] or insulating material [171]. It is a manifestation of the influence on the magnetic order of one of the magnetic layers by the other one, and thus it has wide range of application in devices. One such example can be the tunneling magnetoresistance [54, 171], where the difference in the resistance which is caused by the relative magnetic alignment of the two magnetic layers in trilayer system is used to read the states of magnetic unit [172]. Eventhough tunneling magnetoresistance is used for the current applications, the discovery of giant magnetoresistance (GMR) effect by Grunberg and Fert [6, 7] had brought a significant increase in the density of magnetic data storage. The existence of such characteristics is hidden in the coupling medium, *i.e.* a medium with delocalized electrons which have high probability of being confined. These electrons are spin-polarized as result of the spin-polarized boundaries. It has been shown that the interaction between magnetic units depends on the distance between the elements [144], *e.g* the interlayer exchange coupling (IEC) between magnetic layers depends on the thickness of the coupling medium [142].

Commonly, magnetic tunneling junctions (MTJ), which have similar trilayer structures like GMR contacts, have in-plane stable axis of magnetization. But there are also materials with out-of plane easy axis that can also be used for MTJ. These devices which are based on perpendicular MTJ have the advantage of spin transfer torque since the demagnetization filed is parallel to the layers [50, 51, 53]. Furthermore, the critical current for switching the magnetic order is significantly reduced for materials of perpendicular magnetic anisotropy [54].

In the last two decades the magnetic storage units were reduced to the nanoscale level. The main drawbacks of writing information in these magnetic units by magnetic filed is described in section 1.3. As reminder, one of the disadvantages is that due to the non-local nature of the magnetic field the stray fields of the magnetic filed could affect the neighboring cells during the process of writing. Whereas, the other one is associated its high consumption of power. One alternative solution was to exploiting the magnetoelectric phenomena, using multi-functional materials [70, 173, 57]. Whereas, the other mechanism employs magnetoelectric coupling relaying on varying the intrinsic charge carries of the magnetic nanostructures. The two ways that are possible to induce a variation of the charge carriers of magnetic systems are external electric filed or charge doping. For instance, it was shown that switching of magnetic tunneling junction based on MgO tunneling barrier, with perpendicular magnetic anisotropy, can be assisted by electric field [54].

In following parts of this chapter the main field of concern is the interplay between interlayer exchange coupling of magnetic layers and surface charging. The process of switching of the interlayer exchange coupling between two Fe layers mediated by Cu layers could be accomplished only with surface/interface charging. We propose a new route to tailor the interlayer exchange coupling of Fe layers via non-magnetic Cu layer.

5.3.1 Fe/Cu_N/Fe

Once we have uncovered the influence of surface charge on the MAE of $3d/5d$ multilayers [82], hence, it could be worthwhile to study the effect of charge injection on IEC. Explicitly,

the influence of surface charging on the mutual IEC will be the topic of discussions. The actual manipulation of IEC by electric means has possible applications in non-volatile two terminal devices, *f.e.* magnetic random access memory (MRAM) device. Even though we have studied various sandwich junction made of two Fe layers separated by Cu spacers ($N \leq 5$), we have selected Fe/Cu₄/Fe/Pt(001) as model system. Additional test calculations were also done for trilayers made of Co.

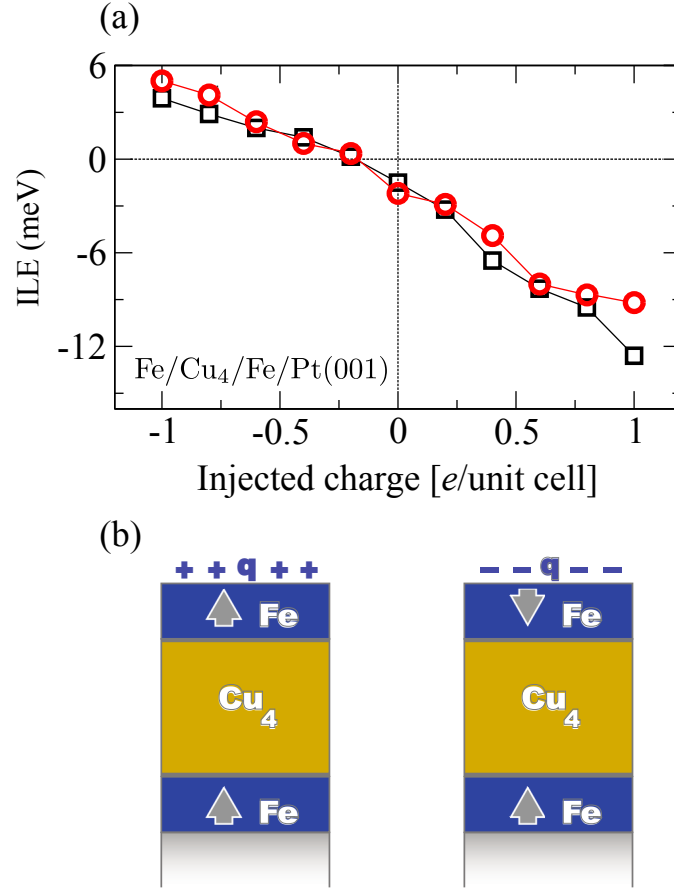


Figure 5.9: (a) Interlayer exchange coupling (IEC) between Fe layers in Fe/Cu₄/Fe/Pt(001) system when it is charged with different amount of electrons (holes). The interlayer exchange coupling is calculated as, $E_{\text{IEC}} = E_{\text{AFM}} - E_{\text{FM}}$, and ferromagnetic and antiferromagnetic orderings have positive and negative signs, respectively. For almost all charge injection the values of E_{IEC} obtained from calculations with (circles) and without (square) spin-orbit coupling are found to be close to each other. (b) A schematic description of Fe/Cu₄/Fe/Pt(001) and the relative alignment of the magnetization as result of charge injection or removal.

The spin magnetic moment of the neutral system for surface Fe layers for both ferromagnetic and antiferromagnetic couplings is $2.77 \mu_B$, whereas the inner Fe layer has spin magnetic moment of $2.60 \mu_B$ and $2.57 \mu_B$, respectively, for FM and AFM cases. When electrons of $1 e$ per unit cell are added (removed) into (from) the ferromagnetically ordered system the spin magnetic moments of the top Fe layer are found to be 2.7 (2.9) μ_B , respectively.

In order to investigate the relative magnetic order (the IEC between the two magnetic layers) for all cases charged and neutral Fe/Cu₄/Fe systems are evaluated. In Fig. 5.9 the IEC of Fe/Cu₄/Fe as function of the injected charge is plotted. For each value of injected charge the IEC is calculated with (circles) and without (square) taking the spin-orbit coupling

into account. For almost all charge injection or removal the values of E_{IEC} obtained from calculations with and without spin-orbit coupling are found to be close to each other. For the neutral system the Fe layers are antiferromagnetically coupled and the IEC is found to be 2.5 meV. Upon removing charge of 1 e per unit cell the AF coupling can be further enhanced, where the value of the IEC is ~ 12 meV.

The most fascinating finding is observed when the Fe/Cu/Fe trilayer is injected with extra electrons, *i.e.* the relative magnetic order is switched from antiferromagnetic coupling to ferromagnetic one. Explicitly, switching from FM to AFM takes place when the system is charged with 0.4 e per unit cell, and when the an extra charge $q \geq 0.4 e$ per unit cell is added the IEC is found to be ~ 3 meV (ferromagnetic coupling). Such tuning of interlayer magnetic order could have significant impact on the process of realizing robust spintronic devices, *e.g.* magnetic random access memory (MRAM). More importantly these results once more show that charge injection could be preferable technique for the switching mechanism of the magnetic orders of elements of spin electronics, as compared to electric field.

The results discussed above are supported by the analysis on the electronic structure of the system. In Fig. 5.10 the difference in the spacial $r = (x, y, z)$ charge distribution from the LDA approximation calculations is presented. In Fig. 5.10(a-d) the difference of the charge densities between the system injected with 1.0 e per unit cell, and the system from which 1.0 e per unit cell is removed are evaluated for both spin channels; majority and minority. It should be noted that the relative alignment of the two magnetic layers in Fe/Cu₄/Fe were coupled ferromagnetically, and the impact of charge doping can be inferred in the spatial charge distribution plots. The blue (red) colors represent higher (lower) number of electrons. The first important information from this plot is accumulation of the net charges at the interfaces of Fe/vacuum and Fe/Pt.

Fig. 5.10(a) shows the difference between the minority charge densities (at $x = 0.05\text{\AA}$ plane) of Fe/Cu₄/Fe on Pt(001) when an extra electrons of 1.0 e per unit cell is added and removed. This spatial charge distribution is a manifestation of the spilling of the minority charge carriers on the surface. Apart from that, similar charge distribution for majority carriers of the top Fe layer (Fig. 5.10(b)) manifest opposite response as compared to the minority carriers. This non-similar response of spatial charge distribution of the injected charge clearly reveals that the effect of interface charging in the Fe/Cu/Fe trilayers is spin-dependent.

For further elaboration on the variation of the charge density along x -direction, similar analysis of the spatial charge distributions on another sample plane ($x = 1.3\text{\AA}$) is plotted Fig. 5.10(c and d). In fact, this sample plane mainly depicts the charge distribution of the bottom Fe layer, and could be possible to observe the spin-dependent response of this layer. From Fig. 5.10(a and c) the spatial charge re-distribution in response to the extra ones for both top and bottom Fe layers is analogous. Once again the spin-dependent spatial distribution of charge density is observed.

The opposite response of majority and minority carriers by interface charging could be confirmed by the spin polarized local density of states (LDOS). The LDOS for the surface Fe layer is shown in Fig. 5.11(a), and the LDOS for bottom Fe layer is also depicted in Fig. 5.11(b). For both cases the density of state of the Fe layers when the system [Fe/Cu₄/Pt(001)] has 1 e per unit cell extra (less) charges is represented with dotted (full) lines. The positive density of states are assigned for the majority carriers, whereas the the negative density of states represent minority carriers. For the surface Fe atom the majority occupied states has one peak at -2 eV, and the minority sates have two peaks of occupied

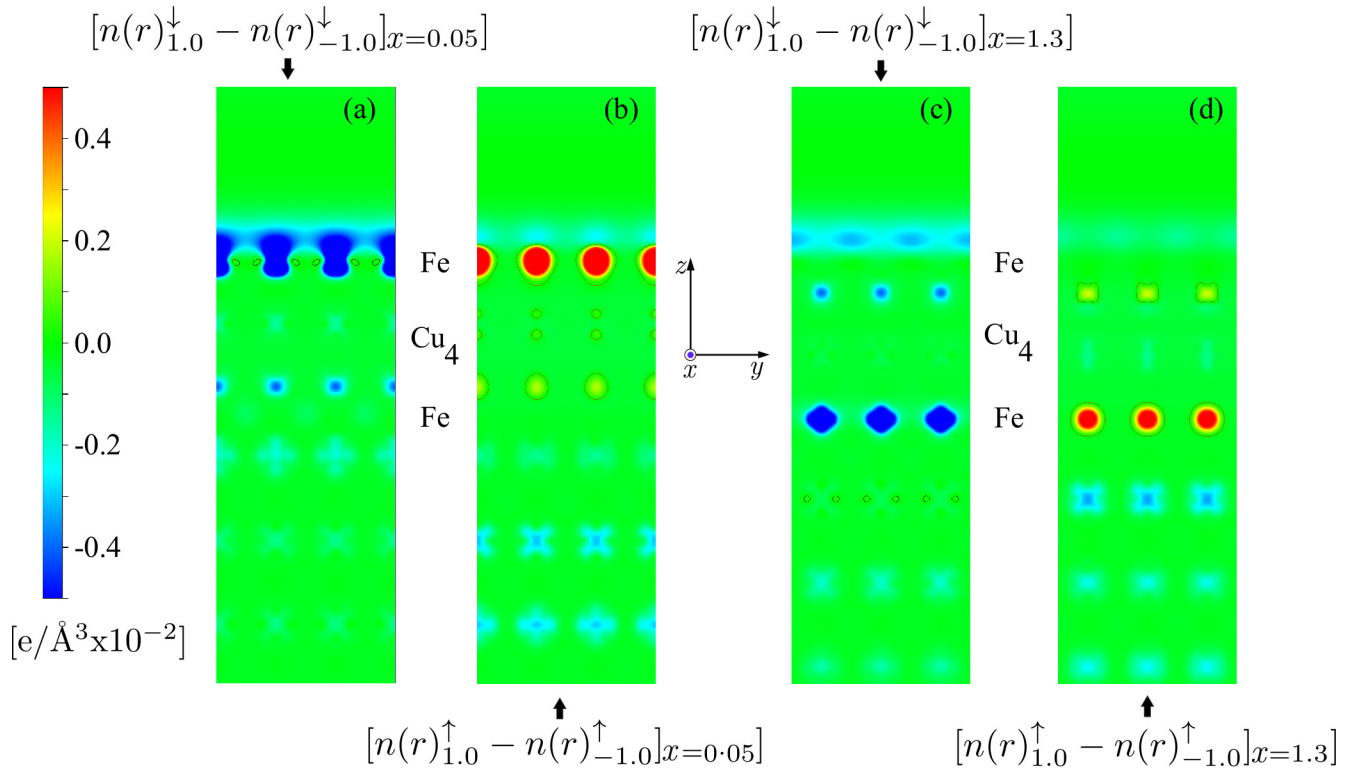


Figure 5.10: The difference between the spacial distribution of charge densities of ferromagnetically coupled Fe/Cu₄/Fe system when it is doped with 1.0 e and 1.0 h . The differences are given for two different planes along the x -axis, namely $x = 0.05 \text{ \AA}$, $x = 1.3 \text{ \AA}$. The charge distributions on each cross-section depicts the variation of the net charges near the top and bottom Fe layers. In both cases the two Fe layers were ferromagnetically aligned. The charge distributions are given in units of $e / \text{\AA}^3$.

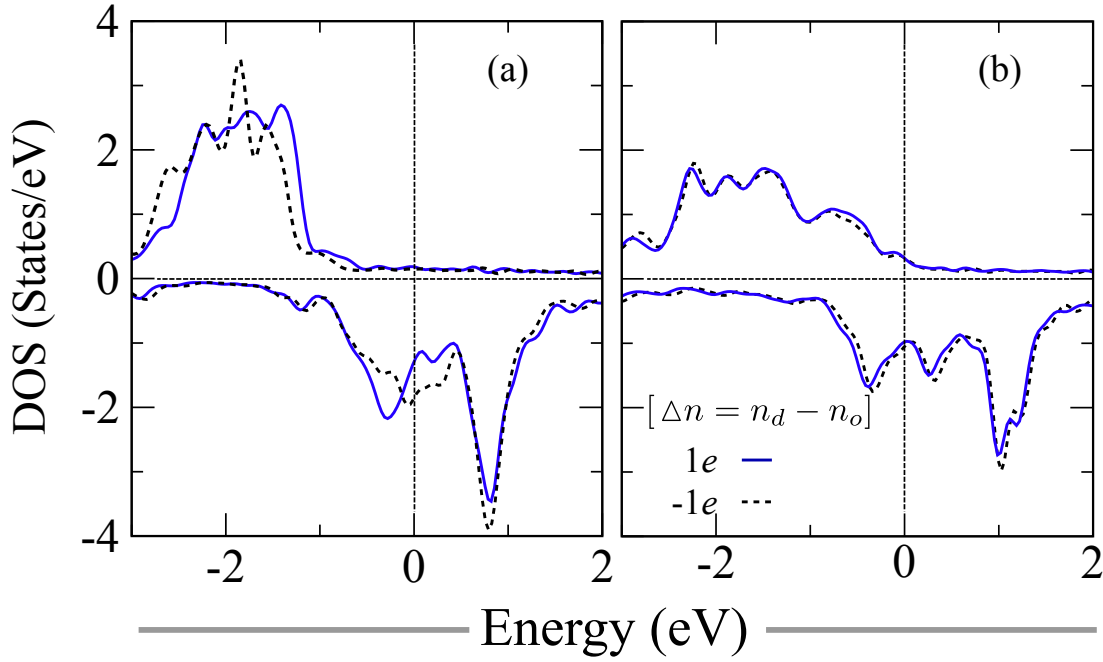


Figure 5.11: The local density of states (LDOS) for both spin up and spin down states of top (a) and bottom (b) Fe layers. The LDOS is plotted for Fe/Cu₄/Fe/Pt(001) system which is charged with extra (less) 1 *e* per unit cell, respectively, is shown in dotted (full) lines. In both cases the two Fe layers were ferromagnetically aligned.

(−0.25 eV) and unoccupied (0.8 eV). It confirms the similar charge re-distribution of same spin channels of the two Fe layers as result of charge injection.

The intricate connection between the LDOS plot and the differences in the spin-dependent spatial charge densities is given as follows; when the net charge in the slab is changed from 1 *e* to -1 *e* per unit cell, the minority peak is shifted to higher energy. Both peaks of the minority LODS are shifted opposite to the majority states. The oppositely affected spin channels are the key reasons for the possible switching of the interlayer exchange coupling between the Fe layers from anti-ferromagnetic to ferromagnetic or vice versa. Besides, the opposite response of the spin up and spin down density of states is in a good agreement with the observation on the spatial charge distribution of the Fe layers, Fig. 5.10.

Besides the discussions on the charge re-distributions the two layers of Fe communicate via the quantum well states within the mediator (Cu). The mutual interaction between the magnetic layers could be described using the difference in the electronic structure for parallel and anti-parallel alignment. Indeed, the valence electrons of parallel and anti-parallel couplings of the superstructures have different spatial distributions. In this case the bottom Fe layer was kept constant and the top Fe layer is rotated by 180° for anti-parallel alignment. Thus, in Fig. 5.12 (a) for both spin channels the LDOS of the bottom Fe layer is plotted, and the DOS for ferromagnetic and anti-ferromagnetic coupling with respect to the top Fe layer is shown by full and dash-dotted lines, respectively. For both magnetic alignments the system was injected with an extra electrons of 1 *e* per unit cell. As result of flipping the top Fe layer, *i.e.* anti-ferromagnetic coupling, the minority density of states just above the Fermi energy becomes less degenerate, and rather smaller changes are observed for majority channel. Similar to Fig. 5.10 the difference in the charge densities are plotted for both spin up and spin down electrons at the cross-section of $x=1.3$, see Fig. 5.10 (b and c). Explicitly,

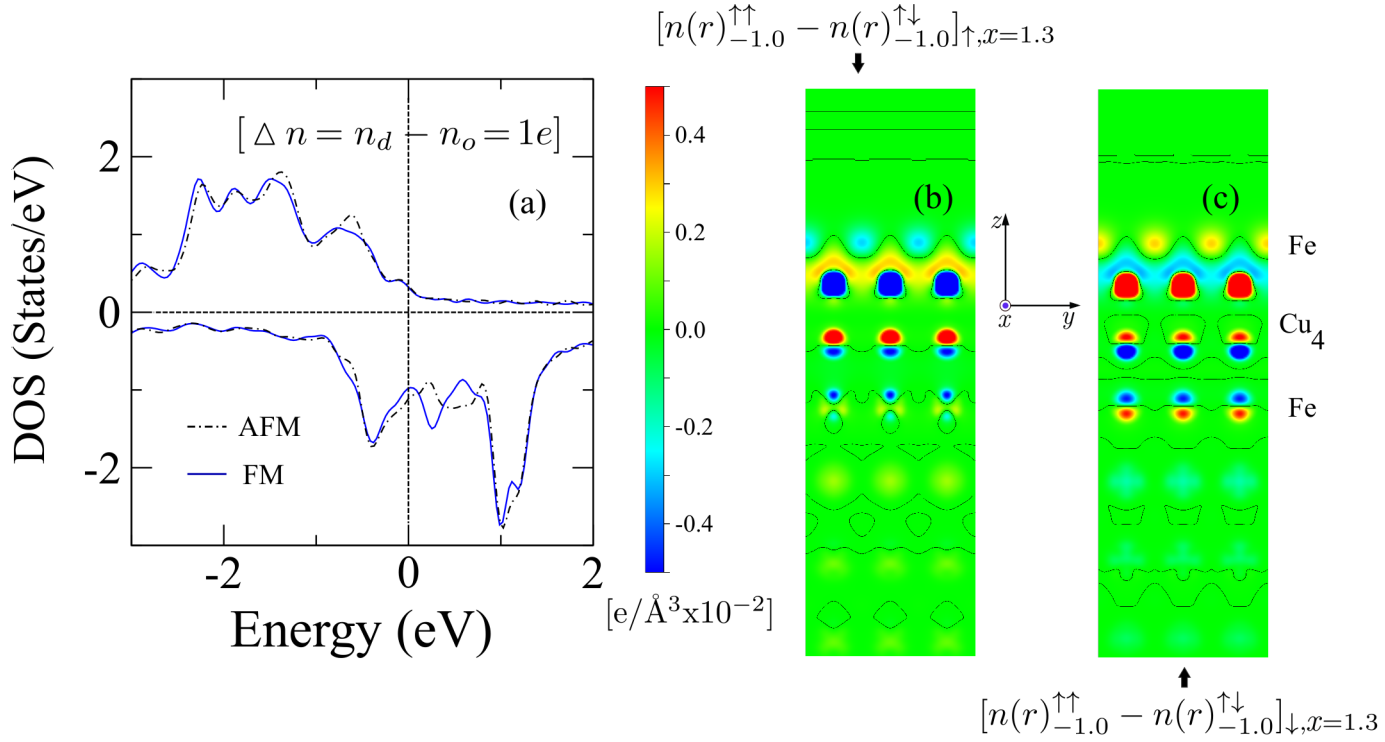


Figure 5.12: (a) The local density of states (LDOS) for both spin up and spin down states of the bottom Fe layer. The LDOS is plotted for ferromagnetic (full line) and antiferromagnetic (dash-dotted line) coupling of the bottom Fe layer with respect to the top one. In both cases the system is charged with extra $1 e$ per unit cell. (b) The difference in the spatial distribution of charge densities between parallel and anti-parallel alignment of Fe/Cu₄/Fe, at a cross-section parallel to the z -axis which intersects at $x=1.3\text{\AA}$. It is plotted for both (b) spin up and (c) spin down channels.

the difference in the spatial charge distribution between ferromagnetic and antiferromagnetic couplings of Fe/Cu₄/Pt(001) is shown. It is clearly seen that for the the minority charge distribution of the bottom Fe layer is affected by the relative magnetic alignment of the two layers, as compared to the majority ones. This contrast corresponds to the the observation in the DOS plot.

Based on the results and discussion provided above one could have some insights about the influence of charge doping on the IEC. Indeed, the nature of the coupling and hence the switching of the IEC depends on the thickness of the spacer and quantum well states therein. On the other hand, the impact of interface charging on Co/Cu₄/Co trilayer was also investigated, and the neutral system is found to have antiferromagnetic coupling ($E_{\text{IEC}} = -5.4$ meV). However, in order to observe a transition to ferromagnetic coupling a rather large amount of charge of the order of 1 e /unit cell should be removed.

5.4 Summary

In this chapter we have revealed a strong effect of surface charging on the MAE of alloyed $3d/5d$ multilayers, using Fe-Pt multilayers as a particular model system. Surface-charging results in a direct change of both magnitude and direction of magnetization and magnetic anisotropy. A remarkable enhancement in MAE upon charge-injection is found in Pt/Fe/Pt(100). In capped multilayers with double Fe-layers, a spin-reorientation occurs due to an enhancement of the hybridization caused by both alloying and charge-doping. Moreover, it was proven that the interlayer exchange coupling across Cu layer can also be tuned by addition or removal of extra charge. It was demonstrated that the charge-removal can switch the magnetic order from antiferromagnetic to ferromagnetic state. These observations lead us to the conclusion that charge injection might be used as a promising technique for engineering novel materials with potential technological applications.

Conclusions

Summarizing everything that has been discussed in the foregoing chapters, we can conclude, that, based on the state-of-the-art *ab initio* calculations, magnetic properties of metallic 1-D and 2-D nanoscale structures can be tailored statically by tuning their geometry, chemical composition. But most interestingly, applying external electric field or surface charging can allow one to dynamically tune such important parameters of spintronics-oriented nanostructures as magnetic moment, magnetic anisotropy value and orientation and the interlayer exchange coupling and ordering.

In linear surface-supported chains, mixing magnetic $3d$ and non-magnetic relativistic $5d$ results in a system with substantial magnetic anisotropy, which can then be tuned in magnitude and direction by exposing the wires to an external electric field.

Going one dimension up, to metallic multilayers, one observes much the same physics as in chains, with the added effect of the confinement of electrons in the direction perpendicular to the film. This finite size effect, boiling down to the presence of spin-polarized quantum well states, causes the above mentioned magnetic characteristics of the system to acquire a thickness dependence. Juggling the stoichiometry and thickness of $3d/5d$ layer-wise alloyed films and playing them against the external electric field one is presented with infinite opportunities of designing a system with predefined and controllable magnetic properties.

And if the effect of the electric field happens to be insufficient, a direct charge injection into the system of alloyed multilayers (decoupled from a metallic bulk) drastically changes the system's electronic and magnetic properties, magnetic anisotropy and interlayer exchange coupling among them. Particularly, adding or removing $1 \bar{e}$ per surface cell can allow one to change the magnetic anisotropy of the system almost by an order of magnitude or even realign the easy axis of magnetization. For coupled magnetic layers such surface charging might even be the only dynamical possibility to reverse the exchange coupling in the system.

Bibliography

- [1] S. A. Wolf, D. D. Awschalom, R. A. Buhrman, J. M. Daughton, S. von Molnár, M. L. Roukes, A. Y. Chtchelkanova and D. M. Treger. *Spintronics: A spin-based electronics vision for the future*. Science (New York, N.Y.), **294**, 1488 (2001).
- [2] P. Gambardella, A. Dallmeyer, K. Maiti, M. C. Malagoli, W. Eberhardt, K. Kern and C. Carbone. *Ferromagnetism in one-dimensional monatomic metal chains*. Nature, **416**, 301 (2002).
- [3] I. Žutić, J. Fabian and S. Sarma. *Spintronics: Fundamentals and applications*. Reviews of modern physics, **76**, 323 (2004).
- [4] G. A. Prinz. *Magnetoelectronics*. Science, **282**, 1660 (1998).
- [5] B. Lenk, H. Ulrichs, F. Garbs and M. Münzenberg. *The building blocks of magnonics*. Physics Reports, **507**, 107 (2011).
- [6] F. S. G. Binasch. P. Grunberg and W. Zinn. *Enhanced magnetoresistance in layered magnetic structures*. Physical Review B, **39**, 4828 (1989).
- [7] L. D. Physique, U. U. Paris-sud and F. Orsay. *Giant Magnetoresistance of (001)Fe/(001)Cr Magnetic Superlattices*. Physical Review Letters, **61**, 2472 (1988).
- [8] S. N. Piramanayagam and T. C. Chong. *Developments in Data Storage: Materials perspective*. John Wiley Sons, Inc., Hoboken, NJ, USA (2011).
- [9] R. Rottmayer, S. Batra, D. Buechel, W. Challener, J. Hohlfield, Y. Kubota, L. Li, B. Lu, C. Mihalcea, K. Mountfield, K. Pelhos, C. Peng, T. Rausch, M. Seigler, D. Weller and X.-M. Yang. *Heat-Assisted Magnetic Recording*. IEEE Transactions on Magnetics, **42**, 2417 (2006).
- [10] I. M. L. Billas, A. Chatelain and W. A. de Heer. *Magnetism from the atom to the bulk in iron, cobalt, and nickel clusters*. Science, **265**, 1682 (1994).
- [11] G. Autès, C. Barreteau, D. Spanjaard and M.-C. Desjonquères. *Magnetism of iron: from the bulk to the monatomic wire*. Journal of Physics: Condensed Matter, **18**, 6785 (2006).
- [12] P. Boski, A. Lehnert, S. Denmler, S. Rusponi, M. Etzkorn, G. Moulas, P. Bencok, P. Gambardella, H. Brune and J. Hafner. *Magnetocrystalline anisotropy energy of Co and Fe adatoms on the (111) surfaces of Pd and Rh*. Physical Review B, **81**, 104426 (2010).

- [13] P. Gambardella, S. Rusponi, M. Veronese, S. S. Dhesi, C. Grazioli, A. Dallmeyer, I. Cabria, R. Zeller, P. H. Dederichs, K. Kern, C. Carbone and H. Brune. *Giant magnetic anisotropy of single cobalt atoms and nanoparticles*. Science (New York, N.Y.), **300**, 1130 (2003).
- [14] J. Honolka, T. Lee, K. Kuhnke, D. Repetto, V. Sessi, P. Wahl, a. Buchsbaum, P. Varga, S. Gardonio, C. Carbone, S. Krishnakumar, P. Gambardella, M. Komelj, R. Singer, M. Fähnle, K. Fauth, G. Schütz, a. Enders and K. Kern. *Complex magnetic phase in submonolayer Fe stripes on Pt(997)*. Physical Review B, **79**, 104430 (2009).
- [15] J. Wiebe, L. Zhou and R. Wiesendanger. *Atomic magnetism revealed by spin-resolved scanning tunnelling spectroscopy*. Journal of Physics D: Applied Physics, **44**, 464009 (2011).
- [16] J. Tersoff and D. R. Hamann. *Theory of the scanning tunneling microscope*. Physical Review B, **31**, 805 (1985).
- [17] R. Wiesendanger. *Single-atom magnetometry*. Current Opinion in Solid State and Materials Science, **15**, 1 (2011).
- [18] F. Meier, L. Zhou, J. Wiebe and R. Wiesendanger. *Revealing magnetic interactions from single-atom magnetization curves*. Science (New York, N.Y.), **320**, 82 (2008).
- [19] A. Heinrich, J. A. Gupta, C. P. Lutz and D. M. Eigler. *Single-atom spin-flip spectroscopy*. Science (New York, N.Y.), **306**, 466 (2004).
- [20] M. Bode. *The environment matters - even on the atomic scale*. Science (New York, N.Y.), **306**, 423 (2004).
- [21] T. Balashov, T. Schuh, A. Takács, A. Ernst, S. Ostanin, J. Henk, I. Mertig, P. Bruno, T. Miyamachi, S. Suga and W. Wulfhekel. *Magnetic Anisotropy and Magnetization Dynamics of Individual Atoms and Clusters of Fe and Co on Pt(111)*. Physical Review Letters, **102**, 257203 (2009).
- [22] N. Nilius, T. M. Wallis and W. Ho. *Development of one-dimensional band structure in artificial gold chains*. Science (New York, N.Y.), **297**, 1853 (2002).
- [23] A. Stekolnikov, F. Bechstedt, M. Wisniewski, J. Schäfer and R. Claessen. *Atomic Nanowires on the Pt/Ge(001) Surface: Buried Pt-Ge Versus Top Pt-Pt Chains*. Physical Review Letters, **100**, 196101 (2008).
- [24] J. Lagoute, C. Nacci and S. Fölsch. *Doping of Monatomic Cu Chains with Single Co Atoms*. Physical Review Letters, **98**, 146804 (2007).
- [25] J.-P. B. Hogler Roser, Elmar Hahn, Harald Brune and K. Kern. *Building one and two dimensional nanostructures by diffusion controlled aggregation at surfaces*. Nature, **366**, 141 (1993).
- [26] D. Wei, C. Gao, K. Zakeri and M. Przybylski. *Pd atomic chain formation as a result of submonolayer deposition of 3d metals on Pd (110)*. Physical review letters, **103**, 225504 (2009).

- [27] P. Gambardella, A. Dallmeyer, K. Maiti, M. Malagoli, S. Rusponi, P. Ohresser, W. Eberhardt, C. Carbone and K. Kern. *Oscillatory Magnetic Anisotropy in One-Dimensional Atomic Wires*. Physical Review Letters, **93**, 077203 (2004).
- [28] N. D. Mermin and H. Wagner. *Absence of ferromagnetism or anti-ferromagnetism in one or two dimensional isotropic Heisenberg models*. Physical Review Letters, **17**, 1133 (1966).
- [29] J. Dorantes-Dávila and G. Pastor. *Magnetic Anisotropy of One-Dimensional Nanostructures of Transition Metals*. Physical Review Letters, **81**, 208 (1998).
- [30] S. Fölsch, P. Hyldgaard, R. Koch and K. Ploog. *Quantum Confinement in Monatomic Cu Chains on Cu(111)*. Physical Review Letters, **92**, 056803 (2004).
- [31] M. Przybylski, M. Dabrowski, U. Bauer, M. Cinal and J. Kirschner. *Oscillatory magnetic anisotropy due to quantum well states in thin ferromagnetic films (invited)*. Journal of Applied Physics, **111**, 07C102 (2012).
- [32] J. S. Park, A. Quesada, Y. Meng, J. Li, E. Jin, H. Son, A. Tan, J. Wu, C. Hwang, H. W. Zhao, A. K. Schmid and Z. Q. Qiu. *Determination of spin-polarized quantum well states and spin-split energy dispersions of Co ultrathin films grown on Mo(110)*. Physical Review B, **83**, 113405 (2011).
- [33] V. Sandomirskii. *Quantum size effect in a semimetal film*. Soviet Physics JETP, **25**, 101 (1967).
- [34] R. K. Kawakami, H. J. Choi, E. J. Escorcía-aparicio, M. O. Bowen, J. H. Wolfe, E. Arenholz and Z. Q. Qiu. *Quantum-well states in copper thin films*. Nature, **398**, 132 (1999).
- [35] T. C. Chiang. *Photoemission studies of quantum well states in thin films*. Surface Science Reports, **39**, 181 (2000).
- [36] O. Brovko, P. A. Ignatiev and V. S. Stepanyuk. *Confined bulk states as a long-range sensor for impurities and a transfer channel for quantum information*. Physical Review B, **83**, 125415 (2011).
- [37] N. V. Smith. *Phase analysis of image states and surface states associated with nearly free electron band gaps*. Physical Review B, **32**, 7 (1985).
- [38] T. Hirahara, T. Komorida, A. Sato, G. Bihlmayer, E. Chulkov, K. He, I. Matsuda and S. Hasegawa. *Manipulating quantum-well states by surface alloying: Pb on ultrathin Ag films*. Physical Review B, **78**, 035408 (2008).
- [39] N. Binggeli and M. Altarelli. *Surface Reactivity and Quantum-Size Effects on the Electronic Density Decay Length of Ultrathin Metal Films*. Physical Review Letters, **96**, 036805 (2006).
- [40] Y. Guo, Y.-F. Zhang, X.-Y. Bao, T.-Z. Han, Z. Tang, L.-X. Zhang, W.-G. Zhu, E. G. Wang, Q. Niu, Z. Q. Qiu, J.-F. Jia, Z.-X. Zhao and Q.-K. Xue. *Superconductivity modulated by quantum size effects*. Science (New York, N.Y.), **306**, 1915 (2004).

- [41] K. Garrison, Y. Chang and P. Johnson. *Spin Polarization of Quantum Well States in copper thin films deposited on a Co(001) substrate*. Physical Review Letters, **71**, 2801 (1993).
- [42] J. J. Paggel, T. Miller and T.-C. Chiang. *Quantum-Well States as Fabry-Pérot Modes in a Thin-Film Electron Interferometer*. Science, **283**, 1709 (1999).
- [43] D. Luh, J. Paggel, T. Miller and T. Chiang. *d-Band Quantum Well States*. Physical review letters, **84**, 3410 (2000).
- [44] M. Cinal. *Origin of magnetocrystalline anisotropy oscillations in (001) face-centred-cubic Co thin films and effect of spd hybridization*. Journal of Physics: Condensed Matter, **15**, 17 (2003).
- [45] K. Yoshimatsu, K. Horiba, H. Kumigashira, T. Yoshida, A. Fujimori and M. Oshima. *Metallic Quantum Well States in Artificial Structures of Strongly Correlated Oxide*. Science, **333**, 319 (2011).
- [46] F. J. Himpsel. *Fe on Au(100): Quantum well states*. Physical Review B, **44**, 59966(R) (1991).
- [47] K. Altmann, W. O'Brien and D. Seo. *Spin-polarized quantum well states*. Journal of Electron Spectroscopy and Related Phenomena, **103**, 367 (1999).
- [48] C. Stamm, S. Egger and D. Pescia. *Quantum oscillations in a confined electron gas*. Nature, **389**, 937 (1997).
- [49] H. Oka, P. A. Ignatiev, S. Wedekind, G. Rodary, L. Niebergall, V. S. Stepanyuk, D. Sander and J. Kirschner. *Spin-dependent quantum interference within a single magnetic nanostructure*. Science (New York, N.Y.), **327**, 843 (2010).
- [50] J. Slonczewski. *Current-driven excitation of magnetic multilayers*. Journal of Magnetism and Magnetic Materials, **159**, L1 (1996).
- [51] L. Berger. *Emission of spin waves by magnetic multilayer traversed by a current*. Physical Review B, **54**, 9353 (1996).
- [52] J. Katine and E. E. Fullerton. *Device implications of spin-transfer torques*. Journal of Magnetism and Magnetic Materials, **320**, 1217 (2008).
- [53] S. Loth, S. Baumann, C. P. Lutz, D. M. Eigler and A. J. Heinrich. *Bistability in atomic-scale antiferromagnets*. Science (New York, N.Y.), **335**, 196 (2012).
- [54] W.-G. Wang, M. Li, S. Hageman and C. L. Chien. *Electric-field-assisted switching in magnetic tunnel junctions*. Nature materials, **11**, 64 (2012).
- [55] N. A. Spaldin and M. Fiebig. *Materials science. The renaissance of magnetoelectric multiferroics*. Science (New York, N.Y.), **309**, 391 (2005).
- [56] M. Fiebig. *Revival of the magnetoelectric effect*. Journal of Physics D: Applied Physics, **38**, R123 (2005).

- [57] S. Sahoo, S. Polisetty, C.-G. Duan, S. Jaswal, E. Tsymbal and C. Binek. *Ferroelectric control of magnetism in BaTiO₃/Fe heterostructures via interface strain coupling*. Physical Review B, **76**, 092108 (2007).
- [58] T. Lonkai, D. Tomuta, U. Amann, J. Ihringer, R. Hendrikx, D. Többens and J. Mydosh. *Development of the high-temperature phase of hexagonal manganites*. Physical Review B, **69**, 134108 (2004).
- [59] T. Kimura, T. Goto, H. Shintani, K. Ishizaka, T. Arima and Y. Tokura. *Magnetic control of ferroelectric polarization*. Nature, **426**, 55 (2003).
- [60] T. Lottermoser, T. Lonkai and U. Amann. *Magnetic phase control by an electric field*. Nature, **430**, 541 (2004).
- [61] H.-C. Ding and C.-G. Duan. *Electric-field control of magnetic ordering in the tetragonal-like BiFeO₃*. EPL (Europhysics Letters), **97**, 57007 (2012).
- [62] P. Babkevich, A. Poole, R. D. Johnson, B. Roessli, D. Prabhakaran and A. T. Boothroyd. *Electric field control of chiral magnetic domains in the high-temperature multiferroic CuO*. Physical Review B, **85**, 134428 (2012).
- [63] A. J. Hearmon, F. Fabrizi, L. C. Chapon, R. D. Johnson, D. Prabhakaran, S. V. Streltsov, P. J. Brown and P. G. Radaelli. *Electric Field Control of the Magnetic Chiralities in Ferroaxial Multiferroic RbFe(MoO₄)₂*. Physical Review Letters, **108**, 237201 (2012).
- [64] Y. Chen, T. Fitchorov, Z. Cai, K. S. Ziemer, C. Vittoria and V. G. Harris. *Electric field controlled magnetic hysteresis loops in a Metglas/PMNPT heterostructure*. Journal of Physics D: Applied Physics, **43**, 155001 (2010).
- [65] S. Brivio, D. Petti, R. Bertacco and J. C. Cezar. *Electric field control of magnetic anisotropies and magnetic coercivity in Fe/BaTiO₃(001) heterostructures*. Applied Physics Letters, **98**, 092505 (2011).
- [66] D. Lebeugle, A. Mougin, M. Viret, D. Colson and L. Ranno. *Electric Field Switching of the Magnetic Anisotropy of a Ferromagnetic Layer Exchange Coupled to the Multiferroic Compound BiFeO₃*. Physical Review Letters, **103**, 257601 (2009).
- [67] D. Chiba, M. Sawicki, Y. Nishitani, Y. Nakatani, F. Matsukura and H. Ohno. *Magnetization vector manipulation by electric fields*. Nature, **455**, 515 (2008).
- [68] H. Ohno, D. Chiba, F. Matsukura, T. Omiya, E. Abe, T. Dietl, Y. Ohno and K. Ohtani. *Electric-field control of ferromagnetism*. Nature, **408**, 944 (2000).
- [69] M. Weisheit, S. Fähler, A. Marty, Y. Souche, C. Poinignon and D. Givord. *Electric field-induced modification of magnetism in thin-film ferromagnets*. Science (New York, N.Y.), **315**, 349 (2007).
- [70] T. Maruyama, Y. Shiota, T. Nozaki, K. Ohta, N. Toda, M. Mizuguchi, A. A. Tulapurkar, T. Shinjo, M. Shiraishi, S. Mizukami, Y. Ando and Y. Suzuki. *Large voltage-induced magnetic anisotropy change in a few atomic layers of iron*. Nature nanotechnology, **4**, 158 (2009).

- [71] Y. Yamada, K. Ueno, T. Fukumura, H. T. Yuan, H. Shimotani, Y. Iwasa, L. Gu, S. Tsukimoto, Y. Ikuhara and M. Kawasaki. *Electrically induced ferromagnetism at room temperature in cobalt-doped titanium dioxide*. *Science* (New York, N.Y.), **332**, 1065 (2011).
- [72] S. Zhang. *Spin-Dependent Surface Screening in Ferromagnets and Magnetic Tunnel Junctions*. *Physical Review Letters*, **83**, 640 (1999).
- [73] N. N. Negulyaev, V. S. Stepanyuk, W. Hergert and J. Kirschner. *Electric Field as a Switching Tool for Magnetic States in Atomic-Scale Nanostructures*. *Physical Review Letters*, **106**, 037202 (2011).
- [74] T. R. Dasa, P. A. Ignatiev and V. S. Stepanyuk. *Effect of the electric field on magnetic properties of linear chains on a Pt(111) surface*. *Physical Review B*, **85**, 205447 (2012).
- [75] Y. Sun, J. D. Burton and E. Y. Tsymbal. *Electrically driven magnetism on a Pd thin film*. *Physical Review B*, **81**, 064413 (2010).
- [76] E. C. Stoner. *Collective Electron Specific Heat and Spin Paramagnetism in Metals*. *Proceedings of the Royal Society A: Mathematical, Physical and Engineering Sciences*, **154**, 656 (1936).
- [77] C.-G. Duan, J. Velez, R. Sabirianov, Z. Zhu, J. Chu, S. Jaswal and E. Tsymbal. *Surface Magnetoelectric Effect in Ferromagnetic Metal Films*. *Physical Review Letters*, **101**, 137201 (2008).
- [78] K. Nakamura, R. Shimabukuro and Y. Fujiwara. *Giant modification of the magnetocrystalline anisotropy in transition-metal monolayers by an external electric field*. *Physical review letters*, **102**, 187201 (2009).
- [79] H. Zhang, M. Richter, K. Koepf, I. Opahle, F. Tasnádi and H. Eschrig. *Electric-field control of surface magnetic anisotropy: a density functional approach*. *New Journal of Physics*, **11**, 043007 (2009).
- [80] K. Shimamura, D. Chiba, S. Ono, S. Fukami, N. Ishiwata, M. Kawaguchi, K. Kobayashi and T. Ono. *Electrical control of Curie temperature in cobalt using an ionic liquid film*. *Applied Physics Letters*, **100**, 122402 (2012).
- [81] L. Juárez-Reyes, G. M. Pastor and V. S. Stepanyuk. *Tuning substrate-mediated magnetic interactions by external surface charging: Co and Fe impurities on Cu(111)*. *Physical Review B*, **86**, 235436 (2012).
- [82] P. Ruiz-Díaz, T. R. Dasa and V. S. Stepanyuk. *Tuning Magnetic Anisotropy in Metallic Multilayers by Surface Charging: An ab-initio Study*. *Physical Review Letters*, **110**, 267203 (2013).
- [83] P. Hohenberg and W. Kohn. *Inhomogeneous Electron gas*. *Physical Review*, **136**, B864 (1964).
- [84] E. D. Joubert. *Density Functionals: Theory and Applications*. Springer, Berlin (1998).

- [85] R. M. Martin. *Electronic Structure, Basic Theory and Practical Applications*. Cambridge University Press (2004).
- [86] W. Kohn and L. J. Sham. *Self consistent equations including exchange and correlation effects*. Physical Review, **140**, A1133 (1965).
- [87] D. M. Ceperley and B. J. Alder. *Ground state of the electron gas by a stochastic method*. Physical Review Letters, **45**, 566 (1980).
- [88] J. P. Perdew and A. Zunger. *Self interaction correction to density functional approximations for many electron systems*. Physical Review B, **23**, 5048 (1981).
- [89] J. Perdew, K. Burke and M. Ernzerhof. *Generalized Gradient Approximation Made Simple*. Physical review letters, **77**, 3865 (1996).
- [90] U. von Barth and L. Hedin. *A local exchange-correlation potential for the spin polarized case. I*. Journal of Physics C: Solid State Physics, **5**, 1629 (1972).
- [91] E. K. U. Gross and R. M. Dreizler. *Density Functional Theory : An Approach to the Quantum Many-Body Problem*. Springer-Verlag, Berlin Heidelberg (1990).
- [92] L. Nordstrom and D. J. Singh. *Planewaves, pseudopotentials, and the LAPW method*. Springer Science+Business media, Inc., second edi edn. (2006).
- [93] L. M. Sandratskii. *Noncollinear magnetism in itinerant-electron systems: Theory and applications*. Advances in Physics, **47**, 91 (1998).
- [94] D. Hobbs, G. Kresse and J. Hafner. *Fully unconstrained noncollinear magnetism within the projector augmented-wave method*. Physical Review B, **62**, 11556 (2000).
- [95] L. Kleinman. *Relativistic norm-conserving pseudopotential*. Physical Review B, **21**, 2630 (1980).
- [96] W. E. P. MacDonald and D. D. Koelling. *A linearised relativistic augmented-plane-wave method utilising approximate pure spin basis functions*. Journal of Physics C: Solid St. Phys., **13**, 2675 (1979).
- [97] P. Boski, S. Dennler and J. Hafner. *Strong spin-orbit effects in small Pt clusters: geometric structure, magnetic isomers and anisotropy*. The Journal of chemical physics, **134**, 034107 (2011).
- [98] J. Kubler and K. Hock. *Density functional theory of non-collinear magnetism*. Journal of Physics F: Metal Phys., **18**, 469 (1988).
- [99] B. J. Austin, V. Heine and L. J. Sham. *General theory of pseudopotentials*. Physical Review, **127**, 267 (1962).
- [100] D. Hamann, M. Schlüter and C. Chiang. *Norm-conserving pseudopotentials*. Physical Review Letters, **43**, 1494 (1979).
- [101] D. Vanderbilt. *Soft self consistent pseudopotentials in a generalized eigenvalue formalism*. Applied optics, **25**, 4228 (1986).

- [102] E. Moroni, G. Kresse, J. Hafner and J. Furthmüller. *Ultrasoft pseudopotentials applied to magnetic Fe, Co, and Ni: From atoms to solids*. Physical Review B, **56**, 15629 (1997).
- [103] J. Hafner and G. Kresse. *Ab initio molecular dynamics for liquid metals*. Physical Review B, **47**, 558(R) (1993).
- [104] P. Giannozzi, S. Baroni, N. Bonini, M. Calandra, R. Car, C. Cavazzoni, D. Ceresoli, G. L. Chiarotti, M. Cococcioni, I. Dabo, A. Dal Corso, S. de Gironcoli, S. Fabris, G. Fratesi, R. Gebauer, U. Gerstmann, C. Gougoussis, A. Kokalj, M. Lazzeri, L. Martin-Samos, N. Marzari, F. Mauri, R. Mazzarello, S. Paolini, A. Pasquarello, L. Paulatto, C. Sbraccia, S. Scandolo, G. Sclauzero, A. P. Seitsonen, A. Smogunov, P. Umari and R. M. Wentzcovitch. *QUANTUM ESPRESSO: a modular and open-source software project for quantum simulations of materials*. Journal of physics. Condensed matter : an Institute of Physics journal, **21**, 395502 (2009).
- [105] G. Kresse and D. Joubert. *From ultrasoft pseudopotentials to the projector augmented-wave method*. Physical Review B, **59**, 1758 (1999).
- [106] P. E. Blochl. *Projector augmented wave method*. Physical Review B, **50**, 17953 (1994).
- [107] J. Repp, G. Meyer, F. E. Olsson and M. Persson. *Controlling the charge state of individual gold adatoms*. Science (New York, N.Y.), **305**, 493 (2004).
- [108] Y. Shen, S. Guo, J. Hu and Y. Zhang. *Charging of nanostructured and partially reduced graphene oxide sheets*. Applied Physics Letters, **101**, 183109 (2012).
- [109] M. Zdrojek, T. Melin, C. Boyaval, D. Stievenard, B. Jouault, M. Wozniak, a. Huczko, W. Gebicki and L. Adamowicz. *Charging and emission effects of multiwalled carbon nanotubes probed by electric force microscopy*. Applied Physics Letters, **86**, 213114 (2005).
- [110] K. Kunc and R. Resta. *External Fields in the Self-Consistent Theory of Electronic States: A New Method for Direct Evaluation of Macroscopic and Microscopic Dielectric Response*. Physical Review Letters, **51**, 686 (1983).
- [111] J. Neugebauer and M. Scheffler. *Adsorbate substrate and adsorbate-adsorbate interaction of Na and K adlayers on Al(111)*. Physical Review B, **46**, 16067 (1992).
- [112] G. Kresse and O. Lebacqz. *Vasp Manual*, <http://cms.mpi.univie.ac.at/vasp/vasp/>.
- [113] G. Makov and M. C. Payne. *Periodic boundary conditions in ab initio calculations*. Physical Review B, **51**, 4014 (1995).
- [114] I. Dabo, B. Kozinsky, N. Singh-Miller and N. Marzari. *Electrostatics in periodic boundary conditions and real-space corrections*. Physical Review B, **77**, 115139 (2008).
- [115] A. D. Corso and A. M. Conte. *Spin-orbit coupling with ultrasoft pseudopotentials: Application to Au and Pt*. Physical Review B, **71**, 115106 (2005).
- [116] D.-S. Wang, R. Wu and A. J. Freeman. *First principle theory of surface magneto crystalline anisotropy and diatomic pair model*. Physical Review B, **47**, 14932 (1993).

- [117] P. Bruno. *Tight-binding approach to the orbital magnetic moment and magneto crystalline anisotropy*. Physical Review B, **39**, 865 (1989).
- [118] H. Schuurmans. *Magnetic anisotropy of free standing Co monolayers and of multilayers which contain Co monolayers*. Physical Review B, **50**, 9989 (1994).
- [119] A. Mosca Conte, S. Fabris and S. Baroni. *Properties of Pt-supported Co nanomagnets from relativistic density functional theory calculations*. Physical Review B, **78**, 014416 (2008).
- [120] E. Y. Tsybal. *Spintronics: Electric toggling of magnets*. Nature materials, **11**, 12 (2012).
- [121] P. Boski and J. Hafner. *Density-functional theory of the magnetic anisotropy of nanostructures: an assessment of different approximations*. Journal of physics. Condensed matter : an Institute of Physics journal, **21**, 426001 (2009).
- [122] S. Baud, C. Ramseyer, G. Bihlmayer and S. Blügel. *Relaxation effects on the magnetism of decorated step edges: CoPt(664)*. Physical Review B, **73**, 104427 (2006).
- [123] B. Lazarovits, L. Szunyogh and P. Weinberger. *Magnetic properties of finite Co chains on Pt(111)*. Physical Review B, **67**, 024415 (2003).
- [124] S. Rusponi, T. Cren, N. Weiss, M. Epple, P. Bulushek, L. Claude and H. Brune. *The remarkable difference between surface and step atoms in the magnetic anisotropy of two-dimensional nanostructures*. Nature materials, **2**, 546 (2003).
- [125] A. Shick, F. Máca and A. Lichtenstein. *Magnetic anisotropy of single 3d spins on a CuN surface*. Physical Review B, **79**, 172409 (2009).
- [126] K.-F. Braun and K.-H. Rieder. *Engineering Electronic Lifetimes in Artificial Atomic Structures*. Physical Review Letters, **88**, 096801 (2002).
- [127] A. A. Khajetoorians, J. Wiebe, B. Chilian and R. Wiesendanger. *Realizing all-spin-based logic operations atom by atom*. Science (New York, N.Y.), **332**, 1062 (2011).
- [128] G. Moulas, A. Lehnert, S. Rusponi, J. Zabloudil, C. Etz, S. Ouazi, M. Etzkorn, P. Bencok, P. Gambardella, P. Weinberger and H. Brune. *High magnetic moments and anisotropies for Fe_xCo_{1-x} monolayers on Pt(111)*. Physical Review B, **78**, 214424 (2008).
- [129] F. J. Himpsel. *Quantum well states as mediator of magnetic coupling in superlattices*. Physical Review Letters, **69**, 844 (1992).
- [130] A. V. de Parga and R. M. Hinarejos, J.J., F. Calleja, J. Camarero, R. Otero. *Quantum oscillations in surface properties*. Surface Science, **603**, 1389 (2009).
- [131] W. B. Su, C. S. Chang and T. T. Tsong. *Quantum size effect on ultra-thin metallic films*. Journal of Physics D: Applied Physics, **43**, 013001 (2010).
- [132] K. He, L. Zhang, X. Ma, J. Jia, Q. Xue and Z. Qiu. *Growth and magnetism of ultrathin Fe films on Pt(100)*. Physical Review B, **72**, 155432 (2005).

- [133] A. Freeman and R. qian Wu. *Electronic structure theory of surface, interface and thin film magnetism*. Journal of Magnetism and Magnetic Materials, **100**, 497 (1991).
- [134] W. Weber, A. Bischof and R. Allenspach. *Oscillatory Magnetic Anisotropy and Quantum Well States in Cu/ Co/Cu (100) Films*. Physical Review Letters, **76**, 4 (1996).
- [135] Z.-Y. Lu, X.-G. Zhang and S. Pantelides. *Spin-Dependent Resonant Tunneling through Quantum-Well States in Magnetic Metallic Thin Films*. Physical Review Letters, **94**, 207210 (2005).
- [136] J. Li, M. Przybylski, F. Yildiz, X. Ma and Y. Wu. *Oscillatory Magnetic Anisotropy Originating from Quantum Well States in Fe Films*. Physical Review Letters, **102**, 207206 (2009).
- [137] U. Bauer, M. Dbrowski, M. Przybylski and J. Kirschner. *Experimental confirmation of quantum oscillations of magnetic anisotropy in Co/Cu(001)*. Physical Review B, **84**, 144433 (2011).
- [138] Van Gelderen P, S. Crampin and J. Inglesfield. *Quantum-well states in Cu/Co overlayers and sandwiches*. Physical review. B, **53**, 9115 (1996).
- [139] M. Cinal and D. Edwards. *Quantum-well states and magnetocrystalline anisotropy in Co/Pd structures*. Physical Review B, **57**, 100 (1998).
- [140] G. Guo. *Magnetocrystalline anisotropy oscillations predicted in Fe/Au (001) superlattices*. Journal of Physics: Condensed Matter, **11**, 4329 (1999).
- [141] M. Tsujikawa and T. Oda. *Finite Electric Field Effects in the Large Perpendicular Magnetic Anisotropy Surface Pt/Fe/Pt(001): A First-Principles Study*. Physical Review Letters, **102**, 247203 (2009).
- [142] P. Bruno and C. Chappert. *Oscillatory coupling between ferromagnetic layers separated by a non-magnetic metal spacer*. Physical Review Letters, **67**, 1602 (1991).
- [143] P. Bruno and C. Chappert. *Ruderman-Kittel theory*. Physical Review B, **46**, 261 (1992).
- [144] O. Brovko, P. Ignatiev, V. Stepanyuk and P. Bruno. *Tailoring exchange interactions in engineered nanostructures: an ab initio study*. Physical review letters, **101**, 036809 (2008).
- [145] P. Lang, L. Nordstrom, R. Zeller, and P.H. Dederichs. *Ab initio calculation of exchnage coupling of Fe and Co monolayers in Cu*. Physical review letters, **71**, 1927 (2004).
- [146] P. A. Ignatiev and V. S. Stepanyuk. *Effect of the external electric field on surface states: An ab initio study*. Physical Review B, **84**, 075421 (2011).
- [147] J. Hu and R. Wu. *Control of the Magnetism and Magnetic Anisotropy of a Single-Molecule Magnet with an Electric Field*. Physical Review Letters, **110**, 097202 (2013).
- [148] C. Liu and S. D. Bader. *Perpendicular surface magnetic anisotropy in ultrathin epitaxial Fe films*. Journal of Vacuum Science & Technology A: Vacuum, Surfaces, and Films, **8**, 2727 (1990).

- [149] T. R. Dasa, P. Ruiz-Díaz, O. O. Brovko and V. S. Stepanyuk. *Tailoring magnetic properties of metallic thin films with quantum well states and external electric fields*. Physical Review B, **88**, 104409 (2013).
- [150] M. Tsujikawa, A. Hosokawa and T. Oda. *Magnetic anisotropy of FePt(001) and Pt-FePt(001) using a first-principles approach*. Physical Review B, **77**, 054413 (2008).
- [151] S. Imada, A. Yamasaki, S. Suga, T. Shima and K. Takanashi. *Perpendicular magnetization of L10-ordered FePt films in the thinnest limit*. Applied Physics Letters, **90**, 132507 (2007).
- [152] C. Andersson, B. Sanyal, O. Eriksson, L. Nordström, O. Karis, D. Arvanitis, T. Konishi, E. Holub-Krappe and J. Dunn. *Influence of Ligand States on the Relationship between Orbital Moment and Magnetocrystalline Anisotropy*. Physical Review Letters, **99**, 177207 (2007).
- [153] S. S. P. Parkin, C. Kaiser, A. Panchula, P. M. Rice, B. Hughes, M. Samant and S.-H. Yang. *Giant tunnelling magnetoresistance at room temperature with MgO (100) tunnel barriers*. Nature materials, **3**, 862 (2004).
- [154] M. Julliere. *Tunneling between ferromagnetic films*. Physics letters, **54**, 225 (1975).
- [155] H. Oka, K. Tao, S. Wedekind, G. Rodary, V. S. Stepanyuk, D. Sander and J. Kirschner. *Spatially Modulated Tunnel Magnetoresistance on the Nanoscale*. Physical Review Letters, **107**, 187201 (2011).
- [156] H. Meyerheim, M. Przybylski, a. Ernst, Y. Shi, J. Henk, E. Soyka and J. Kirschner. *Correlation of structure and magnetism of ultrathin Co films on Pd(001) prepared by thermal and pulsed laser deposition*. Physical Review B, **76**, 035425 (2007).
- [157] S. Valvidares, T. Schroeder, O. Robach, C. Quirós, T.-L. Lee and S. Ferrer. *Structural and magnetic properties of bcc Co films on Pt(001) studied by magnetic resonant surface x-ray diffraction, STM, and magneto-optical Kerr effect*. Physical Review B, **70**, 224413 (2004).
- [158] S. Sun. *Monodisperse FePt Nanoparticles and Ferromagnetic FePt Nanocrystal Superlattices*. Science, **287**, 1989 (2000).
- [159] D. Weller, L. Folks, M. Best, E. E. Fullerton, B. D. Terris, G. J. Kusinski, K. M. Krishnan and G. Thomas. *Growth, structural, and magnetic properties of high coercivity Co/Pt multilayers*. Journal of Applied Physics, **89**, 7525 (2001).
- [160] S. Razee, J. Staunton and F. Pinski. *First-principles theory of magnetocrystalline anisotropy of disordered alloys: Application to cobalt platinum*. Physical Review B, **56**, 8082 (1997).
- [161] A. Ebbing, O. Hellwig, L. Agudo, G. Eggeler and O. Petravic. *Tuning the magnetic properties of Co nanoparticles by Pt capping*. Physical Review B, **84**, 012405 (2011).
- [162] C. J. Aas, K. Palotás, L. Szunyogh and R. W. Chantrell. *The effect of a Pt impurity layer on the magnetocrystalline anisotropy of hexagonal close-packed Co: a first-principles study*. Journal of physics. Condensed matter, **24**, 406001 (2012).

- [163] J. Jaworowicz, V. Zablotskii, J.-P. Jamet, J. Ferre, N. Vernier, J.-Y. Chauleau, M. Kisielewski, I. Sveklo, A. Maziewski, J. Gierak and E. Bourhis. *Magnetic coercivity of focused ion beam irradiated lines in a Pt/Co(1.4 nm)/Pt film*. Journal of Applied Physics, **109**, 093919 (2011).
- [164] M. Abes, J. Venuat, A. Carvalho, J. Arabski, D. Muller, G. Schmerber, E. Beaurepaire, P. Panissod, a. Dinia and V. Pierron-Bohnes. *Magnetic nanopatterning of CoPt thin layers*. Journal of Magnetism and Magnetic Materials, **286**, 297 (2005).
- [165] M. Suzuki, H. Muraoka, Y. Inaba, H. Miyagawa, N. Kawamura, T. Shimatsu, H. Maruyama, N. Ishimatsu, Y. Isohama and Y. Sonobe. *Depth profile of spin and orbital magnetic moments in a subnanometer Pt film on Co*. Physical Review B, **72**, 054430 (2005).
- [166] J. J. Hauser. *Magnetic proximity effect*. Physical Review, **187**, 580 (1969).
- [167] C. Fowley, Z. Diao, C. C. Faulkner, J. Kally, K. Ackland, G. Behan, H. Z. Zhang, A. M. Deac and J. M. D. Coey. *Local modification of magnetic anisotropy and ion milling of Co/Pt multilayers using a He⁺ ion beam microscope*. Journal of Physics D: Applied Physics, **46**, 195501 (2013).
- [168] K. Nakamura, R. Shimabukuro, T. Akiyama, T. Ito and A. Freeman. *Origin of electric-field-induced modification of magnetocrystalline anisotropy at Fe(001) surfaces: Mechanism of dipole formation from first principles*. Physical Review B, **80**, 172402 (2009).
- [169] A. Lehnert, S. Denner, P. Boski, S. Rusponi, M. Etzkorn, G. Moulas, P. Bencok, P. Gambardella, H. Brune and J. Hafner. *Magnetic anisotropy of Fe and Co ultrathin films deposited on Rh (111) and Pt (111) substrates: An experimental and first-principles investigation*. Physical Review B, **82**, 094409 (2010).
- [170] H. Gleiter, J. Weissmüller, O. Wollersheim and R. Würschum. *Nanocrystalline materials: a way to solids with tunable electronic structures and properties?* Acta materialia, **49**, 737 (2001).
- [171] M. Y. Zhuravlev, A. V. Vedyayev and E. Y. Tsymbal. *Interlayer exchange coupling across a ferroelectric barrier*. Journal of Physics. Condensed matter : an Institute of Physics Journal, **22**, 352203 (2010).
- [172] M. Kryder. *After Hard Drives What Comes Next?* IEEE Transactions on Magnetics, **45**, 3406 (2009).
- [173] M. Fechner, P. Zahn, S. Ostanin, M. Bibes and I. Mertig. *Switching Magnetization by 180 with an Electric Field*. Physical Review Letters, **108**, 197206 (2012).

Publications (Veröffentlichungen)

The results presented in this thesis have been partly published in the following articles:
Teile der vorliegenden Arbeit wurden an folgenden Stellen veröffentlicht:

1. T. R. Dasa, P. A. Ignatiev, and V. S. Stepanyuk
Effect of the electric field on magnetic properties of linear chains on a Pt(111) surface
Phys. Rev. B **88**, 104409 (2012)
2. P. Ruiz-Díaz, T. R. Dasa, and V. S. Stepanyuk
Tuning Magnetic Anisotropy in Metallic Multilayers by Surface Charging: An Ab Initio Study
Phys. Rev. Lett. **110**, 267203 (2013)
3. T. R. Dasa, P. Ruiz-Díaz, O. O. Brovko, and V. S. Stepanyuk
Tailoring magnetic properties of metallic thin films with quantum well states and external electric fields
Phys. Rev. B **85**, 205447 (2013)
4. Brovko Oleg O., Ruiz-Díaz Pedro, Dasa Tamene R., Stepanyuk Valeri S.
Controlling magnetism on metal surfaces with non-magnetic means: electric fields and surface charging: (TOPICAL REVIEW)
J. Phys.: Condens. Matter, **26** 093001 (2014).
5. T. R. Dasa, and V. S. Stepanyuk
Switching the interlayer magnetic order of Fe/Cu_N/Fe trilayers by surface charging and alkali metals
to be submitted.

Curriculum vitae (Lebenslauf)

Name	Tamene Regassa, Dasa
Geburtsdatum	18.03.1984
Geburtsort	Addis Ababa, Ethiopia
Staatsangehörigkeit	äthiopisch
Familienstand	Ledig
Adresse (privat)	Gütchen-Str. 3, D-06108, Halle/Saale
Adresse (dienstlich)	Weinberg 2, D-06120, Halle/Saale

Ausbildung und Qualifikation

1989-1997	Primary school, Addis Ababa (Ethiopia)
1997-2001	High school, Addis Ababa (Ethiopia)
2001-2005	Bachelor of science in physics, Addis Ababa University, College of Natural Sciences, Physics Department, Addis Ababa (Ethiopia)
2007-2009	Masters of science in Materials Science, Addis Ababa University, College of Natural Sciences, Materials Science Program, Addis Ababa (Ethiopia)
2009-2010	Master Universitario di II livello NANO-MICRO (Second level NANO-MICRO Master), Università Degli Studi Di Trento (University of Trento), Facoltà di Scienze (Faculty of Science), Trento (Italy)
2010-	Doktorand and der Martin-Luther-Universität Halle-Wittenberg und der International Max-Planck Research School for Nanoscience and Technology, wissenschaftlicher Mitarbeiter am Max-Planck-Institut für Mikrostrukturphysik, Halle, Deutschland

Erklärung

Ich versichere hiermit, die vorliegende Dissertation

**Exploring the effect of electric field and surface
charging on magnetic properties of nanostructures :
an *ab initio* Study**

selbständig und ohne fremde Hilfe verfasst und keine anderen als die von mir angegebenen Quellen und Hilfsmittel verwendet zu haben. Den benutzten Werken wörtlich oder inhaltlich entnommene Stellen sind als solche gekennzeichnet.

Halle (Saale), 12.06.2014

Tamene Regassa Dasa

Erklärung

Ich versichere hiermit, dass ich mich an keiner wissenschaftlichen Hochschule im Geltungsbereich des deutschen Grundgesetzes bereits früher um den Doktorgrad beworben habe.

Halle (Saale), 12.06.2014

Tamene Regassa Dasa

Acknowledgments

I would like to acknowledge the enormous support of my supervisor Prof. Valery S. Stepanyuk, and I am indebted to him. I also thank Prof. Dr. Wolfram Hergert for monitoring my study and for the fruitful discussions.

Greatful to say the incredible support, from our group members Oleg O. Brovko, Pedro Ruiz-Díaz, Srijan K. Saha and Ilia Sivkov, was very useful. I am also thankful for the support that I got from our former group members: Pavel Ignatiev, Larissa Niebergall, Kun Tao and Nikolay Negulyaev.

I would like to thank Prof. Dr. Eberhard Gross and Prof. Dr. Jürgen Kirschner, directors of the Max-Planck Institute of Microstructure Physics (MPI), for an interesting working environment that I have experienced.

I sincerely thank the secretary of the theory department Ina Goffin, for her help in all administrative related issues, and I also thank Udo Schmidt for being supportive in matters related to our calculational facilities. I have enjoyed the time with the colleagues from the MPI, as well as the IMPRS school members.

I am very thankful for my parents, sisters and brother for their motivation and support.

Once again I thank you all!

Halle (Saale),

12.06.2014